SPECTROSCOPIC STUDY OF SURFACE TREATMENTS FOR Nb SRF CAVITY

Puneet Veer Tyagi

Supervised by

Dr. Shigeki Kato

Department of Accelerator Science

School of High Energy Accelerator Science

The Graduate University for Advanced Studies

2011 (School Year)

A Ph.D. Thesis

Spectroscopic Study of

Surface Treatments for Nb SRF Cavity

By
Puneet Veer Tyagi

SUPERVISOR CERTIFICATE

This is to certify that the thesis entitled **"SPECTROSCOPIC STUDY OF SURFACE TREATMENTS FOR NB SRF CAVITY"** describes the original work done by **Puneet Veer Tyagi**, under my supervision for the degree of **Doctor of Philosophy** of the Graduate University for Advanced Studies, Japan. Mr. Puneet Veer Tyagi has fulfilled the required formalities as per the university rules known to us.

Dr. Shigeki Kato
Associate Professor
KEK/The Graduate University for Advanced Study
Japan

THESIS DEDICATED

TO

MY FAMILY

Especially to my wife Payal
for her consistent encouragement through out my Doctoral course.
She suffered a lot, staying alone in India but never complaint.

Everybody has difficult years, but a lot of times the difficult years end up being the greatest years of your whole entire life, if you survive them.
Brittany Murphy, Seventeen Magazine, September 2003

Contents

List of Figures

List of Tables

Acknowledgments

Time goes by so fast. The last three years were highly eventful and every day presented new challenges and opportunities. This period has brought me valuable new experiences in both a scientific and personal perspective. Realizing the unique opportunity to obtain a Ph.D. degree would not have been possible without the contributions of many people.

Foremost, I would like to thank Dr. Shigeki Kato for my integration in his group and allowing me to work in a nice scientific environment as well as discussing many topics of vacuum science and surface science with me. He fearlessly accepted me as a PhD candidate and was the main creator of the great ideas, techniques and whole background of this thesis. We experienced together all the ups and downs of routine work, the shared happiness of success and the depression of failure. He managed to teach me how to work independently (which is very important), but at any time, his useful advice was available to me. These three years, I spent as a part of surface analysis laboratory proved to be very helpful for me in developing new scientific ideas and skills. I would like to thank you for your help and sharp views, which really improved the quality of the thesis. On the personal side, he did not hesitate to invite his students to become an extended part of his family, I appreciate this immensely.

I am very grateful to Dr. M. Nishiwaki who sets many things for me to start on my project. I gained a lot from her experience and expertise. I learned useful things from her on experimental side.

I am highly indebted to Dr. H. Hayano and Dr. T. Saeki for allowing me to work in STF and providing me their kind help and advices during the experiments.

I express my gratitude to Dr. M. Sawabe and all the technical staff of STF for their kind help in performing electropolishing and buffered chemical polishing experiments.

Two people with whom I enjoyed every moment in Tsukuba are Dr. Noguchi and Mr. Chouhan. They helped me in all spheres of life: during experiments as well as in daily life. I am fortunate to have colleagues like them. I also admire Mrs. Sonam Chouhan (wife of Mr. Vijay Chouhan), who cooked delicious food for me and invited many times for a nice food.

I would like to acknowledge the Japanese government (MEXT : Ministry of Education, Culture, Sports, Science and Technology) for financial support in the form of Monbukagakusho scholarship.

I am very thankful to Mr. Y. Aizawa, S. Hasegawa and other Sokendai staff for their valuable help in all administrative processes.

I am highly obliged to Ulvac-PHI for providing me the TOF-SIMS analysis of our cavity EP 1 sample and Applied Surface Technologies, USA for providing the dry ice cleaning equipment.

Also outside of science, there were people whose help and support was very important. I greatly admire my parents: Mr. Ajai Veer Singh Tyagi and Mrs. Sushila Tyagi. They have always encouraged me and supported me all the time from the joining of research program till today in every aspect. I also wish to express my feelings for my brother Dr. Vineet Veer Tyagi and sister in law Dr. Richa K. Tyagi for their full-fledged co-operation and inspiration. They are the ones who have always boosted my moral in carrying out my work. I also admire my niece Ananya, my little angel, who did not directly contributed to my thesis but gave me a lot of humor when talking to her. I forgot all the work stress when listening her childish talks and freshen myself.

Finally, I would like to mention the great love and care of my wife Dr. Payal Tyagi during the last year of my thesis. I can't simply express her contribution in words. She has helped me in every aspects like thesis modification, moral support etc. Without her love and care, it would have been difficult for me to achieve my goals. Above all, I thank almighty God for providing me strength, motivation and courage.

Abstract

The superconducting radio frequency (SRF) cavities are being used worldwide in particle accelerators to achieve a high energy beam of charged particles. These cavities are made of high purity niobium (Nb) material and work at 2 K temperature. The inner surface of these cavities plays the most important role in order to obtain good performances in terms of the high field gradient. Therefore, the surface treatments associated with SRF cavities are the key issues toward the achievement of the high field gradient larger than 35 MV/m during vertical test of the nine-cell cavity for International Linear Collider (ILC). In the recent years, extensive research has been done to enhance the cavity performance by applying improved surface treatments such as mechanical grinding, buffered chemical polishing (BCP), electropolishing (EP), electrochemical buffing (ECB), mechanochemical polishing (MCP), tumbling, etc., followed by various post-treatment methods such as ultrasonic pure water rinse, alcoholic rinse, high pressure water rinse (HPR), hydrogen per oxide rinse and baking etc. to obtain smooth and contaminant free surface.

Among all surface treatments, the EP followed by HPR seems to be the salient surface treatment method and used worldwide as a final surface treatment which provides the promising results. However, as a result of the EP process at laboratory level, some contaminants such as sulfur, fluorine, and carbon have been identified at the surface, which might be the sources of field emission when a high electric field is excited in a SRF cavity and limit the performance. Therefore it is of interest to characterize the status of surface after the EP process as well as see the effect of HPR with the help of surface analytical tools. The use of surface analytical tools will enable to find the optimum conditions of the surface treatments necessary for the mass production of efficient SRF cavities.

In this thesis, the efforts have been made to understand the behavior of EP inside a real cavity based on different EP conditions and see the effect of HPR with different pressures and doses. The total work can be summarized as follows :

(1) The theory and working principle of SRF cavities have been introduced. The manufacturing procedure, engineering and various surface treatment methods have been discussed in details. A wide literature survey has been done.

(2) The main experimental setups such as surface analytical system, scanning electron microscope, electropolishing system, HPR facility and clean room etc. have been introduced. The necessary systems for experiments such as three loadlock systems attached with surface analysis system, vacuum

suitcases, experimental setup to carried out lab-HPR experiments etc. were constructed.

(3) A series of cavity EP experiments by using a real Nb test cavity attached with six Nb disc type samples were carried out with different EP conditions in the same manner as ILC cavities are processed.

(4) The experimental results with high current density and aged EP acid solution showed a greater existence of sulfur and fluorine at the Nb surfaces in comparison of the experiment with fresh EP acid which confirms the sulfur generation is proportional to the aging of the EP acid solution. The chemical state of sulfur was confirmed as a mixture of SO_4^{--} and SO_3^{--}.

(5) The experimental results with low current density demonstrated that the low current is quite helpful in order to mitigate the sulfur and fluorine at the Nb surfaces.

(6) Two laboratory EP experiments were also conducted with low and high current density. The experimental results were quite consistent with the cavity EP experiments and showed that low current density was very helpful in order to mitigate sulfur/sulfide from the surface.

(7) The HPR experiment was conducted on BCPed samples in order to demonstrate the effect of different pressures and doses which might be very helpful to optimize the HPR parameters. The thicker oxide layer was formed on Nb surface in proportional to high pressure and dose.

(8) The dry ice cleaning (DIC) was also tried on Nb samples after the lab EP. The results showed that the dry ice cleaning was not so effective in order to mitigate sulfur and fluorine form Nb surface while some hydrocarbons/dust particles were removed.

Chapter 1 Introduction

1.1. International Linear Collider

The International Linear Collider (ILC) will accelerate the electron and positron beams up to a center of mass energy of 500 GeV - 1 TeV [1.1, 1.2]. The electron - positron collision in the terascale energy region would explore the unknown regions of science. The International Technology Recommendation Panel (ITRP) committee for ICFA (International Committee for Future Accelerators) has decided to use superconducting radio frequency (SRF) technology for the accelerating structures (cavities). The tesla type nine-cell accelerating cavity is adopted as a baseline cavity for ILC. These cavities should provide a high accelerating E-field gradient individually in order to shorten the length of ILC. The goal of average accelerating E-field gradient in each cavity has been set to 35 MV/m in qualification test. The ILC will requires ~ 16000 SRF cavities with the operating accelerating E-field of 31.5 MV/m [1.2].

Fig. 1.1 : The baseline two tunnels design of ILC..

Figure 1.1 shows the two tunnels baseline design of the ILC accelerator in the Reference Design Report (RDR) in which one tunnel is proposed to use as a RF power source installation and supporting tunnel for the maintenance of the main tunnel. In the Technical Design Report (TDR), there will be changed to ILC baseline with single tunnel to reduce the construction cost of the ILC.

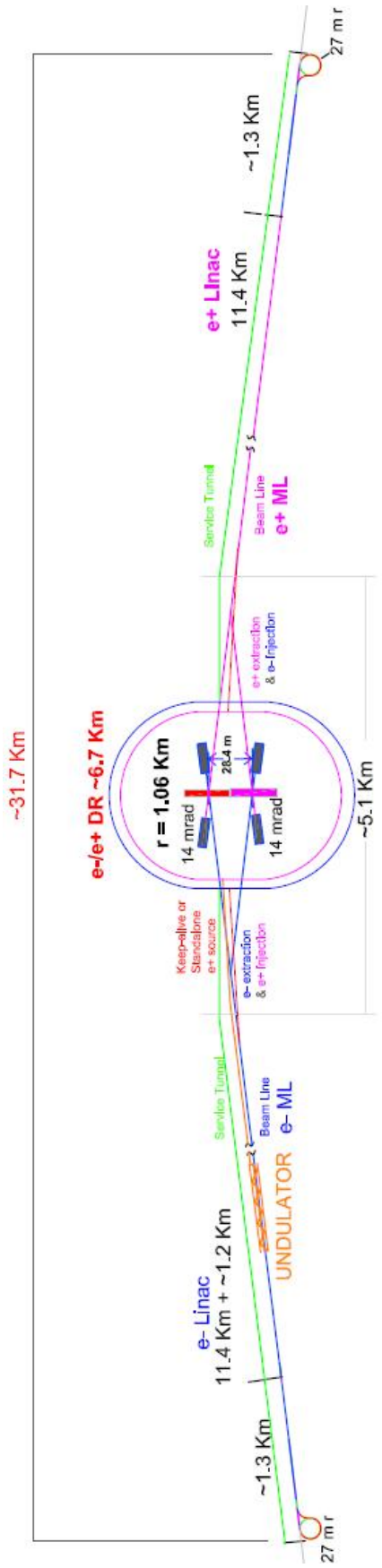

Fig. 1.2 : The schematic layout of 500GeV center of mass energy machine [1].

1.2. Superconducting Radio Frequency Cavity

1.2.1. RF Cavity : A space surrounded by the conducting walls in which infinite number of resonant electromagnetic modes can sustain is called a cavity. The cavities can be operated by the DC power or rf power depending upon the users choice. In order to accelerate charged particles, a cavity should provide an electric field E longitudinal with the velocity of charged particles. The magnetic field inside a cavity can provide deflection but can not accelerate the charged particles beam. The acceleration achieved by charged particles beam can be obtain by the Lorentz force equation [1.3]:

$$\vec{a} = q\frac{\left(\vec{E} + \vec{V} \times \vec{B}\right)}{m} \tag{1.1}$$

The cavities operated with the DC electric fields are able to provide the energies of only a few MeV and the higher energies can be achieved only by the transfer of energy from a rf resonant circuit. The energy can be transferred from a wave to a particle efficiently only when the cavity is tuned i.e. the cavity is excited at the same time of the charged particles passing through the cavity. The rf cavities work as a mode* transformer and an impedance# transformer during the excitation. A rf cavity can be considered as an equivalent of LCR circuit (fig 1.2 a, b) :

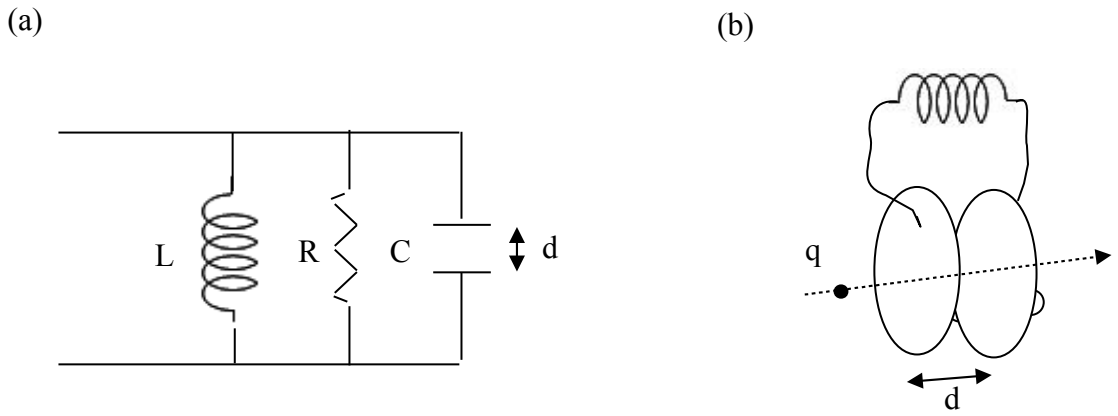

Fig. 1.3 : (a) An equivalent LCR circuit of rf cavity. (b) Simple lumped LC circuit representing a rf cavity [1.4, 1.5].

1.2.2. Electromagnetic Modes in a Cavity : The electromagnetic modes inside a cavity are given by the Maxwell's equations [3] :

$$\left(\nabla^2 - \frac{1}{c^2}\frac{\partial^2}{\partial t^2}\right)\begin{Bmatrix}\vec{E}\\ \vec{H}\end{Bmatrix} = 0 \tag{1.2}$$

* Mode transformer (TEM ⟶ TM), # Impedance transformer (low ⟶ high)

If there is no surface resistance at the cavity wall then Maxwell's equations satisfy the boundary conditions :

The tangential E field : $\vec{n}\times\vec{E}=0$ (1.3)

Normal magnetic field : $\vec{n}.\vec{E}=0$ (1.4)

For a fixed shape, there is an infinite number of solutions for Maxwell's equations with sinusoidal time dependence. Assuming the solution of equation 1.2 is $\sim e^{-i\omega t}$

Now Maxwell's equations can be written as :

$$\left(\nabla^2-\frac{\omega^2}{c^2}\right)\begin{Bmatrix}\vec{E}\\ \vec{H}\end{Bmatrix}=0 \tag{1.5}$$

where $\boldsymbol{\omega}$ is the angular frequency of electromagnetic waves and $\boldsymbol{c}$ is velocity of light.

From equation 1.5 it can be concluded that for an efficient acceleration we should choose a shape of cavity and mode where :

(1) The Electric field should be along the particle trajectory.

(2) There should not be any Magnetic field along the particle trajectory.

(3) Velocity of the electromagnetic field and particle should be matched well.

1.2.3. Accelerating Field in a Cavity: Accelerating field (gradient) seen by the charged particles passing through a cavity can be written as [1.3-1.5]:

$$\vec{E}_{acc}=\frac{1}{L}\int E_z(z)\cos(\omega z/\beta c)\,dz \tag{1.6}$$

Where $L=N\frac{\lambda}{2}$ is a reference length for the particles moving with the velocity of light.

1.2.4. Energy Stored and Power Dissipation in a Cavity : The total energy stored in a cavity at a time is give by [3-5]:

$$U=\frac{\varepsilon_0}{2}\int dV\left(E^2\right)=\frac{\mu_0}{2}\int dV\left(H^2\right) \tag{1.7}$$

From equation 1.7, it can be concluded that the total energy is oscillating between electric and magnetic field because of sinusoidal time dependence of the field with a phase shift of 90^0.

The total power dissipation in the cavity is given by :

$$P=\frac{R_s}{2}\int da\left(H_{\parallel}\right)^2 \tag{1.8}$$

Where $\boldsymbol{R_s}$ is the surface resistance of the cavity wall.

1.2.5. Quality Factor (Q_0) : Quality factor is a measure of the performance of a cavity. It is given by the energy stored in a cavity divided by the energy lost in cavity walls because of surface

resistance of walls [1.4, 1.5].

$$Q_0 = \frac{\omega_0 U}{P_{diss}} = \omega \frac{\mu_0}{R_s} \frac{\int dV\left(H^2\right)}{\int da\left(H_{\|}\right)^2} \tag{1.9}$$

1.2.6. Geometrical Factor (G) and Shunt Impedance (R_{sh}) : The geometrical factor of a cavity is the product of quality factor and surface resistance of the cavity wall. It is basically shape and electric mode dependent quantity which is independent of the size (frequency), number of cells and the material of a cavity [4,5].

$$G = QR_s = 2\pi \frac{\eta}{\lambda} \frac{\int dV\left(H^2\right)}{\int da\left(H_{\|}\right)^2} \tag{1.10}$$

where $\boldsymbol{\eta}$ is the impedance of vacuum which is 377 Ω.

The shunt impedance of a cavity depends on the mode geometry of the cavity and proportional to the number of cells in a cavity. The shunt impedance of a cavity can be written as :

$$R_{sh} = \frac{V^{2_c}}{2\mathrm{P}_{diss}} \tag{1.11}$$

Where $\boldsymbol{V_c}$ is the accelerating voltage.

1.2.7. RF Cavity with External Coupling : In reality, the cavities are used with an external coupling to provide the power from a klystron to a charged particles beam. In such case :

The total power loss in a cavity is given by [1.4, 1.5] : $P_{tot} = P_{diss} + P_e$ (1.12)

Where $\boldsymbol{P_e}$ is the power leaking out from the input coupler.

Similarly, the quality factor can be described as :

$$Q_L = \omega_0 \frac{U}{P_{tot}} \tag{1.13}$$

and

$$Q_e = \omega_0 \frac{U}{P_e} \tag{1.14}$$

therefore

$$\frac{1}{Q_L} = \frac{1}{Q_0} + \frac{1}{Q_e} \tag{1.15}$$

Where $\boldsymbol{Q_L}$ is called as a loaded quality factor.

A coupling parameter can be defined as : $\beta = \frac{Q_0}{Q_e} = \frac{P_e}{P_{diss}}$ (1.16)

Now, $\boldsymbol{Q_L}$ can be written as :

$$\frac{1}{Q_L} = \frac{1+\beta}{Q_0} \tag{1.17}$$

1.2.8. Design Consideration of a Cavity : To design a cavity following parameters are important to be considered [1.4-1.6].

Quantity	Consideration
Critical field ($\frac{H_{S,max}}{E_{acc}}$)	Minimum
Field emission ($\frac{E_{S,max}}{E_{acc}}$)	Minimum
Shunt impedance, current loss ($\frac{\langle H_{s^2} \rangle}{E_{acc^2}}$)	Minimum
Dielectric loss ($\frac{\langle E_{s^2} \rangle}{E_{acc^2}}$)	Minimum

Table 1.1 : The required design parameters for designing a cavity.

1.3. Cavity Fabrication

1.3.1. Flow Chart of a Cavity Fabrication from Nb Mother Material :

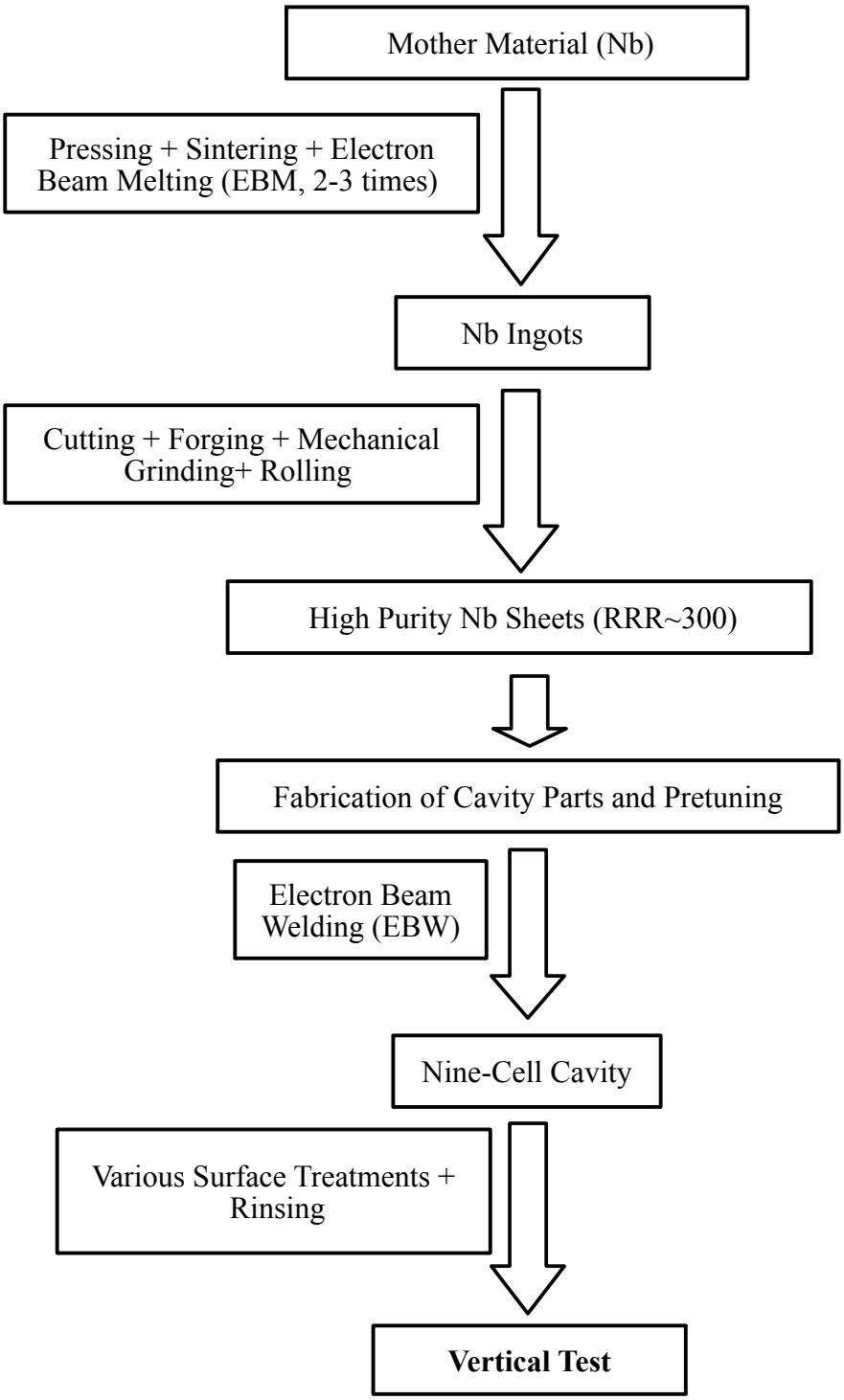

1.3.2. Nb Production : The mineral containing niobium (Nb) material is obtained from the mines. The Nb is then separated from the pyrochlore ($NaCaNb_2O_6F$) mineral. The mines containing pyrochlore mineral are mostly situated in Brazil. The separation of Nb from the pyrochlore ore is done in the following manners [1.7, 1.8]:

1. The pyrochlore ore is crushed and the magnetite is separated magnetically.
2. The ore is then chemically processed to give a concentrate ranging from 55 to about 60% niobium oxide (Nb_2O_5).
3. The mixture of Nb_2O_5 and aluminum powder are reacted to reduce the oxide to Nb.
4. The powder is pressed, sintered and electron beam melted to get the pure Nb ingots.

1.3.3. Nb Ingots : The sintered Nb is moved to the electron beam melting (EBM) facility to melt down. Figure 1.3 (a) and (b) show the schematic of an EBM and EBM of sintered Nb respectively [1.8, 1.9].

(a) (b)

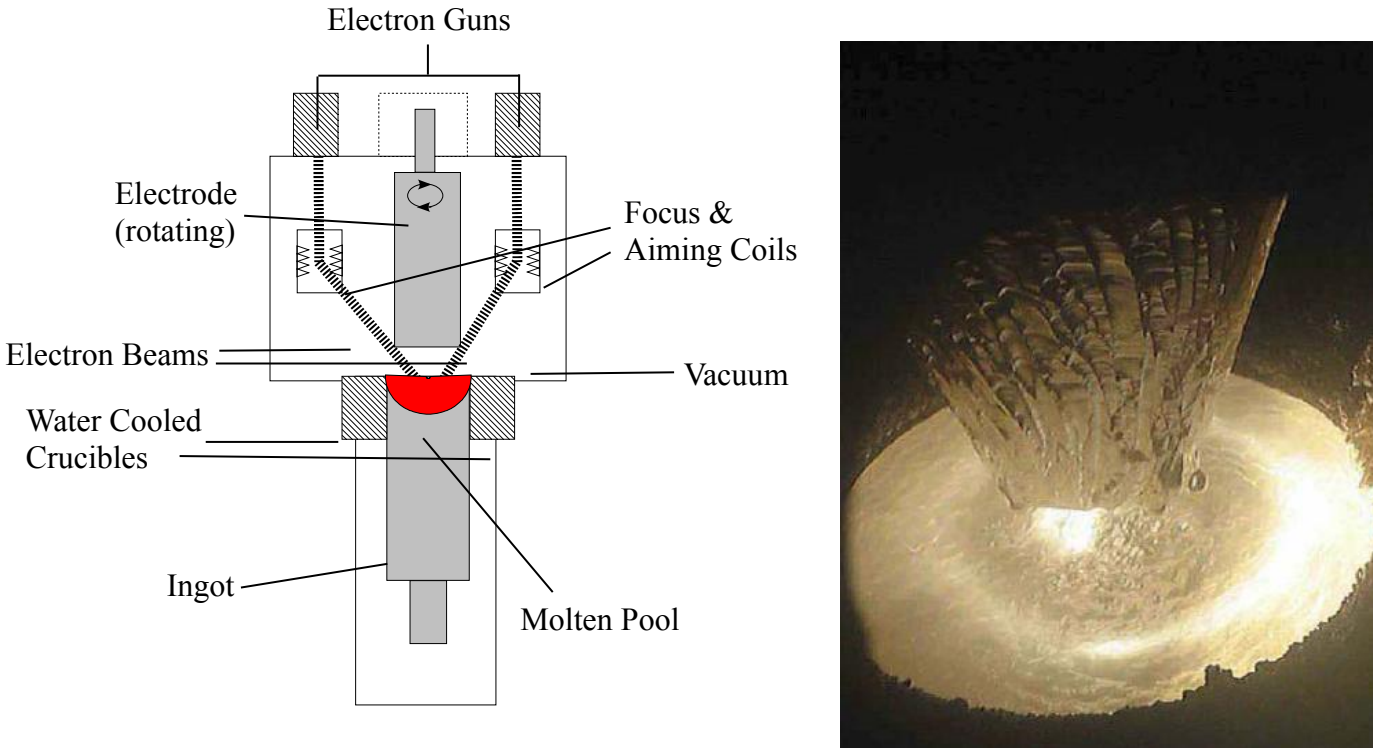

Fig. 1.4 (a) Schematic of EBM procedures. (b) Nb ingot during EBM [1.8].

A typical EBM machine contains a vacuum chamber and electron guns. The electrode (which is to be melted, sintered Nb in this case) is rotated during the melting. The electron beams are focused by using the focusing coils on to the material (sintered Nb) to be melted. The Nb drops are then fallen down in a molten pool on the ingot and is passed to a water cooled copper cylinder. During the meltdown of Nb, all the impurities are evaporated and pumped out by using a vacuum pump. The

ingot formed during the melting of Nb is continuously withdrawn and the rate of withdrawn should be carefully adjusted with the rate of material to insure proper outgassing and complete melting of the material. After getting Nb ingots this process is repeated 3-4 times (EB refining) to get the high purity Nb ingots.

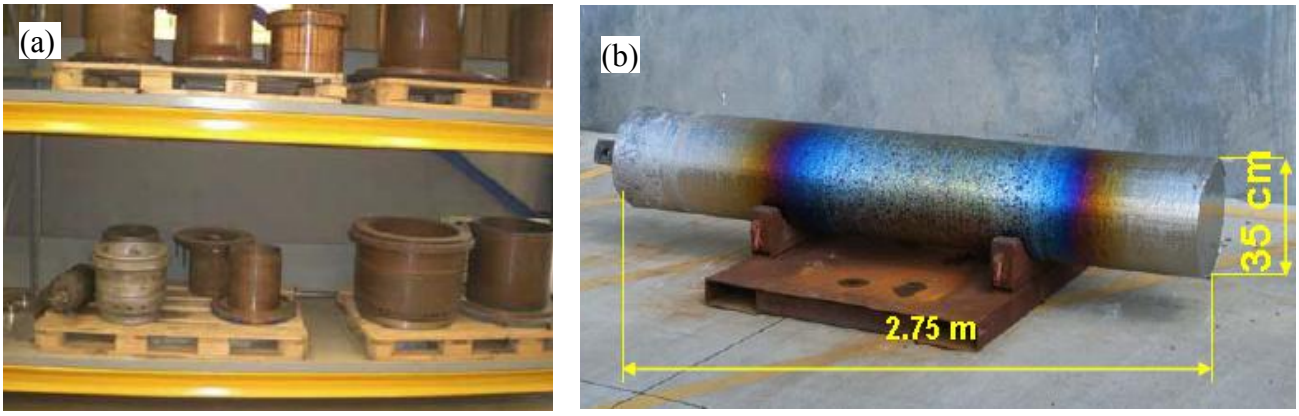

Fig. 1.5 : (a) The crucibles used in EBM. (b) Nb ingot produced after EBM [1.8].

1.3.4. Nb Sheets : The high purity Nb sheets are prepared from the Nb ingots. To produce a sheet from Nb ingot, the Nb ingots are first forged and then moved to a rolling machine. The forging dies of 1500-2000 ton are used for forging [1.8, 1.9].

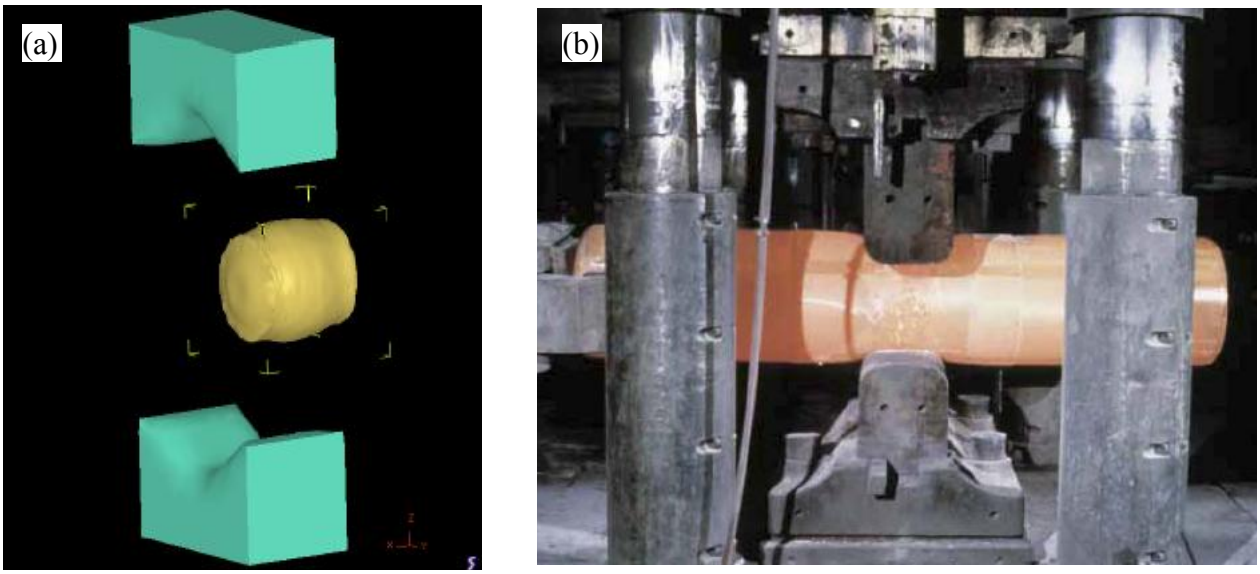

Fig .1.6 (a) The schematic of forging procedure containing Nb ingot in between. (b) Forge machine at ATI Wang company [1.8].

The forged Nb blocks are then moved to a rolling machine where the Nb sheets are prepared. There are two types of rolling methods : hot rolling and cold rolling can be used for rolling depending upon choice. If the temperature during rolling is maintained above the crystallization temperature of

Nb then it is called as a hot rolling and if temperature is lower than the crystallization temperature of Nb then it is called as a cold rolling.

Fig. 1.7 : (a) Cold rolling machine at ATI wang company. (b) Hot rolling machine at ATI Wang company [1.8].

The top surface of Nb sheets is much damaged during the fabrication. The Nb sheets are then polished to remove the damaged layer of the surface. The defects such as point defects, interstitial, line dislocation etc. are then recovered by annealing (recrystallization) at 800 ^{0}C. The RRR measurement (purity check) of a Nb sheet is done after the recrystallization.

1.3.4.1. Residual Resistance Ratio (RRR) : In order to check the purity of the Nb sheets, the RRR measurement is carried out. The ratio of electrical resistivity of a metal at a normal temperature to the critical temperature (T_c) is called the residual resistance ratio (RRR). The impurities present in metals affect the electrical resistivity of the metals which lower the RRR value [1.8, 1.9].

$$RRR = \frac{\rho(295\,K)}{\rho(4.2\mathrm{K})} \tag{1.18}$$

If there are some known impurities present in the metal then equation 1.18 can be written as :

$$RRR = \frac{\rho(295\,K)}{\rho(4.2\mathrm{K}) + \sum_i \frac{\partial \rho_i}{\partial C_i} C_i} \tag{1.19}$$

where C_i is thermal conductivity of impurities.

Following table (1.2) gives the expected RRR contribution for 1 wt ppm impurities for Nb :

Element	RRR Contribution
H	2640
N	4230

C	4380
O	5580
Ti	53700
Zr	102000-239000
Hf	200000
W	261000-721000
Mo	717000
Ta	1149000

Table 1.2 : Expected RRR contribution for 1 wt ppm impurities for Nb [1.8, 1.9].

1.3.5. Fabrication of Cavity Parts : The fabrication of cavity parts can be summarized in following steps :

1. Deep drawing with hydraulic press is made and cups are prepared.
2. The mechanical measurement of cups are done in order to check the shape of the cups.
3. The cups are cleaned by ultra sonic cleaning and rinsing.
4. The iris region is trimmed and cups are reshaped if needed.
5. The trimmed cups are then cleaned once again.
6. The rf measurement of cups is performed to check the size and length of cavity by measuring frequency of resonance.

(b)

(c)

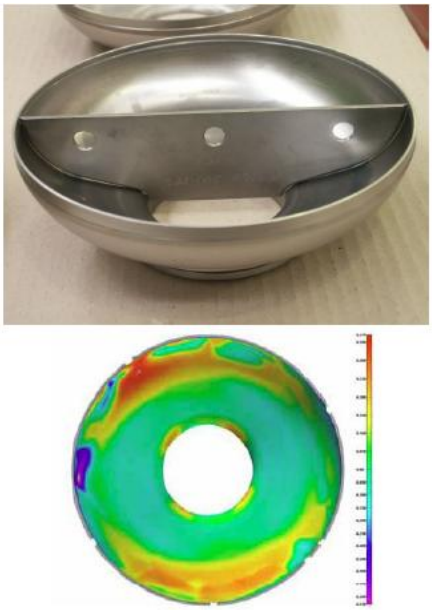

(d)

Fig. 1.8 : (a) Deep drawing of cavity. (b) The cups. (c) Mechanical shape measurement of cup. (d) RF measurement of dumbbell [1.8].

1.3.6. Nine-Cell Cavity : All the cavity parts are cleaned very well and buffered chemical polishing (BCP) followed by rinsing is done prior to weld them. The cleaned cavity parts are moved to electron beam welding (EBW) facility and sequentially welded. After welding of iris and stiffening rings, the mechanical measurement and rf measurement of the dumb-bells are performed and dumb-bells are reshaped if needed. After reshaping of the dumb-bells, the dumb-bells are trimmed (equator regions) and chemically etched (BCP, 20-40 μm) followed by rinsing. The inner surface of the dumb-bell is visually checked and local grinding is done if needed. Then after, the equator regions are welded by using an EBW.

(b)

Fig. 1.9 : (a) Welded cavity parts. (b) Nine-cell cavity after welding [1.8].

1.3.6.1. Electron Beam Welding : In order to avoid the contaminations during welding of the cavity parts, electron beam welding (EBW) is used. The EBW is operated under good vacuum in the range of 10^{-3} Pa. The welding is overlapped at the end of welding to avoid accumulation of impurities and wait to cool down before opening the chamber.

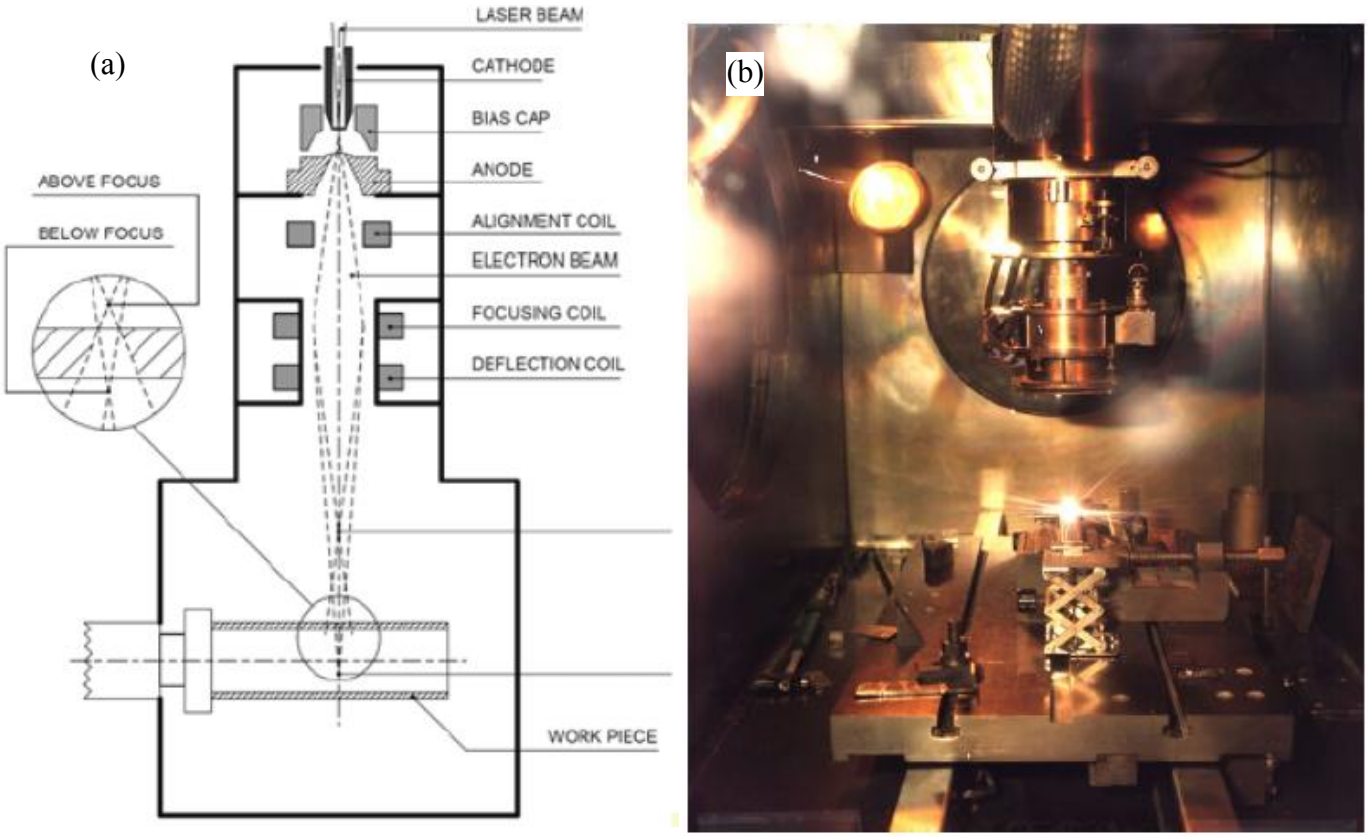

Fig. 1.10 : (a) Schematic view of an EBW machine. (b) The inside picture of an EBW machine [1.8].

The welding sequence can be given as following :

1. Two cups are welded to form a dumb bell.
2. Stiffening ring is welded at the iris.
3. Two dumb-bells are welded together at equator position to form a single cell cavity.
4. More dumb-bells are added one by one.
5. End groups are added in the end.
6. For the mass production, welding of all dumb bells is done.

1.3.7. Cavity Inspection and Tuning : After the fabrication, all the cells are inspected and tuned. The eccentricity measurement of all the cells is done to ascertain the center of each cell, the inner surface is then inspected to ensure that there is no surface damages and field profile measurement (to check the frequency shift) is also performed in order to tune a cavity. Small mechanical adjustments are made to get the flat field and desired frequency.

1.3.8. Surface Finishing and Cleaning : Many contaminants and impurities are introduced at top surface of cavities and the surface layer is damaged during the deep drawing and EBW. In order to achieve a good performance of the cavities, removal of damaged surface layer and the impurities incurred during the fabrication is necessary. There are various surface treatment processes such as mechanical centrifugal barrel polishing (CBP), buffered chemical polishing (BCP), electropolishing (EP), electrochemical buffing (ECB), mechanochemical polishing (MCP) followed by various rinsing procedures are applied to the cavities. The ultrasonic degreasing in detergent is done in advance for all the cavities to remove grease, oil, finger prints from the surface before applying any of the surface treatments [1.9-1.13].

1.3.8.1. Mechanical Centrifugal Barrel Polishing (CBP) : The CBP was developed in KEK in 2001. It is a simple and easy polishing method but a very slow (removal rate ~5 μm/hr.) process. In CBP, the plastic stones and an abrasive liquid is added inside the cavity and cavity is rotated [1.9-1.11]. Because of the rotation of cavity, these plastic particles are rubbing the cavity surface and hence material is removed resulting in a finished surface.

(a) New

Coarse **Medium** **Fine**

(b) Used

Fig. 1.11 : The plastic stones of different sizes for CBP. (a) New (b) used.

The surface roughness depends on the plastic stones size. For the bulk removal large particles are used. The removal rate also depends on particle size as well as rotation speed.

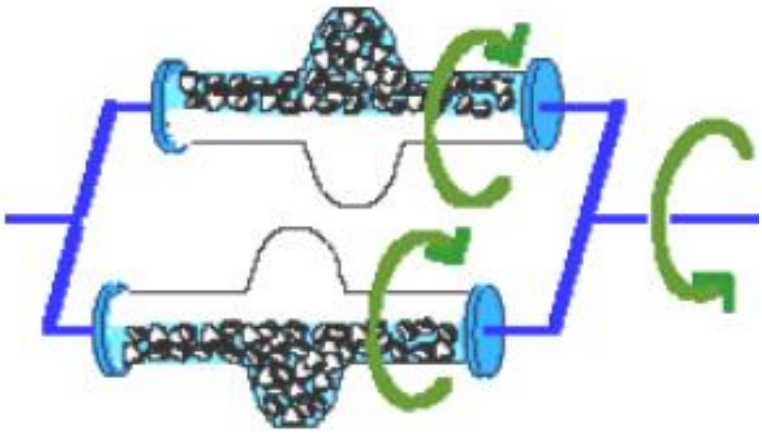

Fig. 1.12 : The schematic of a CBP process.

1.3.8.2. Buffered Chemical Polishing : The cavity requires interior chemistry to remove the damaged layer during welding and exterior chemistry to remove the oxide layer. The chemical etching is used to remove the oxide layer of surface which comes from fabrication steps of the cavity. The BCP is one of the chemical treatments widely used for cavity surface treatment and gives fairly good surface smoothness. The BCP electrolyte contains a mixture of hydrofluoric acid (HF, 49 wt%), nitric acid (HNO_3, 69.5 wt%) and ortho-phosphoric acid (H_3PO_4, 85 wt%) in the ratio of 1 : 1 : 1 or 1 : 1 : 2 by volume respectively. The chemistry of BCP can be written as following [1.13-1.15]:

Oxidation :

$$NO_3^- + 4\,H^+ + 3\,e^- \longrightarrow NO + 2\,H_2O \quad (1.20)$$

$$2\,Nb + 5\,H_2O \longrightarrow Nb_2O_5 + 10\,e^- + 10\,H^+ \quad (1.21)$$

$$6\,Nb + 10\,HNO3 \longrightarrow 3\,Nb2O5 + 10\,NO + 5\,H_2O \quad (1.22)$$

Reduction :

$$Nb_2O_5 + 14\,HF \longrightarrow 2\,H_6NbO_2F_7 + H_2O \quad (1.23)$$

$$Nb_2O_5 + 12\,HF \longrightarrow 2\,HNbF_6 + 5\,H_2O \quad (1.24)$$

$$Nb_2O_5 + 10\,HF \longrightarrow 2\,NbF_5 + 5\,H_2O \quad (1.25)$$

$$Nb_2O_5 + 10\,HF \longrightarrow 2\,H_2NbOF_5 + 3\,H_2O \quad (1.26)$$

$$HNbF_6 + HF \longrightarrow H_2NbF_7 \quad (1.27)$$

The BCP reaction is an exothermic reaction therefore we need to control temperature very well during the reaction. The phosphoric acid is used as a buffer to slow the reaction rate. The typical etch rate is ~ 8 μm/min with mixture of 1 : 1 : 1 which is used for cavity subcomponents and ~3 μm/min for the mixture of 1 : 1 : 2. The etching rate is depending on the position also which is higher (2X) at an iris than an equator as well as a temperature gradient from one end to another end. The usual acid temperature during BCP is maintained at 10 - 15 ^{0}C to control the reaction rate and avoid the hydrogen absorption. The typical surface roughness after BCP is of the order of few micrometers (2-5 μm).

1.3.8.3. Electropolishing : These days EP is commonly used as a final surface treatment of SRF cavity as it gives much smother surface than BCP. The EP is an electrochemical process in which the typical mixture of hydrofluoric acid (HF, 40 wt%) and sulfuric acid (H_2SO_4, 96 wt%) in a volumetric ratio of 1 : 9 is used as an electrolyte. The cathode, made of aluminum is a long rod which is inserted from one end of the cavity and the Nb cavity itself works as an anode and a voltage is applied between these two electrodes. The anodization of Nb in H_2SO_4 results in the growth of Nb_2O_5 and F^- ions from HF dissolves Nb_2O_5 which gives a current flow through the electrolyte. The basic reactions can be written as following [1.15-1.18]:

Oxidation :

$$2\,Nb + 5\,SO_4^{2-} + 5\,H_2O \longrightarrow Nb_2O_5 + 10\,H^+ + 5\,SO_4^{2-} + 10\,e^- \quad (1.28)$$

Reduction (hydrogen formation at an aluminum cathode) :

$$2\,H^+ + 2\,e^- \longrightarrow H_2 \quad (1.29)$$

Oxido-reduction :

$$2\,Nb + 5\,H_2O \longrightarrow 5\,H_2 + Nb_2O_5 \quad (1.30)$$

The Nb_2O_5 is dissolved in HF and niobium fluoride, oxofluoride (from equation 1.23 to 1.27) are formed. The fluorosulfate or oxysulfate and pyrosulfuryfluoride are made with sulfuric acid as sulfuric acid is considered as hydrated sulfur trioxide (SO_3, H_2O).

$$NbF_5 + 2\ (SO_3, H_2O) \longrightarrow NbF_3(SO_3F)_2 + 2\ H_2O \qquad (1.31)$$

$$2\ NbF_5 + 14\ SO_3 \longrightarrow Nb_2O(SO_4)_4 + S_2O_5F_2 \qquad (1.32)$$

The typical I-V characteristic of an EP process is given by fig. 1.12. The region AB : concentration polarization occurs and Nb is diluted, BC : instability, CD : after formation of viscous layer on Nb surface current density is limited (this region is the best condition for EP) and DE : additional cathodic process such as oxygen generation occurs. The voltage limitation in a plateau region (CD) depends on the diffusion coefficient of the viscous layer.

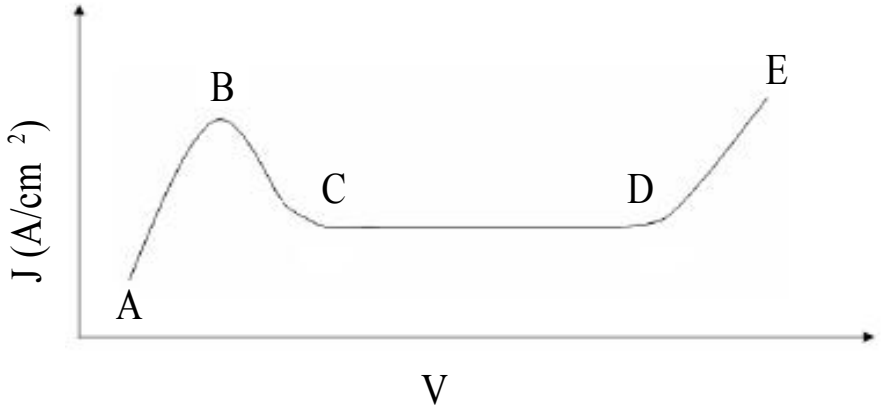

Fig. 1.13 : A Typical I-V characteristic curve for the EP [1.16].

The EP is an exothermic reaction and hence temperature is raised during EP which leads rise in current density. The Current density also depends on HF/H_2SO_4 ratio and decreases linearly with the lower ratio. Therefore, to achieve the best EP conditions we need to get a balance between all the EP parameters such as the electrolyte ratio, applied voltage to the anode, temperature etc. The current oscillations are also observed during the EP process because of dynamic balance between oxide formation and dissolution of Nb. The current oscillations are the indication of a good process i.e. the good balance of EP parameters. Typical etch rate by the EP process is maintained at 0.3 μm/min and surface roughness after the EP is of the order of 0.5 - 1 μm.

1.3.8.4. Rinsing : After the surface treatments of Nb cavities, some chemical residues such as sulfur, fluorine from the etching acids and dust particles are attached on the surface which are a hurdle in achievement of the high accelerating gradient (E_{acc}) and high Q_0 value of the SRF cavities. Therefore post-polishing processes of inner surface has a great role in achievement of good

performances of the SRF cavities. To remove these contaminants from the cavity inner surface, various rinsing processes such as ultra pure water rinse, ultrasonic pure water rinse, alcoholic rinse, detergent rinse, high pressure water rinse (HPR) with ultra pure water, dry ice cleaning have been used. After the rinsing cavities are assembled in clean room and moved to vertical test facility for vertical test [1.19-1.21].

1.4. Motivation and Aim

The performance of Nb SRF cavities is mainly limited by the following four factors :

1. Surface residual resistance.
2. Multipacting.
3. Field Emission.
4. Quench.

Among all the four limiting factors, the field emission depends on the contaminants present at the inner surface of the cavities. As it's described before, there are many steps involved in the fabrication of a cavity therefore the chances of inclusion of the contaminants are greatly enhanced. These contaminants are necessary to be removed in order to obtain good performances of the SRF cavities in terms of the achievement of high field gradient, hence the final surface treatment of SRF cavities is required. Although the good performances have been obtained lately by using EP followed by various post EP treatments, still much research and efforts are required to improve the processes to get consistently good results for the mass production. Some surface studies [1.21, 1.22] on Nb surface after the surface treatments have been done in the past, however surface study concerning contaminants present at the surface as a result of the surface processing have not been done so far. Therefore it is of interest to investigate the Nb surface and identify the chemical compositions present at the surface after the surface processing with different conditions.

In this thesis, the great efforts will be made to understand the behavior of surface treatments inside a real Nb cavity in order to obtain a very smooth and clean surface necessary for the mass production. The surface analytical tools such as x-ray photoelectron spectroscopy, secondary ion mass spectroscopy and scanning electron microscope etc. will be employed for the surface characterization after the surface treatments. The aim of our work is to find causes of low performances of Nb SRF cavities and optimum conditions for the surface processing to get an ultra smooth and clean surface. The use of optimum conditions will enhance the mass production with reduced cost.

1.5. References

[1.1] The International Linear Collider : Global design effort baseline configuration document.

[1.2] Barry Barish "Introduction to the ILC : Lecture I-1, I-2", linear collider school, Villars-sur-Ollon, Switzerland, 25 Oct.-5 Nov. 2010.

[1.3] David J. Griffiths, "Introduction to Electrodynamics", Addison Wesley.

[1.4] Hasan Padmsee et al. "Handbook of rf superconductivity for Accelerators" John Wiley & Sons.

[1.5] Jean Delayen "Lecture on fundamentals of superconductivity, surface resistance, rf and cavities, microphonics", linear collider school, Villars-sur-Ollon, Switzerland, 25 Oct.-5 Nov. 2010.

[1.6] Jean Delayen "Lecture on Cavity design", linear collider school, Villars-sur-Ollon, Switzerland, 25 Oct.-5 Nov. 2010.

[1.7] Jean Delayen "Lecture,4 on cavity fabrication", linear collider school, Villars-sur-Ollon, Switzerland, 25 Oct.-5 Nov. 2010.

[1.8] Hiroaki Umezawa " Impurities analysis of high purity niobium in industrial production" Matériaux et techniques, 91(2003), 33.

[1.9] Jean Delayen "Lecture on surface preparation", linear collider school, Villars-sur-Ollon, Switzerland, 25 Oct.-5 Nov. 2010.

[1.10] G. Issarovitch et al "Development of centrifugal barrel polishing for treatment of superconducting cavities", Pproc. of SRF 2003, travemünde/lübeck, germany.

[1.11] CA Cooper and LD Cooley "Mirror smooth superconducting RF cavities by mechanical polishing with minimal acid use" FERMILAB-PUB-11-032-TD**.**

[1.12] P. A. Jacquet "electrolytic method for obtaining bright copper surfaces", Nature(London), 135, 1076 (1935).

[1.13] C. Boffo et. al. "Optimization of the BCP Processing of Elliptical Nb SRF Cavities", Proc. of the COMSOL Users Conference, 2006, Italy.

[1.14] A. Aspart and C.Z. Antoine "Study of the chemical behavior of hydrofluroic, nitric and sulfuric acids mixtures applied to niobium polishing", Applied surface science, 227(2004), 17.

[1.15] Srinivas Bhashyam "Comparison of electropolishing and buffered chemical polishing – a literature review" td-03-046 report for fermi lab.

[1.16] F. Eozenou et. al., “Electropolishing of niobium: best EP parameters”, WP 5.1.1.4, Care report-06-010-SRF.

[1.17] K. Saito, “Development of electropolishing technology for superconducting cavities”, Proc. of PAC 2003, Portland, U.S.A.

[1.18] A. Aspert et. al., “Aluminum and sulfur impurities in electropolishing baths”, Physica C, 441(2006), 249.

[1.19] D. Sertore et. al., “Study of the high pressure rinsing water jet interactions", Proc. of EPAC08, Genoa, Italy

[1.20] TESLA Technology Collaboration, “Final surface preparation for superconducting cavities”, TTC-Report 2008-05.

[1.21] E. Cavaliere et. al., “High Pressure Rinsing Parameters Measurements”, Physica C 441 (2006), 254.

[1.22] Hui Tian et. al., “Surface studies of niobium chemically polished under conditions for superconducting radio frequency (SRF) cavity production”, applied surface science 253 (2006), 1236.

Chapter 2 Experimental Setups

2.1. Surface Analysis System

To characterize the surface condition and elemental composition present after the surface treatments, a surface analysis system (fig. 2.1) was used [2.1]. The surface analysis system is consist of a main chamber, the three loadlock systems and a sample storage chamber. The system is maintained at extremely high vacuum (XHV).

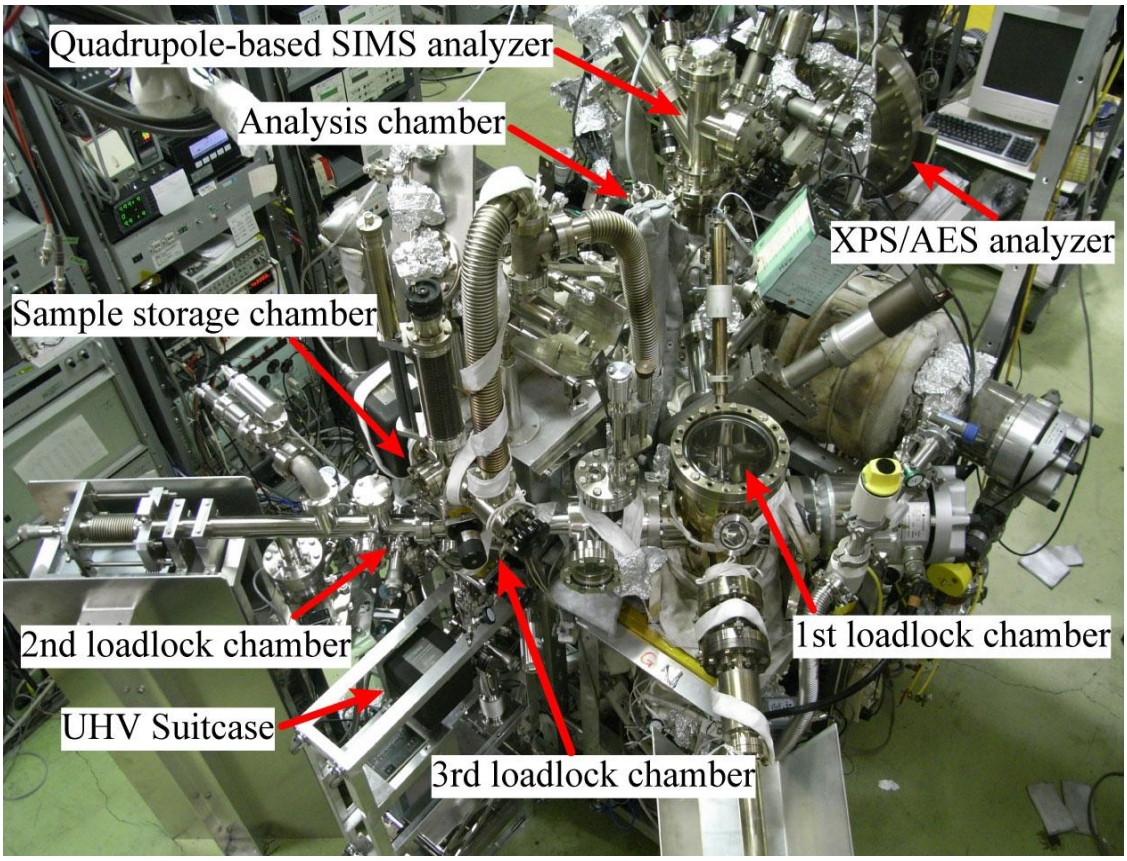

Fig. 2.1 : Surface analysis system connected with an UHV suitcase via three loadlock chambers. It's base pressure is maintained of the order of 10^{-9} Pa.

2.1.1. Main Chamber for Surface Analysis : The main chamber consists of an electron energy analyzer, an ion mass spectrometer, a x-ray source, an electron gun, an ion gun for depth profiling, an extractor gauge, a sample manipulator and a residual gas analyzer. The analysis system (fig 2.1) is capable of executing Auger electron spectroscopy (AES), secondary ion mass spectrometry (SIMS) with argon ion etching and XPS with probing area of 2 mm. Table 2.1 summarizes the details about analysis techniques.

Technique	End-use	Pros.	Cons.
X-ray photoelectron spectroscopy (XPS)	Analysis of the binding energy of emitted photo electrons by the irradiation of Al/Mg x-rays on samples	. Quantification is relatively easy . It doesn't damage the sample's surface after the analysis . It gives the information about the chemical state of elements present at the surface	. lateral resolution is not that good except micro-XPS
Secondary ion mass spectrometry (SIMS)	Investigation of the mass of secondary ions generated by the argon ion sputtering on samples	. Sensitivity is very high	. Sputtering is necessary therefore surface is damaged specially in case of the dynamics SIMS analysis . Quantification is difficult due to the sensitive ion probabilities to many sample properties
Auger electron spectroscopy (AES)	Analysis of the kinetic energy of emitted auger electrons by the irradiation of e-beam on samples	. Lateral resolution is good . Sensitivity is high	. Signal to noise ratio is sometimes very weak . Long time exposure to e-beam and high e-current damages the sample's surface

Table 2.1 : Brief description of the analysis techniques installed in the main chamber.

2.1.1.1 X-ray Photoelectron Spectroscopy : The X-ray photoelectron spectroscopy (XPS) is a quantitative spectroscopic technique which measures the elemental composition, empirical formula, chemical state and electronic state of the elements present at top surface

of a material [2.2-2.4]. When a sample surface is irradiated by the soft X-rays photons (1-2 keV), the X-ray excitation of inner shell electrons of the target atoms induces direct emission of photoelectrons. These photoelectrons are then collected and passed through an electron analyzer to a detector where the kinetic energy of these photoelectrons is measured. The kinetic energy of these photoelectrons is the characteristic of an element and hence provides the valuable information about the chemical composition present at top 1-10 nm of the material. The peak position and the peak area in a XPS spectrum are used to identify and evaluate the total relative atomic composition present on the surface. The peak shape gives unique information about the chemical shifts or chemical bonds of the elements.

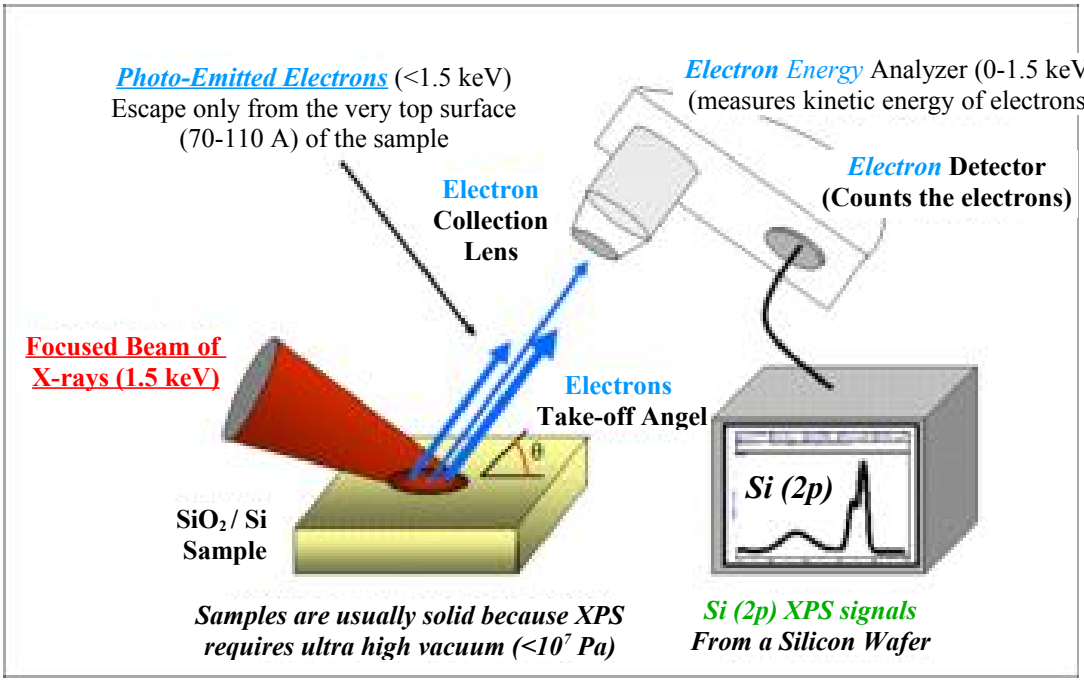

Fig. 2.2 : The schematic view of a XPS system.

A typical XPS spectrum is the plot of binding energy of photoelectrons versus electrons count/number of electrons and the electron binding energy of each of the emitted electrons can be determined by using an equation that is based on the work of Ernest Rutherford (1914):

$$E(binding) = E(photon) - (E(kinetic) + \Phi) \qquad (2.1)$$

where $E_{binding}$ is the binding energy (BE) of the electron, E_{photon} is the energy of X-ray photons being used, $E_{kinetic}$ is the kinetic energy of the electron as measured by the instrument and Φ is the work function of the spectrometer used (not of the material).

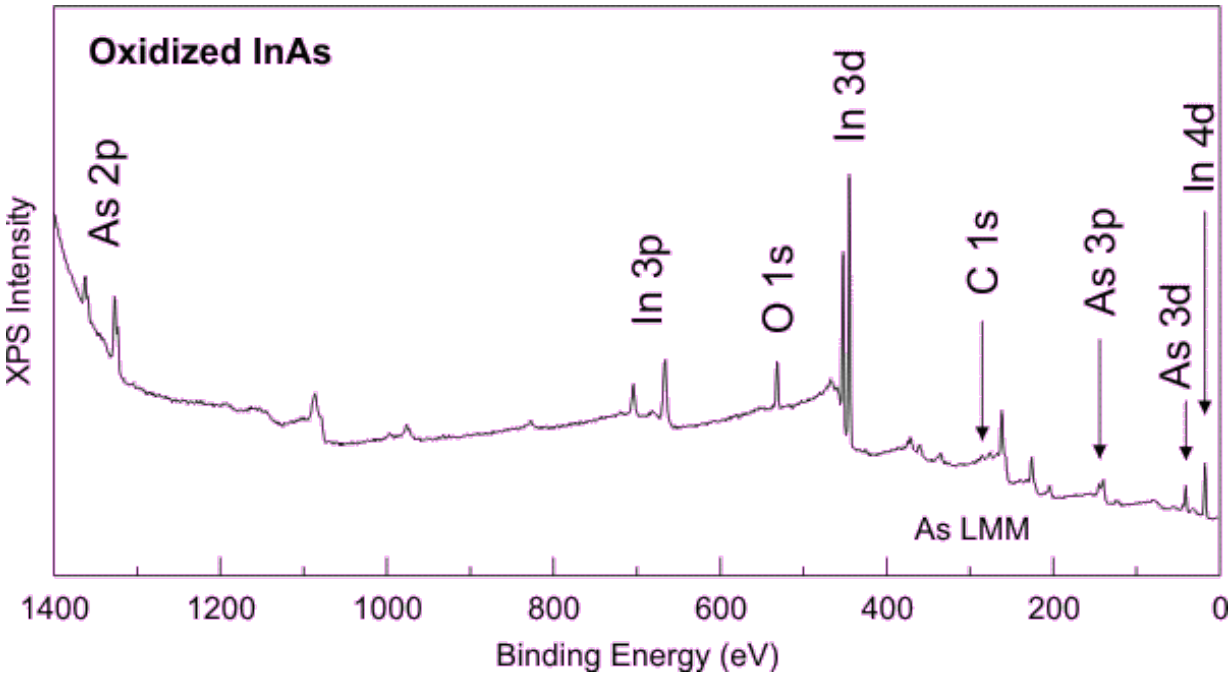

Fig. 2.3 : A typical XPS survey spectrum.

2.1.1.1.1. Components of a XPS System : The main components of a XPS system include :

1. A source of X-rays (usually Al or Mg).
2. An ultra-high vacuum (UHV) stainless steel chamber with UHV pumps.
3. An electron collection lens.
4. An electron energy analyzer.
5. An electron detector system.
6. A complementary sample introduction vacuum chamber (loadlock system).
7. A sample stage.
8. A set of stage manipulators.

2.1.1.2. Secondary Ion Mass Spectrometry : Secondary ion mass spectrometry (SIMS) is a surface analytical technique used in materials science and surface science to analyze the elemental composition of solid surfaces and thin films based on their atomic mass. The SIMS uses sputtering of the sample surface to get their atomic composition [2.2-2.4]. The sample surface is sputtered by a focused primary ion beam and secondary ions are ejected from the surface as a result of sputtering. These secondary ions are collected and analyzed by a mass spectrometer which measures the mass to charge ratio of each ion and determines the elemental, isotopic, or molecular composition of the surface.

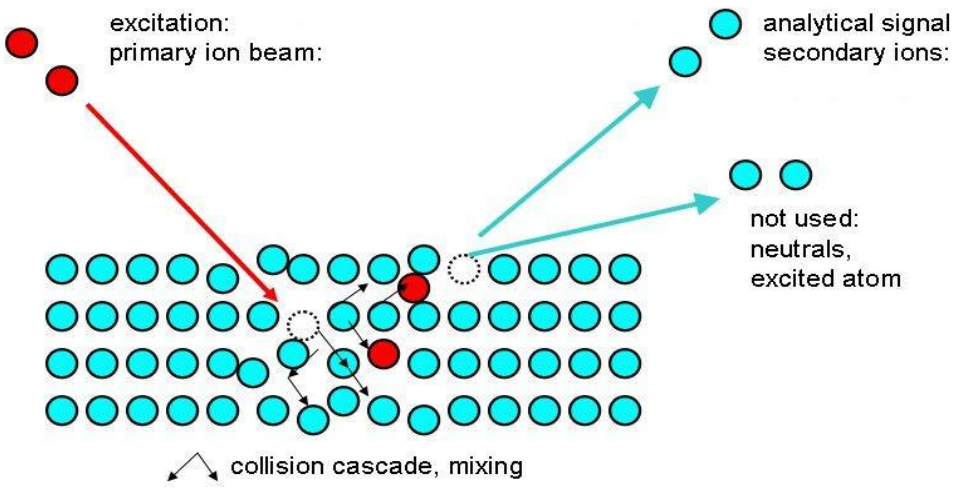

Fig. 2.4 : The schematic view of SIMS principle.

The SIMS sensitivity is very high and able to detect elements present in the parts per billion ranges. A typical SIMS spectrum which is the plot of secondary the ions intensity versus ion mass number consists of two mass spectra of positive ions and negative ions.

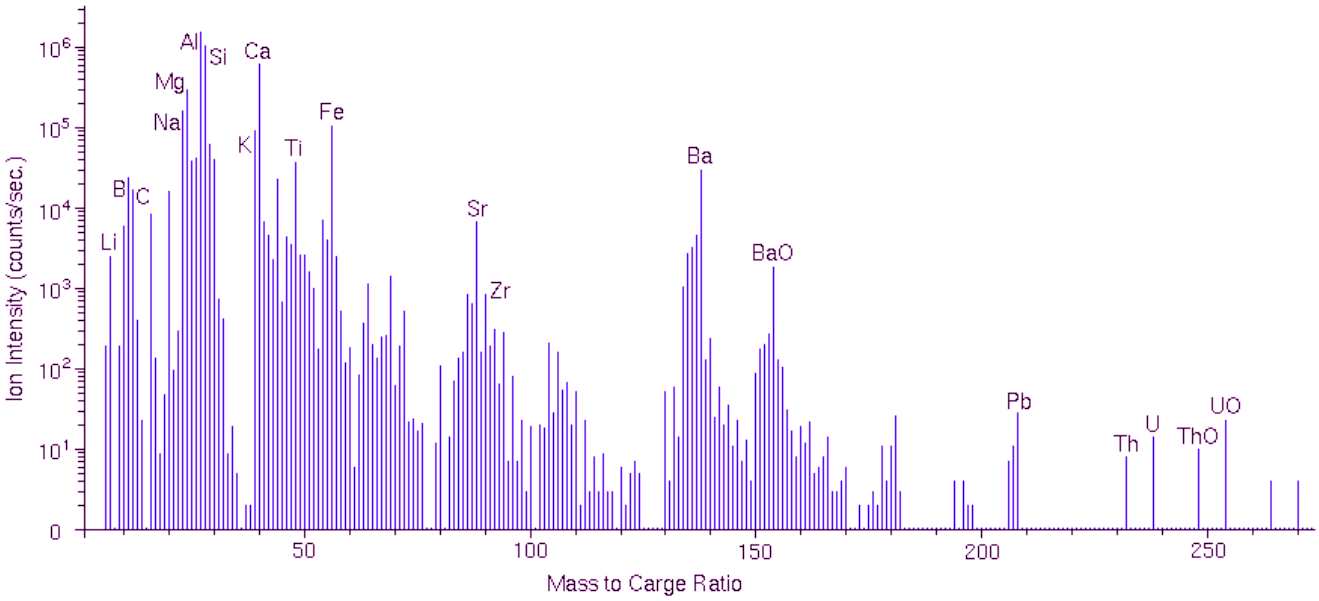

Fig. 2.5 : The typical SIMS mass spectrum.

2.1.1.2.1 Components of a SIMS Instrument : Following are the main components of a SIMS instrument :

1. Primary ion gun (generating the primary ion beam).
2. Primary ion column, for accelerating and focusing the beam onto the sample.

3. A stainless steel ultra high vacuum chamber with UHV pumps.

4. A complementary attached vacuum chamber for sample introduction (loadlock system).

5. A sample stage with manipulators.

6. A secondary ion extraction lens followed by mass analyzer separating the ions according to their mass to charge ratio.

7. An Ion detection unit.

2.1.1.3. Auger Electron Spectroscopy : The Auger electron spectroscopy (AES) utilizes the emission of low energy electrons in the Auger process for determining the composition of the surface layers of a sample [2.2-2.4]. The Auger effect is an electronic process resulting from the inter- and intrastate transitions of electrons in an excited atom. When an atom is bombarded by a photon beam or a beam of electrons with the energies in the range of 2 keV to 50 keV, a core state electron can be removed and a hole is created. As this is an unstable state, the core hole can be filled by an outer shell electron, in which the electron moving to the lower energy level loses an amount of energy equal to the difference in orbital energies. This transition energy can be coupled to a second outer shell electron resulting the emission of secondary electron (Auger electron) from the atom if the transferred energy is greater than the orbital binding energy. The kinetic energy of the emitted electron can be given by :

$$E(kinetic) = E(corestate) - E(binding) - E(C) \qquad (1.34)$$

where $\boldsymbol{E}_{CoreState}$, $\boldsymbol{E}_{binding}$ and E_C are respectively the core level, first outer shell and second outer shell electron energies, measured from the vacuum level. Figure 2.6 illustrates two schematic views of the Auger process.

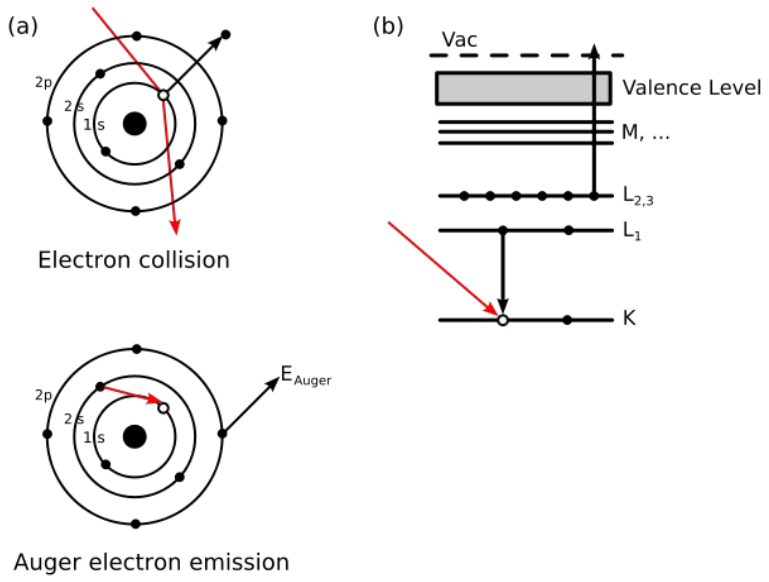

Fig. 2.6 (a), (b) : Schematic views of the Auger process.

A typical AES spectrum (fig 2.7) is the plot of kinetic energy of auger electrons versus electron count/number of electron. The peak intensity gives the quantification information of element present on the surface.

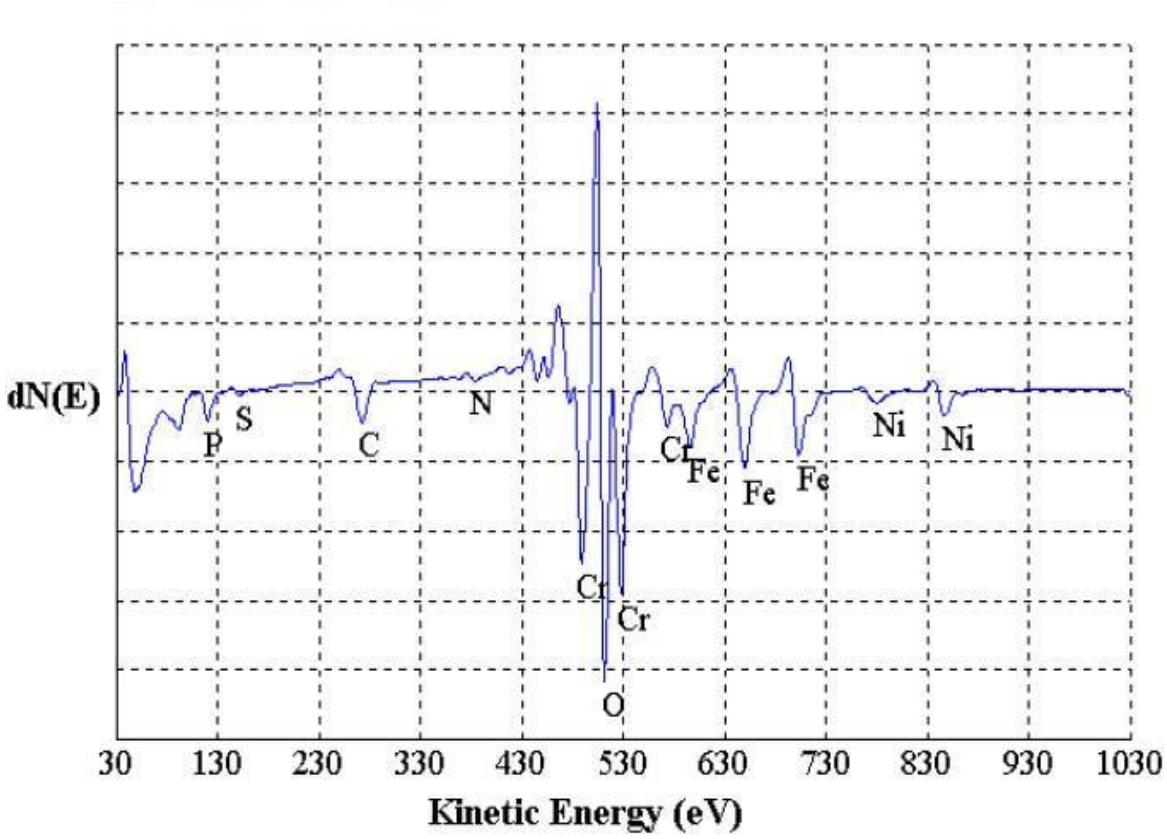

Fig. 2.7 : A typical AES survey spectrum.

2.1.1.3.1: Components of an AES Instrument : An AES system requires the following components :

1. A Primary electron gun.
2. An ultra-high vacuum (UHV) stainless steel chamber with UHV pumps.
3. An electron collection lens.
4. An electron energy analyzer.
5. An electron detector system.
6. A complementary vacuum chamber for sample transfer (loadlock system).
7. Sample mounts and a sample stage.
8. A set of stage manipulators.

2.1.2. Vacuum System for Surface Analysis System :

In order to achieve XHV in the main chamber, a titanium sublimation pump (TSP) and two turbo molecular pumps (TMPs) in sequence are used. Each loadlock chamber contains one TMP and the sample storage chamber is equipped with one ion pump. Figure 2.8 shows the schematic of vacuum system of the analysis system.

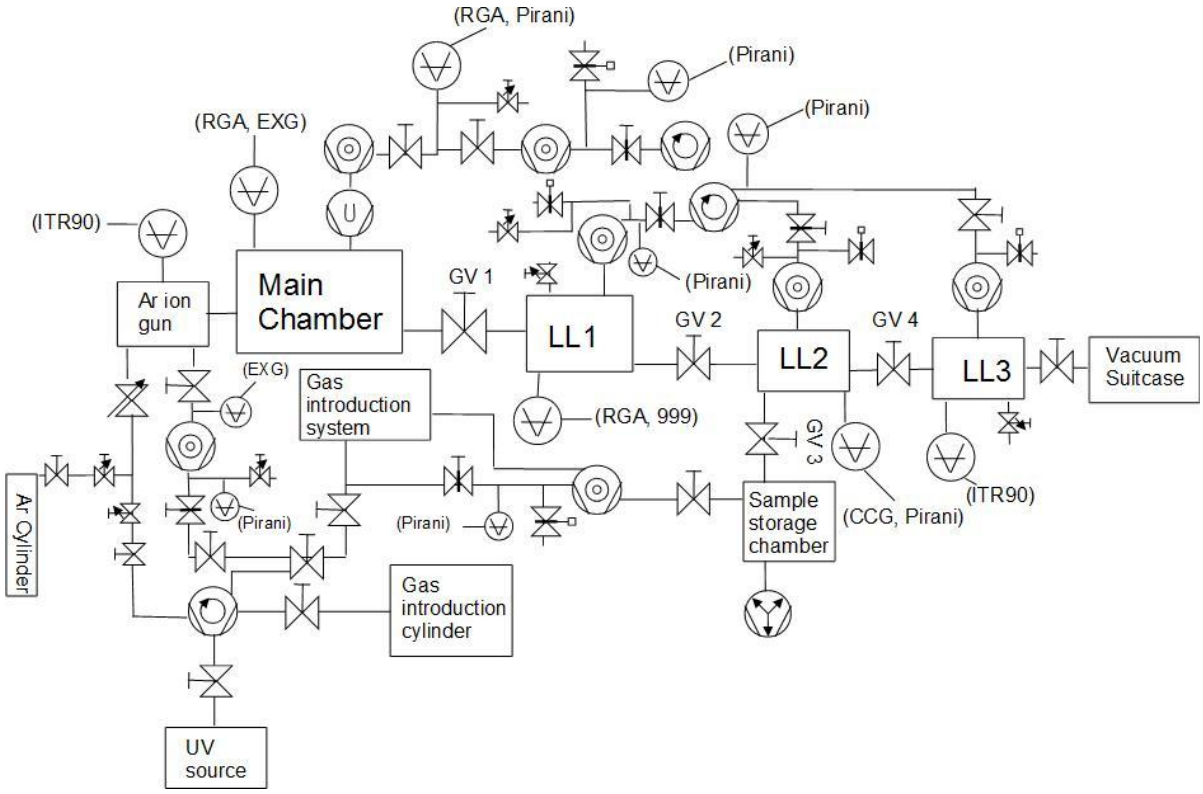

Fig. 2.8 : Vacuum system for analysis system. (RGA : residual gas analyzer, EXG : extractor gauge, ITR 90 and 999 : combination gauges, CCG : cold cathode gauge, GV : gate valve, UV source : ultraviolet source).

2.1.3. Three Loadlock Systems : The analysis chamber can be connected to an UHV suitcase (section 2.2) via three loadlock chambers. The sample can be transferred from suitcase to the analysis chamber with the help of these three loadlock systems without exposing them in to the air. The mechanism of transferring the sample from suitcase to the main chamber through the loadlock systems is follows :

1. At first, the suitcase is connected to loadlock 3 (LL3) chamber and waiting until UHV is achieved.

2. After achievement of UHV in LL 3, the gate valve of suitcase and gate valve 4 are opened and the sample is transferred to the head of loadlock 2 (LL2) motion drive with help of a linear motion drive of the suitcase.

3. If there are multiple numbers of samples kept in a carousel kept in to the suitcase then carousel is transferred to the sample storage chamber (section 2.1.4) to keep samples in UHV.

4. To transfer the carousel to the sample storage chamber, gate valve 3, gate valve 4 and a gate valve of the suitcase are opened. By opening the gate valves 3 and 4 and to the suitcase; the LL 2, the sample storage chamber, the LL 3 and the suitcase are connected and the carousel is transferred from the linear motion drive of suitcase to linear motion drive of the sample storage chamber via LL 2.

5. Samples can be transferred to a head of the LL 2 motion drive from the sample storage chamber one by one with the help of a linear motion drive of the sample storage chamber and by opening the gate valve 3.

6. After receiving the sample at the head of LL 2 motion drive, the gate valves 3 and 4 are closed and gate valve 2 is opened and sample is transferred to LL 1.

7. When sample is transferred to LL 1, the gate valve 1 is opened and sample is transferred to the main chamber for surface analysis.

8. In a case, when we don't need to connect the suitcase, expose the LL 1 chamber to nitrogen and mount the sample directly to LL 1 rack. After achievement of UHV, sample is transferred to the main chamber.

2.1.4. Sample Storage Chamber : A sample storage chamber, which maintains the base pressure of 10^{-8} Pa, is connected to the LL 2 chamber. The chamber is mainly used to keep remaining samples in carousel in UHV while the analysis for one sample is going on. The sample storage chamber contains a linear motion drive to move the sample carousel to LL 2 chamber and sample is transferred to the head of LL2 drive.

2.2. Vacuum Suitcases and Multiuse UHV System

After the surface treatments, the samples were carried from the clean room to a surface analysis system by using a vacuum suitcase to prevent dust particles and contaminants from atmosphere. The vacuum suitcases (fig 2.9 (a)) are maintained at the base pressure of the order of 10^{-6}~10^{-7} Pa. The suitcases consist of a rack and pinion system with a rotary drive to transfer the carousel with coupons, a gate valve, an ion pump and a battery driven power supply for ion pump.

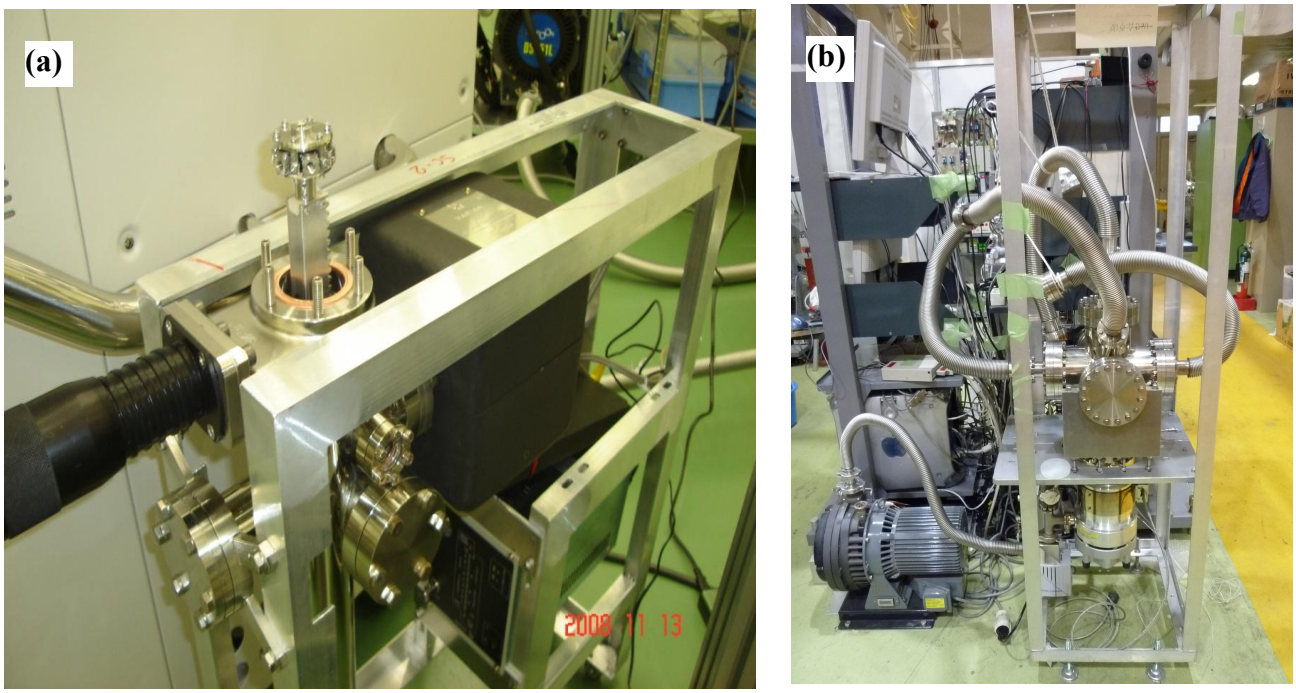

Fig. 2.9 : (a) An UHV suitcase with carousel, (b) Multiuse UHV system.

A multiuse UHV system (MUS, fig 2.9 (b)) is used for pumping down the suitcases which consists of a turbo-molecular pump followed by a scroll pump and one MKS 999 gauge to measure pressure from atmospheric to XHV. There are totally 4 ports in MUS to connect the suitcases and can be pumped down from atmospheric pressure to UHV simultaneously. After reaching to UHV, the ion pump of the suitcase is started and gate valve to the MUS is closed.

2.3. Scanning Electron Microscope

The scanning electron microscope (SEM) of JSM 6500F was used to observe the surfaces after the surface treatment. It has magnification ranges from X25~X500,000. Figure 2.10 shows the picture of SEM. The SEM is also equipped with an energy dispersive X-ray spectroscopy detector, which can be used for an elemental analysis of the surfaces. A field emission scanner (FES) is also installed in SEM main chamber. The purpose of FES is to find the location of a field emitter present on the sample surface.

Fig. 2.10 : The picture of the JSM 6500F scanning electron microscope.

The pressure in the sample stage chamber is maintained of the order of 10^{-5} Pa with the help of TMP. The pressure at electron gun chamber is maintained at 10^{-7} Pa with the help of ion pumps used in a differential pumping system.

The procedures to operate the SEM system can be described as follows :

1. Fix the sample on a sample holder by using a carbon tape and install the holder into the specimen exchange chamber of SEM.
2. Evacuate the specimen exchange chamber of SEM and wait for about 20 minutes until the pressure in this chamber reaches to a high vacuum.

3. After achieving a high vacuum, sample holder is transferred to main chamber with the help of a loadlock system attached with specimen exchange chamber.

4. Check the state of electron gun. If normal, open the electron gun valve and select an appropriate accelerating voltage and an ideal focusing position.

5. Start the observations.

6. If the use of EDX is necessary, EDX should be previously cooled by liquid N_2 for 1 hour at least. During the observations with SEM, EDX can be used synchronously. However, the magnification of SEM, at which EDX can work normally, is < X 3,000.

7. After the observations, at first, reduce the accelerating voltage of the electron gun to ~1 kV and adjust the focus position to more than 10 mm and then, close the gun valve.

8. Adjust the position of the carrier for the sample holder to the right place.

If it is needed to exchange the sample, firstly transfer the sample holder to specimen exchange chamber and vent the chamber by pushing the "VENT" button. The N_2 gas will flow in to the specimen exchange chamber until atmospheric pressure is achieved.

Afterwards open the chamber and exchange the samples.

2.4. Electropolishing System

The electropolishing (EP) is used as a surface treatment for the SRF cavities to remove the damaged layer making the surface smoother. In this study, two kinds of EP systems were used for the experiments. One is a laboratory EP system which is used for EP of the Nb plate attached with the Nb samples ($20\times14\times2.8$ mm^3) at laboratory scale and another is cavity EP system, which is used for EP of a real Nb SRF cavity for ILC.

2.4.1. Laboratory Electropolishing System : The Laboratory EP system is situated at chemical laboratory, KEK. The system contains one movable shaft and a vessel made of PTFE containing EP acid. A Nb plate (with samples) can be attached with the movable shaft and dipped in the EP acid during the EP. The Nb plate works as an anode and two Al plates (dipped in the EP acid) are used as cathodes. The EP process is fully computer controlled.

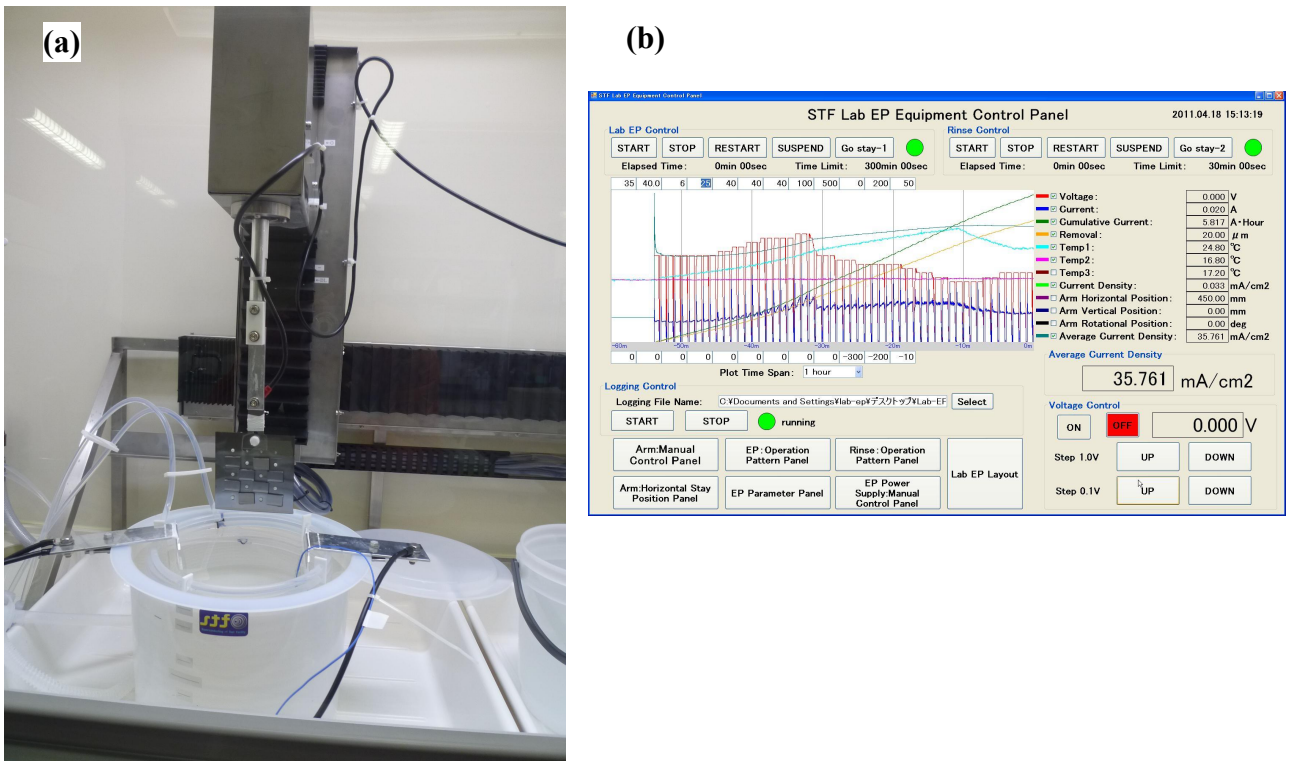

Fig. 2.11 : (a) The laboratory EP system. The Nb plate with samples (anode) is attached with movable shaft and two Al plates (cathodes) are dipped in the EP acid. (b) Control software of the laboratory EP process.

2.4.2. Cavity Electropolishing System : The cavity EP system at STF, KEK contains a horizontal EP bed as shown in figure 2.6. Both ends of a cavity are fixed at the end parts of EP beds. These end parts of bed are containing gears and cavity can be rotated during the EP process.

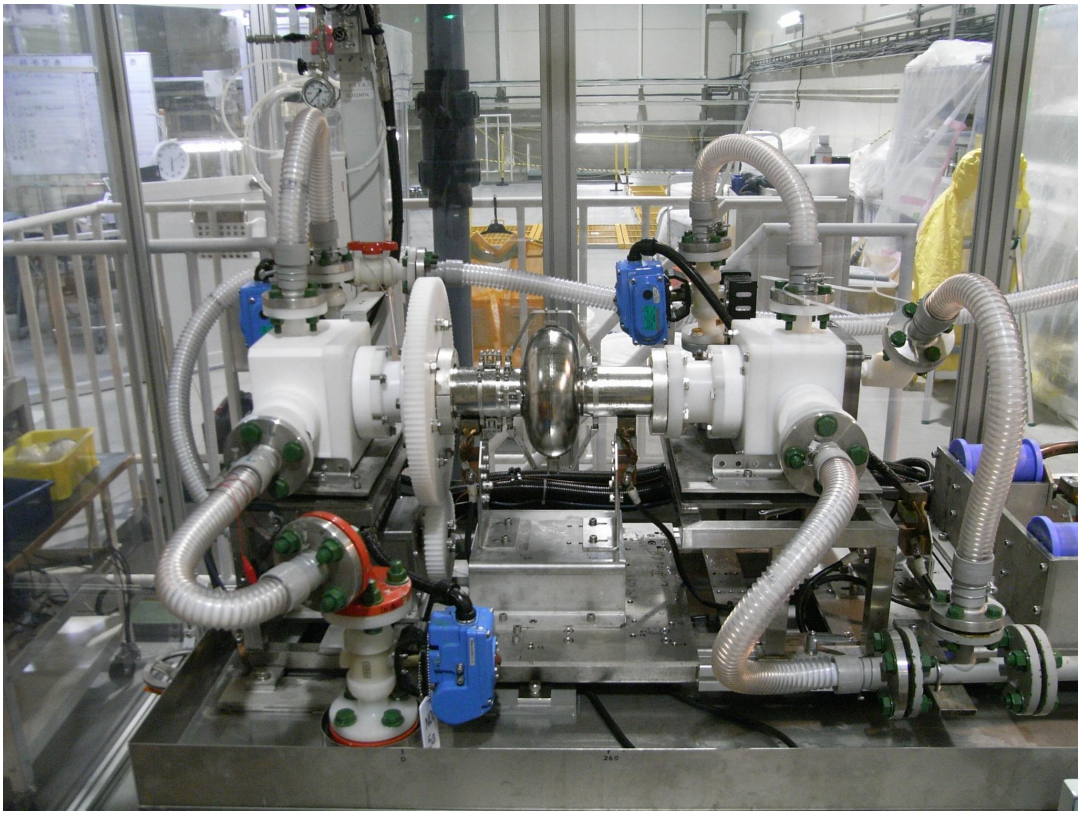

Fig. 2.12 : The EP bed with a single cell cavity (the acid is circulated through the left to right side).

The EP bed is connected to an EP acid tank of the capacity of 1000 liter and the EP acid is circulated through the cavity during EP. The EP bed is also connected to an ultra pure water (UPW) tank for rinsing of the cavity after the EP process and a nitrogen gas cylinder for leak check. All the piping and connections are made of PTFE material and air tight as PTFE is resistant to EP acid solution. The EP bed is flexible to move vertically to drain the EP acid and rinsed water after the process. All the process including movement of EP bed is computer controlled.

2.5. Clean Room

The preparation for an electropolishing (EP) experiment such as sample mounting to the cavity and removal of the samples after the EP was done in the clean room in order to avoid the contaminations from the atmosphere at sample surface. There are two clean rooms at the superconducting rf test facility (STF), which are categorized as class 1000 clean room and class 10 clean room (which is situated inside the class 1000 clean room). The class 1000 clean room is equipped with pure water and ultra pure water taps. Both the clean rooms have facility to use nitrogen, argon and compressed air inside the rooms. A clean bench was also used to carry out the dry ice cleaning experiment as well as sample handling after the experiments. A clean booth was used to cover the chamber during the transformation of the samples.

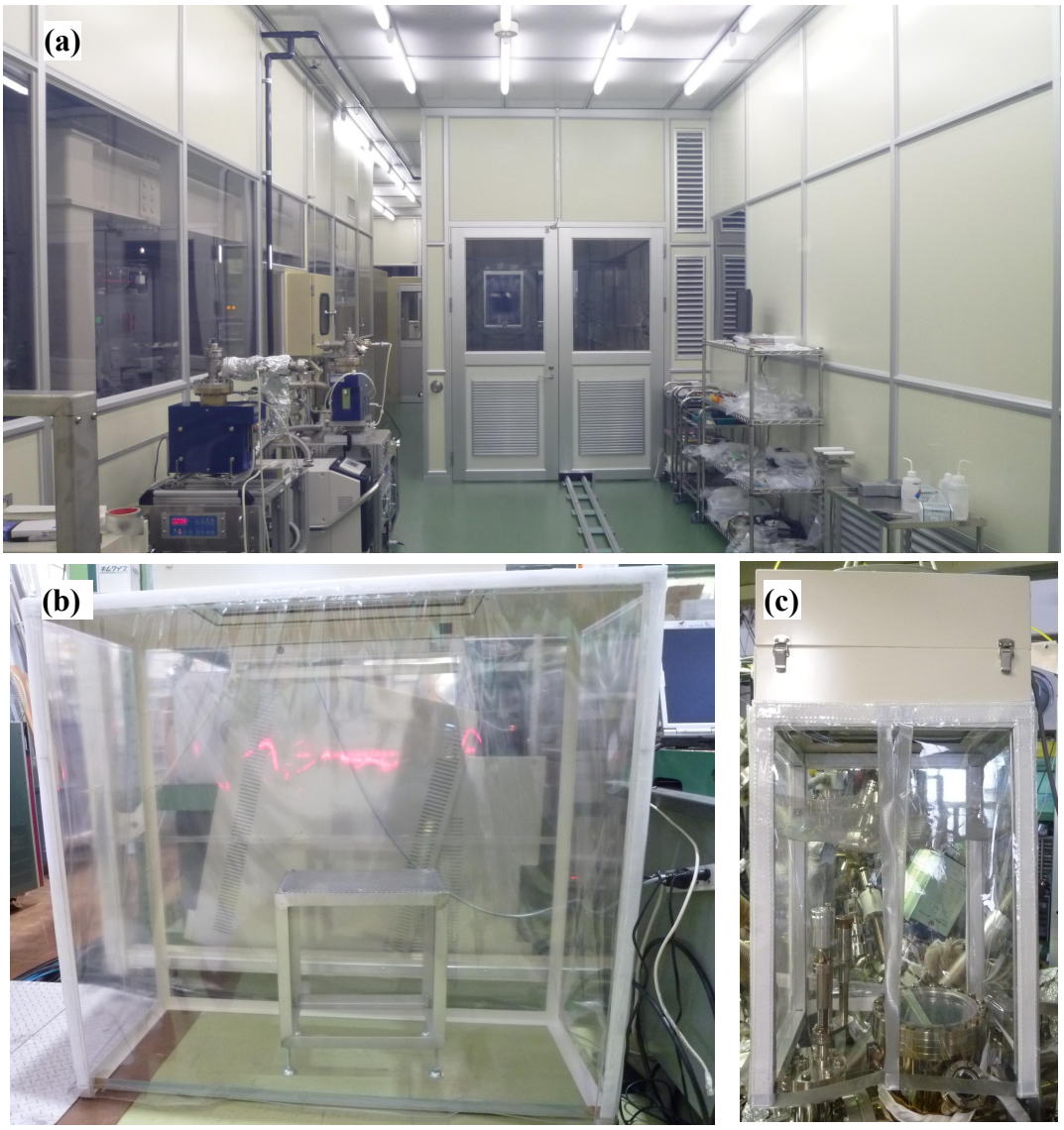

Fig. 2.13 : (a) The class 10 clean room, (b) A clean booth and (c) A clean bench.

2.6. High Pressure Rinsing System

In order to remove the contaminants from the EPed surface, all the cavities are subjected to high pressure rinsing (HPR) by UPW. To perform the HPR experiment two kinds of systems were used: laboratory HPR system and cavity HPR system.

2.6.1. Laboratory High Pressure Rinsing System : For the HPR experiment with different pressures at laboratory scale, a commercial Kranzle high pressure washer machine (fig 2.15) was used. The HPR machine is capable to use at any pressure in between 0 to 15 MPa. The HPR machine contains a lance, a gun and a pump. The nozzle of the lance was made of ceramic with the diameter of 1 mm. The HPR machine can be connected directly to UPW tap in STF. This equipment is handled manually.

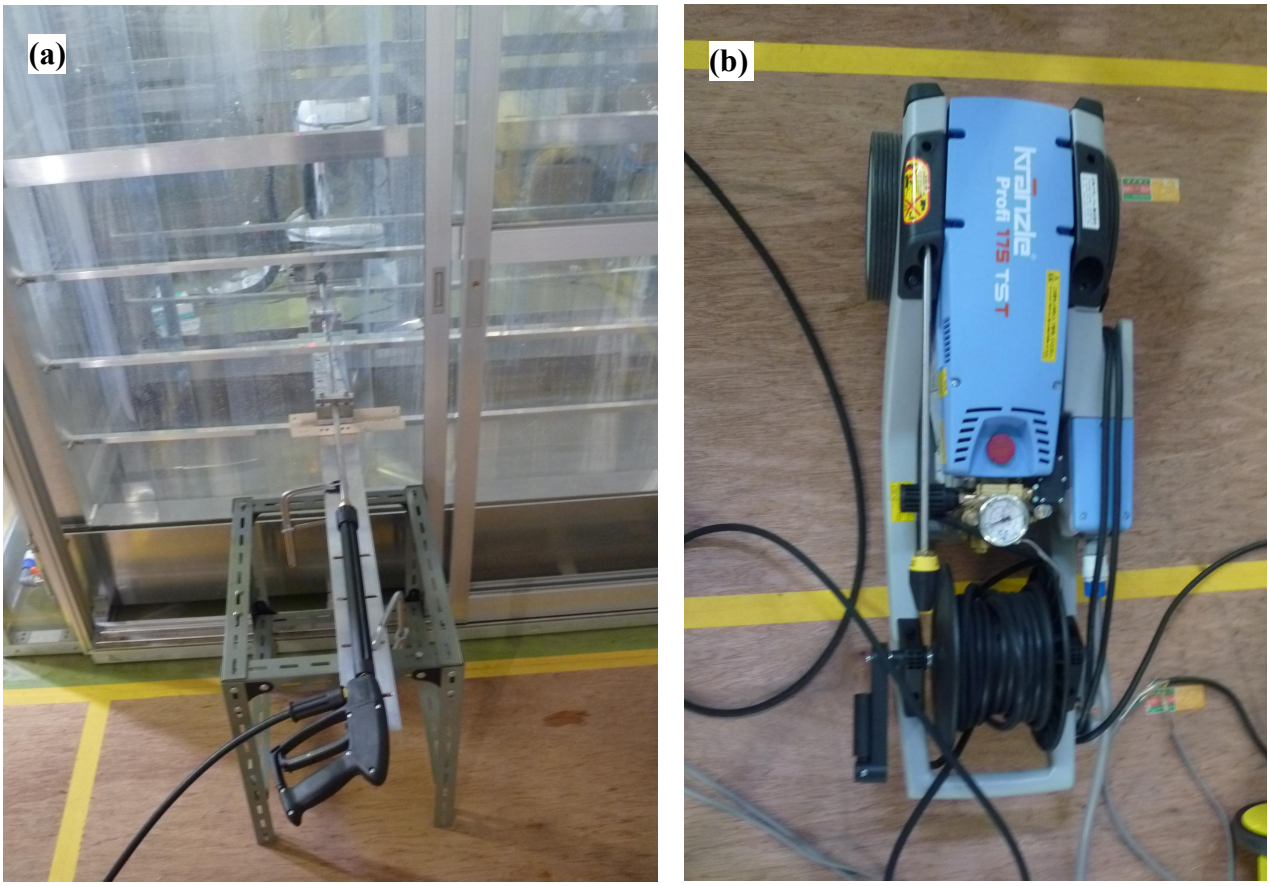

Fig. 2.14 : The laboratory high pressure system. (a) The lance with the water gun and (b) The Kranzle high pressure washer machine.

2.6.2. Cavity High Pressure Rinsing System : The cavity HPR system (fig 2.16) is situated in the clean room at STF, KEK. All the cavities are moved for HPR after their surface

treatments. The cavity HPR system contains a vertical wand made of stain-less-steel. The wand contains 8 nozzles of the diameter of 0.6 mm. The cavity is rotated around wand and can be moved linearly up and down during HPR. Usual operating high pressure is of the order of 8 MPa.

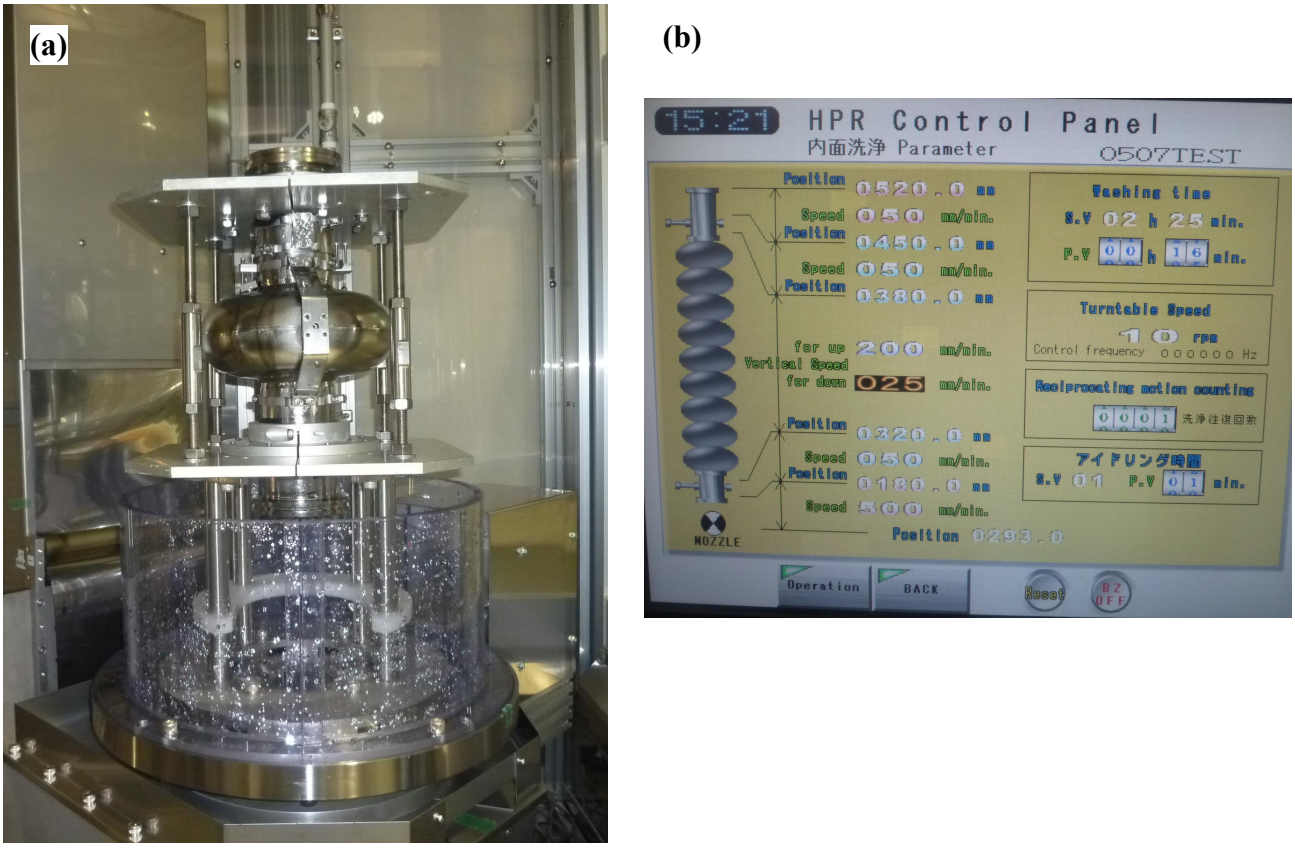

Fig 2.15 : (a) The Cavity High Pressure system. (b) HPR control system.

2.7. Dry Ice Cleaning System

The dry ice cleaning [2.5, 2.6] can be another candidate to clean the Nb surfaces after their surface treatments. The dry ice cleaning system contains one CO_2 cylinder and a gun with a nozzle of the diameter of 1 mm to spray the dry ice particles. This gun contains one expander and the dry ice particles are generated by expanding CO_2 gas. The gun can be connected to a CO_2 cylinder through a stain-less-steel flexible hose.

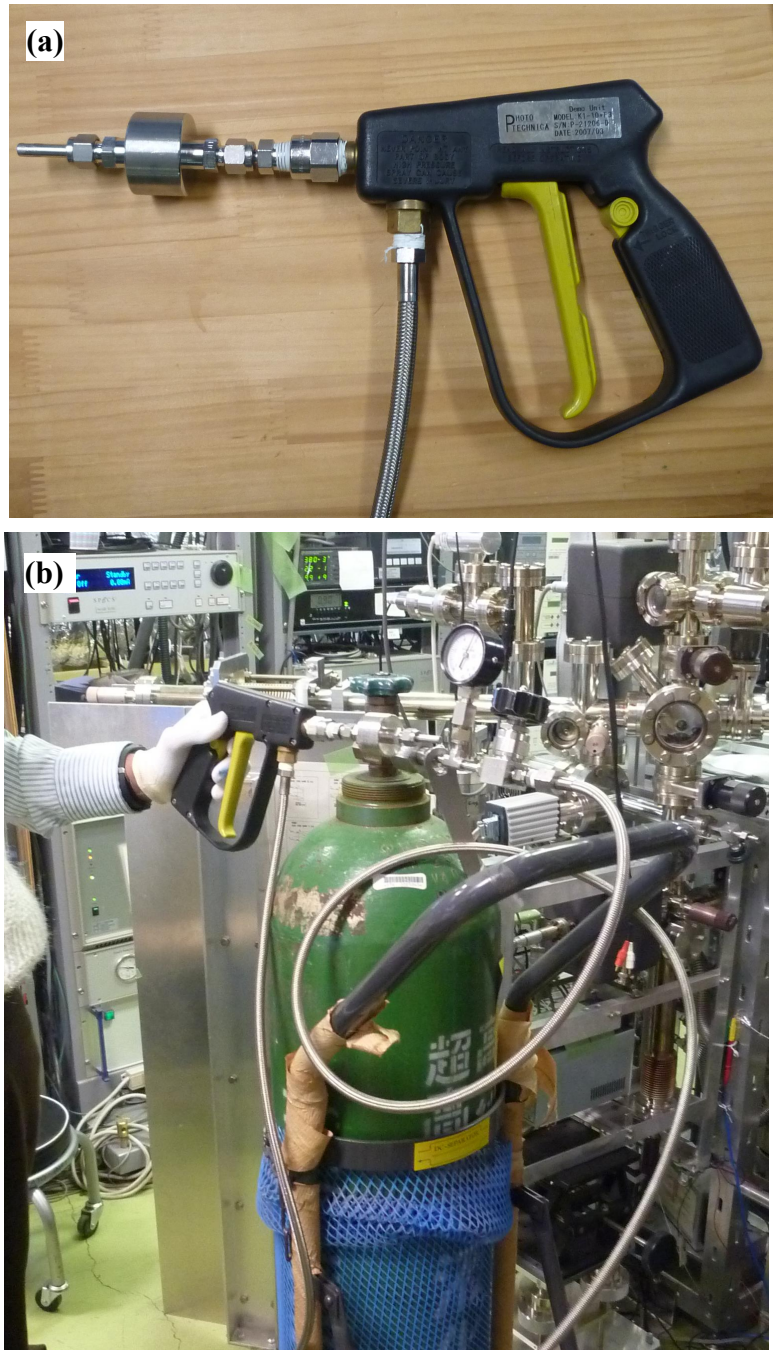

Fig. 2.16 : (a) The DIC gun. (b) The CO_2 cylinder connected with DIC gun.

2.8. References

[2.1] Michiru Nishiwaki "PhD Thesis", 2006, KEK, Japan.

[2.2] D. Briggs and M.P. Seah "Practical surface analysis by auger and x-ray photoelectron spectroscopy " John Wiley & Sons.

[2.3] Frank de Groot "Core level spectroscopy of solids", CRC Press, Tayler & Francis group.

[2.4] www. wikipedia.org.

[2.5] D. Reschke et. al., "First experience with dry-ice cleaning on srf cavities" Proceedings of linac 2004, lübeck, Germany.

[2.6] D. Proch, et. al., “Dry-ice cleaning for SRF applications”, Proceedings of 10th workshop on RF Superconductivity, Tsukuba, Japan,

Chapter 3 Experimental Procedures

3.1. Electropolishing Experiments

3.1.1. Laboratory Electropolishing : The Nb samples can be electropolished by utilizing a laboratory EP system. The rectangular type samples (20×14×2.8 mm^3) made from a high purity Nb sheet were used for the laboratory EP. These samples are first fixed on a Nb base plate (100×100×2.8 mm^3) then this plate is moved to the laboratory EP set up and hanged on a Nb shaft. The base plate contains 20 holes of the diameter of 2 mm in order to fix the samples and two holes of 5 mm diameter to fix the plate at a Nb shaft. All the samples have a tap hole of same size as the base plate's holes (2 mm of diameter). A number of samples (maximum up to 20) can be mounted at the Nb base plate with the help of PTFE screws and EPed at the same time. In order to start the EP process, the Nb plate is immersed into the EP acid and a voltage is applied between electrodes (Nb plate is made an anode and Al plate is made a cathode). The Nb plate along with samples is twisted with a maximum angle of 180^0 and a speed of around 5 rpm during the EP to agitate the EP process. The time taken by the EP process depends on the removal rate of Nb as well as the required removal thickness. After finishing the EP process, the plate is moved into the UPW beaker and rinsing with UPW is performed.

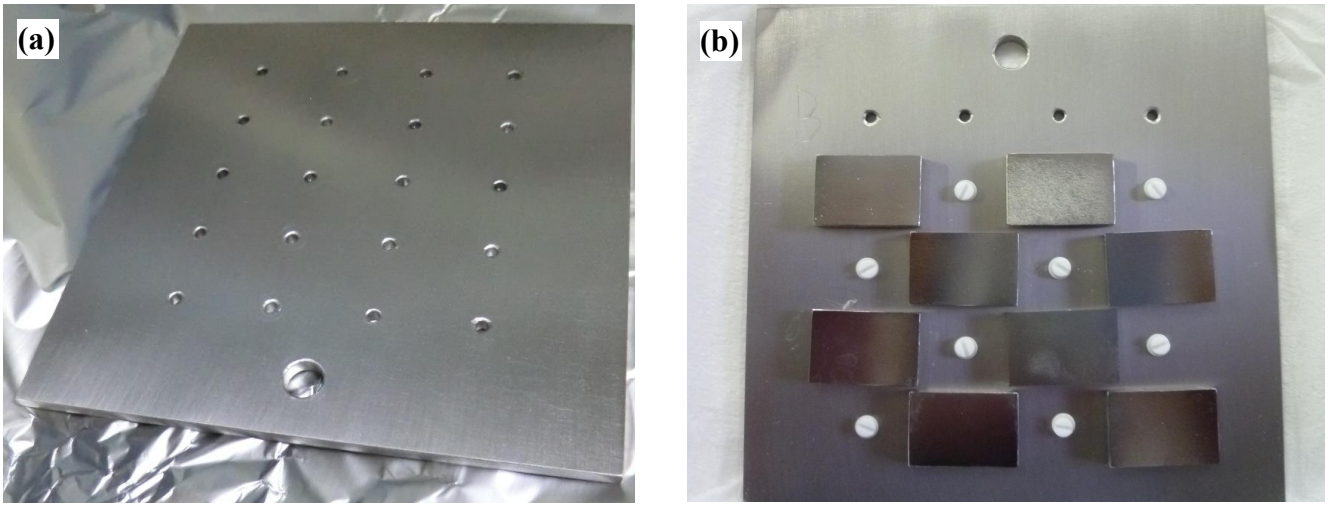

Fig 3.1 (a) Nb base plate and (b) Nb samples mounted on the base plate.

After the rinsing of Nb plate, all the samples are detached from the base plate and kept into the small boxes in UPW. The boxes are then brought to the surface analysis laboratory and kept into the clean booth. The Nb samples are exposed to atmosphere in the clean booth in order to perform the cleaning experiments. All the samples are then moved into the vacuum chamber by using a clean bench.

3.1.2. Test Cavity Electropolishing : In order to understand the EP performance inside a cavity in terms of the contaminants left by the EP acid solution on the surface of a cavity, a real Nb SRF cavity attached with the Nb sample coupons was used for the electropolishing experiments. The cavity was drilled with six holes of 8 mm in diameter at three typical positions, namely “equator”, “iris” and “beam pipe”. The six disc type samples of the same diameter as of holes of the cavity and of a thickness of 2.8 mm were fixed at the cavity holes with the help of specially designed supports for the cavity. These Nb samples were prepared from a high purity niobium sheet supplied from Tokyo Denkai Co. Ltd. The specifications of the niobium sheets were same as that of the nine-cell SRF cavity fabrication at KEK.

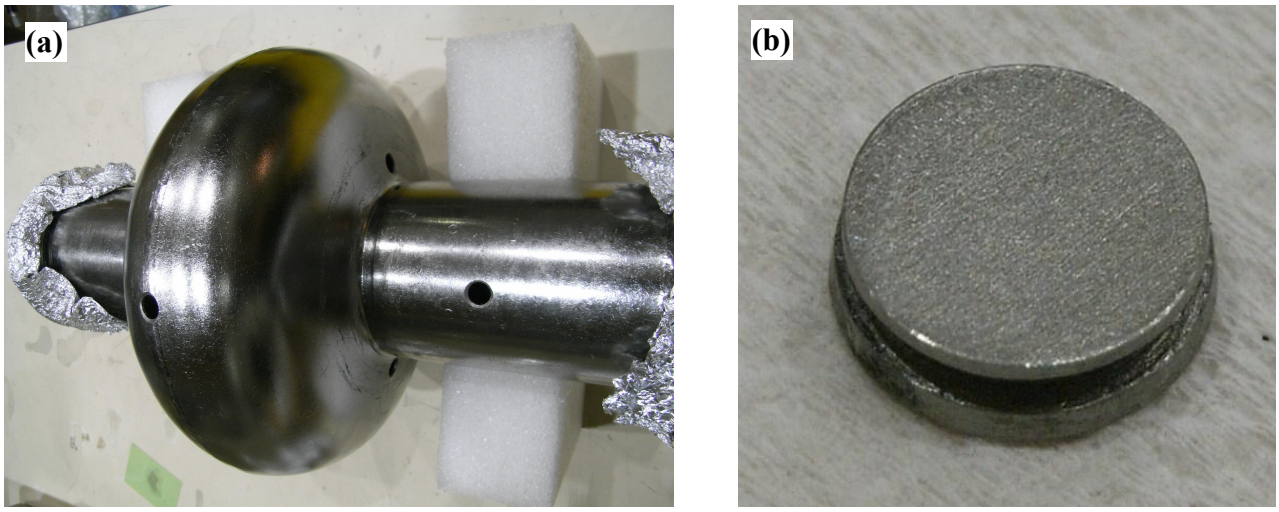

Fig. 3.2 : (a) Sample cavity with six holes at "equator", "iris" and "beam pipe" positions. (b) Disc type sample used for electropolishing.

The fixing of the samples at holes of the cavity was done in class 10 in order to clean room to avoid dust particle contaminants. After mounting all the six samples at the cavity holes, this cavity was moved to EP bed for the electropolishing experiment. The same EP bed can be used for the EP of a single cell or nine cell cavity.

The details of the EP experiment are as follows :

1. The cavity is mounted on the EP bed and cavity beam pipes are fixed at EP bed.
2. A long aluminum rod is also inserted into the cavity which works as a cathode during the EP.
3. The cavity acts as an anode and an electrical contact is made to cavity which can be maintained during the rotation of cavity.

Fig. 3.3 : The cavity assembled with six Nb disc type samples.

4. After fixing the cavity and all its components, nitrogen leak check is performed.

5. If everything is ok then flow of EP acid starts from the left to right with the flow rate of 5 l/min and cavity starts to rotate.

6. Then a voltage is applied to the anode and cavity starts to rotate with a rotational speed of 1 rpm and EP process is begun.

7. After a certain time (depending on depth removal), the power is cut off and cavity is moved to vertical position to drain the EP acid.

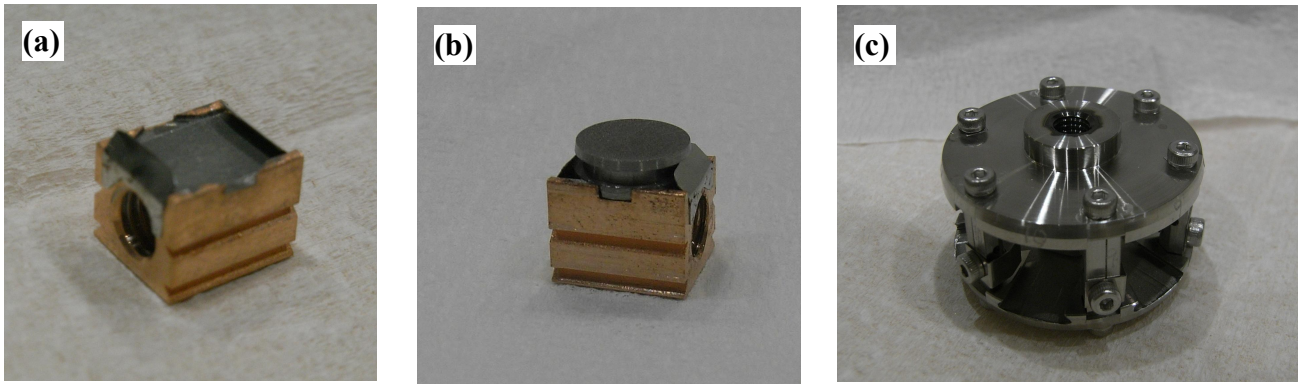

Fig. 3.4 : (a) Cu plated sample holder, (b) Sample sitting on the sample holder and (c) Six sample carousel.

8. After 10 min., a flow of UPW starts from the top of a cavity to remove the acid residues from the cavity inner surface.

All the operations are software controlled. After the EP process, the cavity is moved into the class 10 clean room. All the samples from cavity are detached in the clean room and fixed at the copper plated sample holder and kept in to a multi sample holder carousel. The carousel containing samples is then kept in a UHV suitcase. The UHV suitcase is then moved to surface analysis laboratory and connected to surface analysis system.

3.2. High Pressure Rinsing Experiments

3.2.1. Laboratory High Pressure Rinsing : The laboratory HPR experiment was performed with different pressures and doses on Nb rectangular type samples after their surface treatments. The laboratory HPR experiment was carried out in order to evaluate the appropriate rinsing pressure and dose which can be effective for a real cavity. The dose is the quantity which measures the total water injected to surface per unit area (l/cm^2). To perform HPR experiment, a sample base plate (made of stain-less-steel) was constructed which was fixed on a slide rail and can slide to scan the sample during HPR. The sample was fixed on the base plate and scanned for different doses. For a fixed dose, the scanning time of the sample was calculated at the beginning of the experiment. A separator was also used which separates the sample in two parts for the samples which were subject to two doses, to avoid the effect of rinsing of another position by side-streams of the water beam. The distance between sample and nozzle was kept 50 mm to get highest pressure and to avoid the spreading of water beam. The experiment was conducted in class 1000 clean room. After the HPR experiment, all the samples were carried in clean box or in UPW to analysis laboratory and analyzed by surface analysis system.

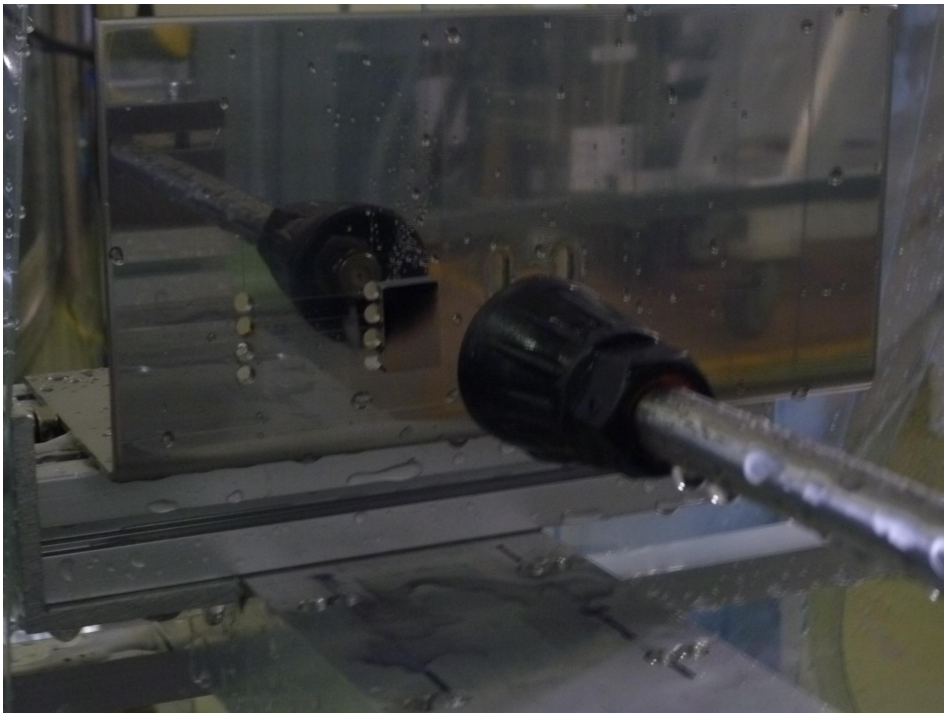

Fig. 3.5 : The Nb sample mounted on the base plate during the laboratory HPR experiment.

3.2.2. Cavity High Pressure Rinsing : The cavity HPR was performed after the cavity EP experiment. The cavity EP experiment was carried out in the same manner as described in section 3.1.2. For the cavity HPR experiment, the cavity attached with Nb disc type samples was moved to cavity HPR facility just after the EP. At the first cavity was showered with UPW to remove dust particles attached with cavity. Then after cavity was moved to HPR position and a stain-less-steel wand containing multiple nozzles was inserted into the cavity. All the operations are computer controlled and rinsing parameters can be set before starting the HPR. The pressure and injected dose were kept similar to usual operating pressure and injected dose in KEK. The cavity was rotating and moving vertically up and down during the HPR. The HPR is stopped after the certain time and the cavity was moved to a class 10 clean room where all the samples were detached. Theses samples were then fixed on copper plated sample holder and kept into the carousel and into the vacuum suitcase same as described in section 3.1.2.

Fig. 3.6 : The Nb cavity assembled with Nb disc type samples during the cavity HPR experiment.

3.3. Dry Ice Cleaning Experiments

The dry ice cleaning (DIC) experiment was conducted on the rectangular type Nb samples after their surface treatments. The DIC was performed in normal environment as well as in nitrogen environment. The ice formation was observed at sample surface during the experiment in normal environment because of the high humidity. In order to avoid ice formation, an experiment was conducted in nitrogen environment as well. The nozzle distance from the sample surface was kept 10 mm in order to get the maximum effect of the DIC. The dry ice flow rate was 2.6 E+6 mm^3 and maximum gas pressure was 6 MPa.

Fig. 3.7 : The dry ice cleaning of the Nb sample in air.

3.4. Surface Analysis Procedure

The surface analysis system as described in chapter 2 was used for analyzing the samples surface and the XPS technique with depth profiling was mainly utilized for the surface analysis. The sample needed to be analyzed, is either mounted directly from atmosphere to LL1 or transferred from suitcase to LL1 via LL 3 and 2. Afterwards, the sample is transferred to main chamber for surface analysis. The surface analysis procedure can be summarized as follows :

(1) The surface of the sample is aligned to the X-rays/electron gun/ion gun with the help of a sample manipulator and an optical (microscope) camera.

(2) Start the analysis by x-ray photoelectron spectroscopy (XPS)/secondary ion mass spectrometry (SIMS)/Auger electron spectroscopy (AES).

(3) In order to get the depth profile, surface is etched by using an Ar ion beam of the energy of 5 keV.

(4) The Ar ion current is first measured by using a Faraday cup. Based on the Faraday current, the etching time is calculated and set corresponding to the sputtered depth.

(5) The sputtered area is 5×5 mm^2 (usually in our case) and the probing area of XPS is 2 mm in diameter.

(6) The XPS analysis is done at a sputtered area.

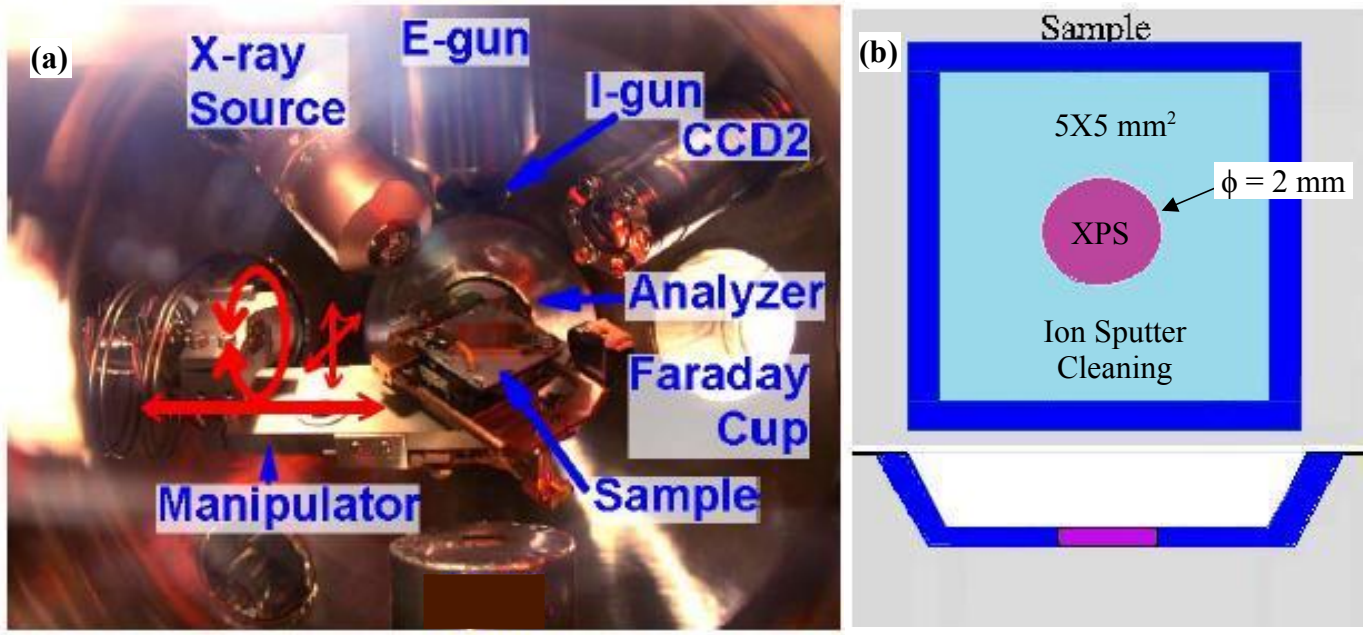

Fig. 3.8 (a) Inner view of the main chamber. (b) Ideal raster and probing area of sample surface : top view and cross-sectional view.

Chapter 4 Experimental Results and Discussions

4.1. Electropolishing Experimental Results

4.1.1. Cavity EP : In order to understand the performance of EP inside a real cavity, a series of cavity electropolishing experiments were conducted. The detailed experimental procedure is given in section 3.1.2 of chapter 3. Table 4.1 gives the brief summary of all the cavity EP experimental conditions and purpose of the experiments.

Experiments	**Average Current Density (mA/cm^2)**	**EP Acid Temperature (^0C)**	**Nb Conc. in EP acid (g/l)**	**Removal Depth (µm)**	**Purpose**
Cavity EP 1	48	25	0	20	To see the effect of fresh EP acid on EP performance in the real cavity
Cavity EP 2	48	25	7.9	50	To see the effect of aged EP acid over the fresh EP acid on EP performance in the real cavity
Cavity EP 3	30	25	6	20	To see the effect of low current density with aged EP acid on EP performance in the real cavity

Table 4.1 : Summary of the experimental conditions of cavity EP experiments.

4.1.1.1. Cavity EP 1 : The first cavity EP experiment was conducted by using the fresh EP acid. The experimental conditions were same as the standard EP conditions for ILC cavities at KEK [4.1]. The table 4.2 summarizes the experimental conditions :

Average Current Density (mA/cm^2)	**EP Acid Temperature (^0C)**	**Nb Conc. in EP acid (g/l)**	**Removal depth (µm)**
48	25	0	20

Table 4.2 : The experimental conditions of cavity EP 1 experiment.

The samples surfaces were characterized by using our surface analysis system and the analysis procedure is described in section 3.4 of chapter 3. Mainly the XPS technique with depth profiling was utilized for the characterization of the samples surface.

Elements	Equator sample surface (atomic %)	Iris sample surface (atomic %)	Beam pipe sample surface (atomic %)
Nb	19	18	16
C	37	40	34
O	44	43	50
F	<0.4	<0.4	<0.4
S	<0.5	<0.5	<0.5

Table 4.3 : Atomic percentages of the elements present on the samples surface after cavity EP 1 experiment.

The XPS analyses of Nb surfaces EPed in the cavity EP 1 experiment show that the surfaces of all the samples were mainly covered with niobium oxide and carbon. Table 4.3 gives the atomic percentages of various elements present on the samples surface after cavity EP 1 experiment.

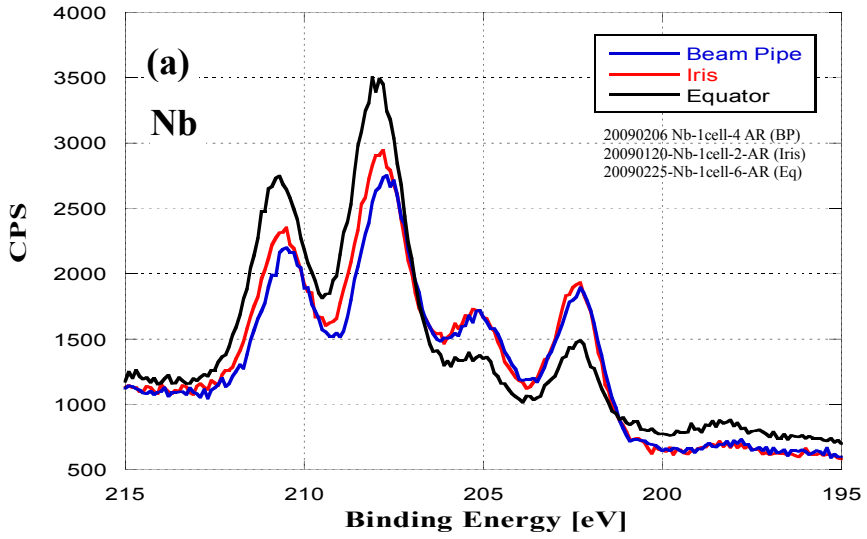

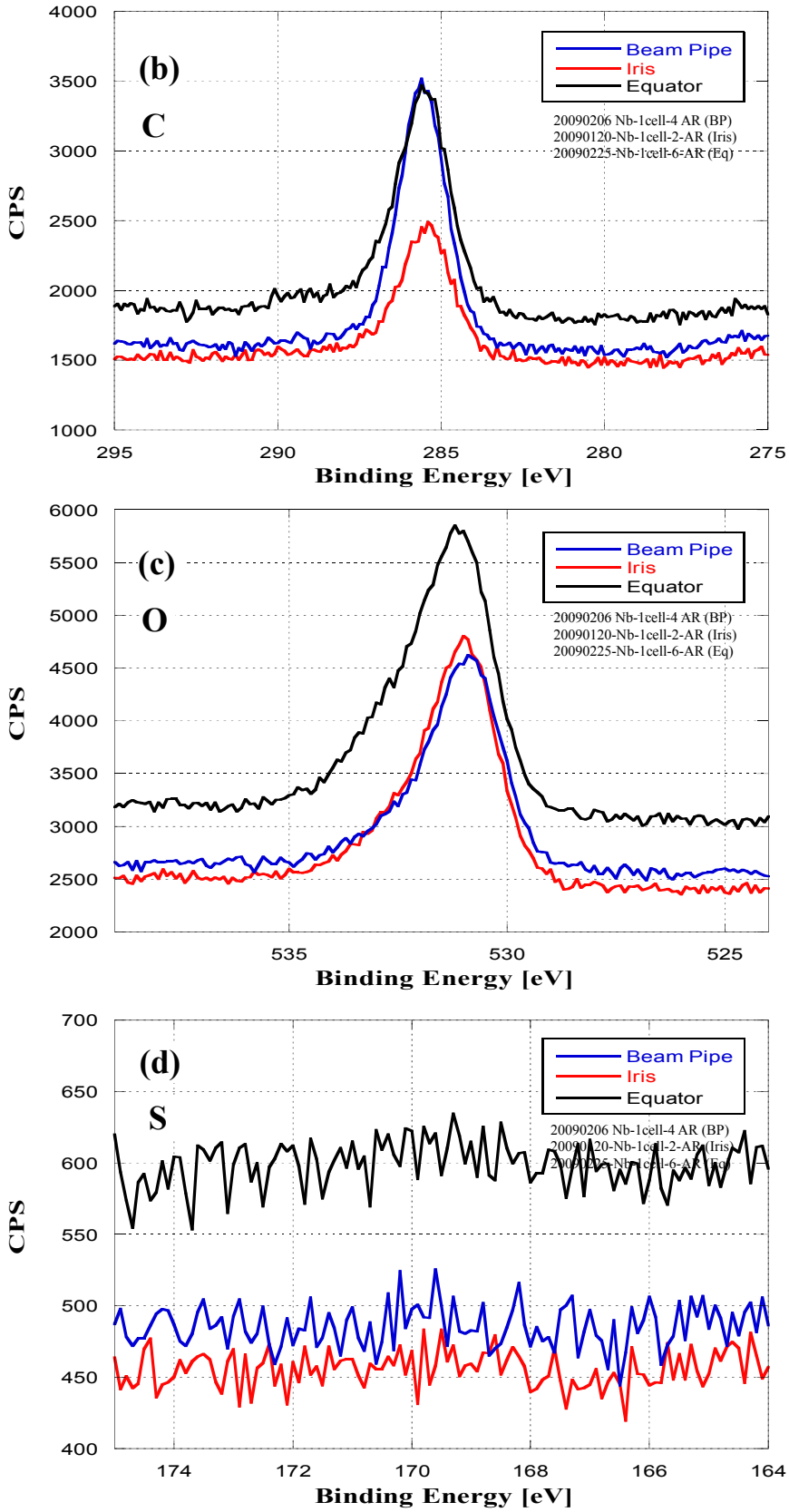

Fig. 4.1 : Comparison of XPS spectra among equator, iris, and beam pipe samples EPed in the cavity EP 1 experiment, (a) Nb spectrum, (b) Carbon spectrum, (c) Oxygen spectrum and (d) Sulfur spectrum.

The XPS results of cavity EP 1 experiment with the fresh EP acid show that the sulfur and fluorine were not detected at Nb surfaces within the detection limit of our XPS and no chemical shift was observed in any of the spectra as shown in fig. 4.1. In addition, a considerable amount of carbon was found on the samples surfaces, which may be due to the lathe operation performed on the samples surface before EP.

The surfaces of all the samples were etched with the help of an Ar ion gun of 5 KeV energy in order to get a depth profile. The depth profiles of all the samples show the thickness of carbon layer was < 1 nm which means carbon was present only at surfaces of samples.

The oxide layer thickness (FWHM) was 1.5 nm at an equator sample surface, 1.8 nm at an iris sample surface and 2 nm in case of a beam pipe sample surface.

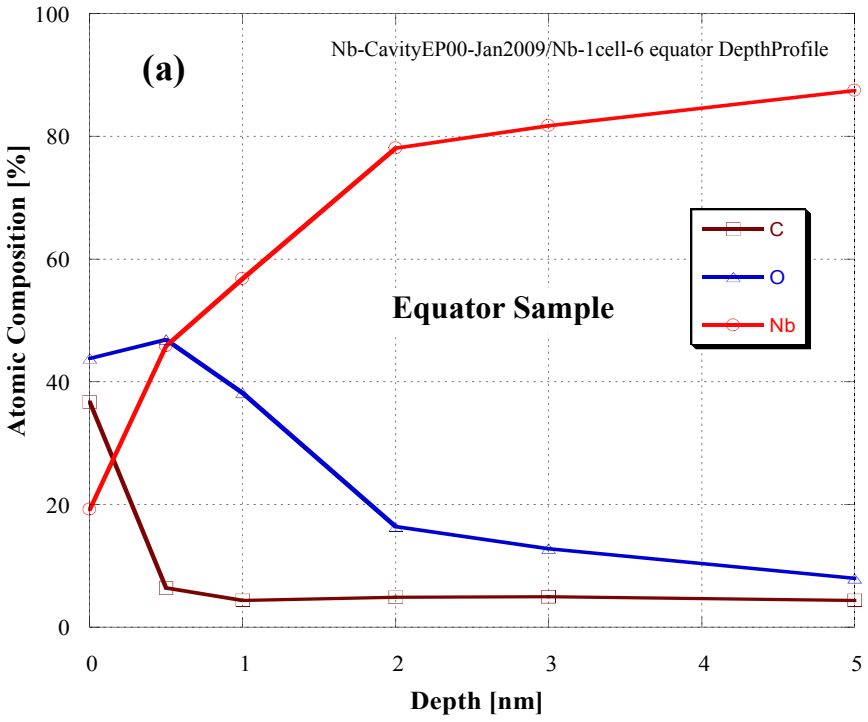

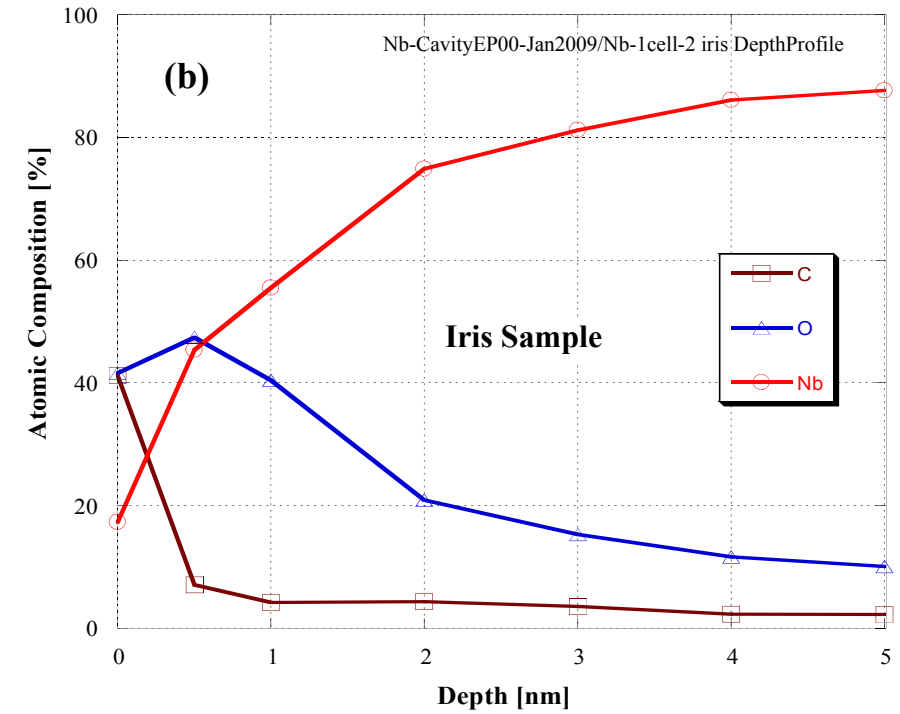

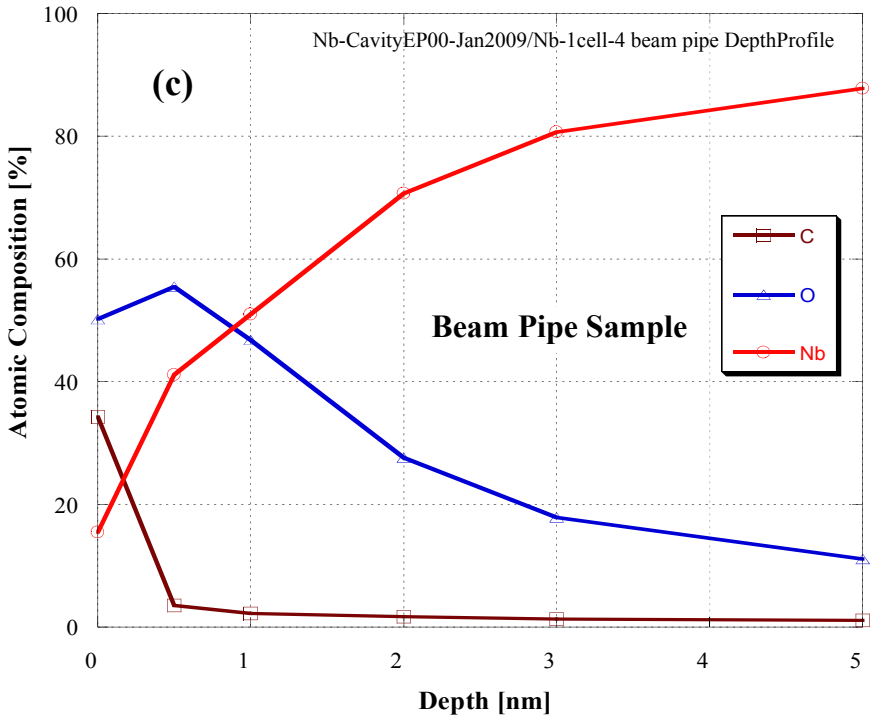

Fig 4.2 : Depth profiles of the EPed samples in the cavity EP 1 experiment up to 5 nm, (a) Equator sample, (b) Iris Sample and (c) Beam pipe sample.

The SEM observations of non sputtered area of the samples show that the surfaces were smooth and covered with many particles of the size of several sub micrometers to a few micrometer.

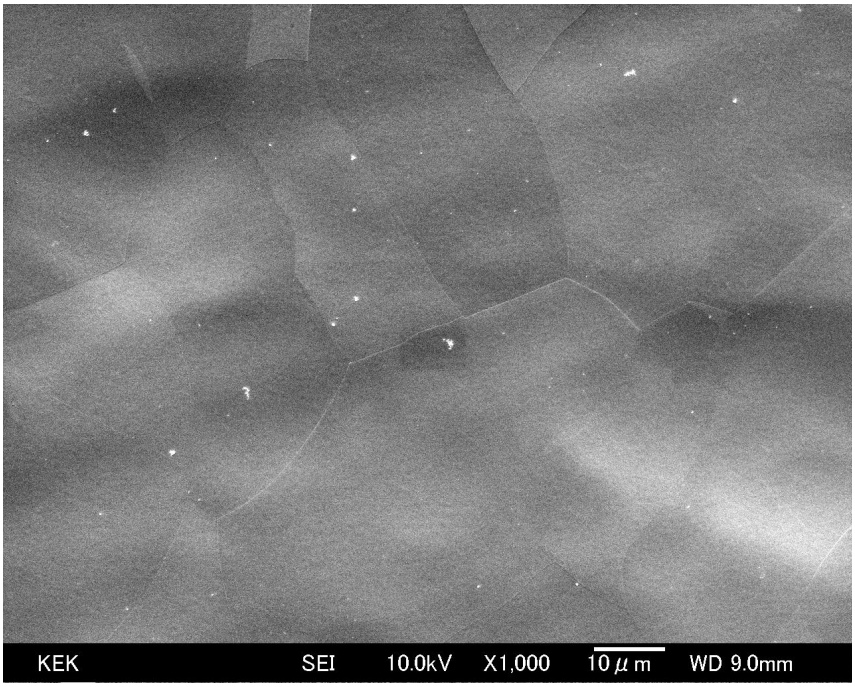

Fig 4.3 : A typical SEM image of the beam pipe sample surface treated in cavity EP 1 experiment.

The ToF (Time of flight)-SIMS images of EPed samples in the cavity EP 1 experiment show the bright spots of sulfur and sulfate in conjunction with the white spots of few micrometer size in SEM image. The sulfur composition was estimated to be several 10 ~ 100 at. ppm.

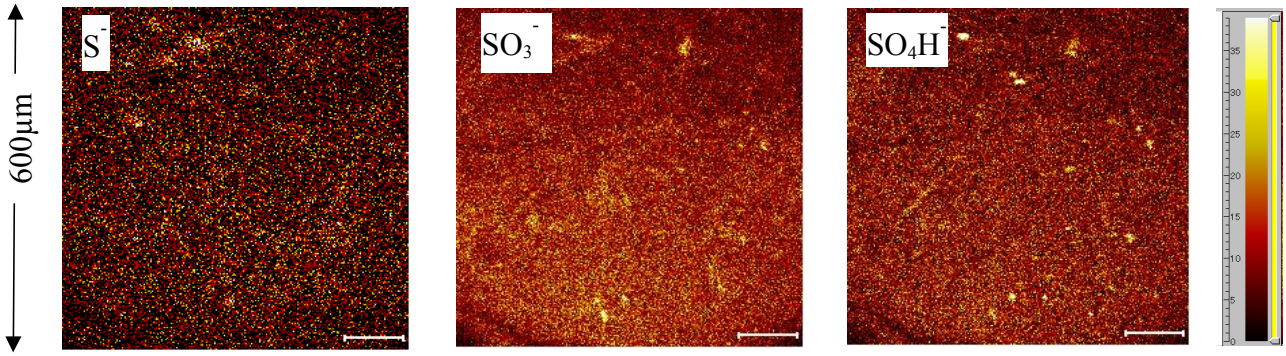

Fig. 4.4 : Secondary ion images with a resolution of 256×256 pixels and a color gradation in 40 steps linearly to the ion intensity of sulfur compound. The brightest dots in each image show sulfur concentrations and it's compounds locally concentrated with a size of around 20 μm.

4.1.1.2 Cavity EP 2 : In reality, the EP acid is reused many times for the EP of ILC cavities, as this is very expensive. Therefore, it is very interesting to see the aging effect of the EP acid on EP performance inside a cavity and the second cavity EP experiment was conducted by using aged EP acid [4.2]. The table 4.4 gives the experimental conditions :

Average Current Density (mA/cm^2)	**EP Acid Temperature (^0C)**	**Nb Conc. in EP acid (g/l)**	**Removal depth (µm)**
48	25	7.9	50

Table 4.4 : The experimental conditions of cavity EP 2 experiment.

The maximum of sulfur was found at the surface of the iris sample while the minimum was found in case of the beam pipe sample surface as described in Table 4.5. Additionally, a notable quantity of nitrogen was found on the surfaces of the iris and equator samples. Table 4.5 gives the atomic percentages of various elements present on the samples surface after the cavity EP 2 experiment.

Elements	**Equator sample surface (atomic %)**	**Iris sample surface (atomic %)**	**Beam pipe sample surface (atomic %)**
Nb	16	10	20
C	18	16	27
N	2	6	0
O	58	59	49
F	3	3	4
S	4	7	2

Table 4.5 : Atomic percentages of the elements present on the samples surface after cavity EP 2 experiment.

The XPS characterizations of the samples surface treated with the aged EP acid show that a significant quantity of sulfur and fluorine was found at the surface and a chemical shift in the oxygen and sulfur spectra peaks was observed.

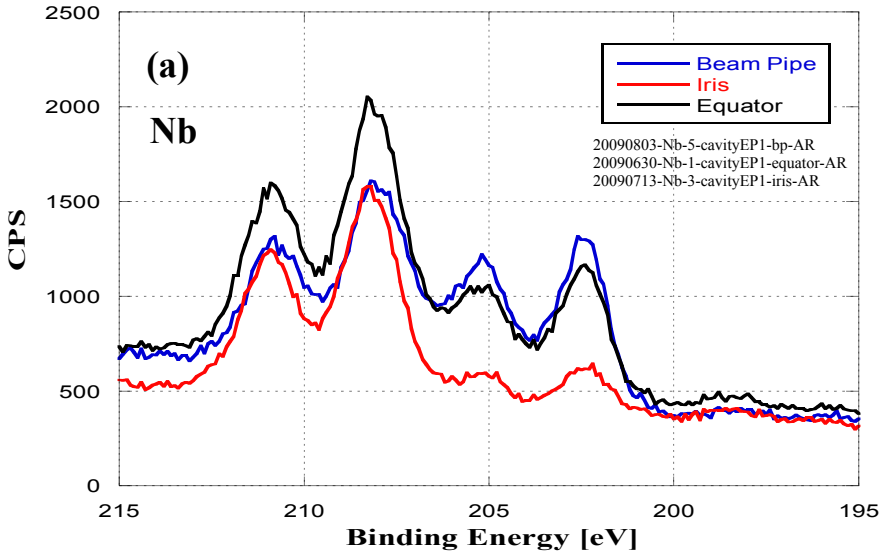
(a)
Nb
Beam Pipe
Iris
Equator
20090803-Nb-5-cavityEP1-bp-AR
20090630-Nb-1-cavityEP1-equator-AR
20090713-Nb-3-cavityEP1-iris-AR
CPS
Binding Energy [eV]

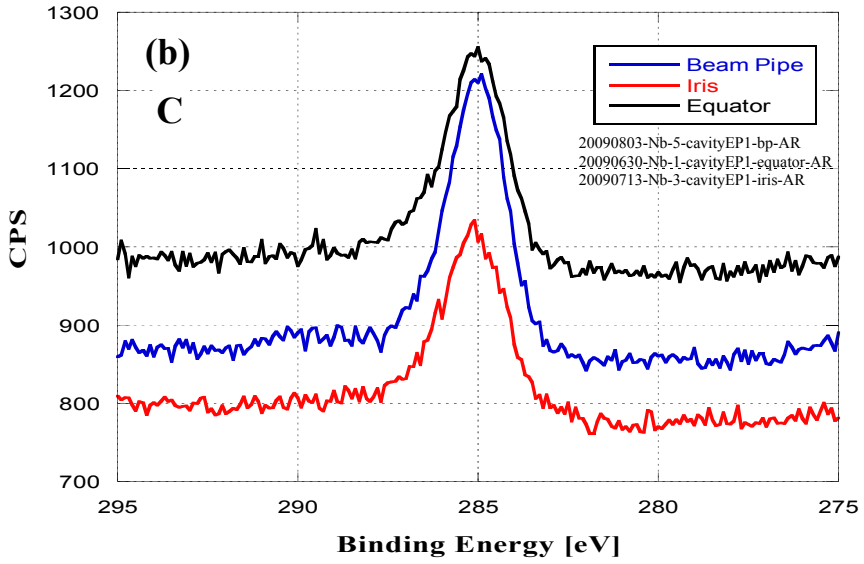
(b)
C
Beam Pipe
Iris
Equator
20090803-Nb-5-cavityEP1-bp-AR
20090630-Nb-1-cavityEP1-equator-AR
20090713-Nb-3-cavityEP1-iris-AR
CPS
Binding Energy [eV]

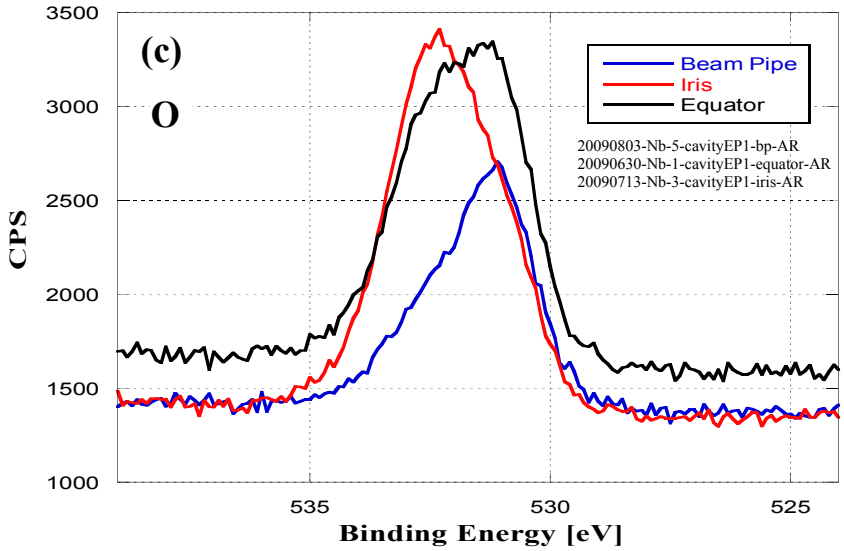
(c)
O
Beam Pipe
Iris
Equator
20090803-Nb-5-cavityEP1-bp-AR
20090630-Nb-1-cavityEP1-equator-AR
20090713-Nb-3-cavityEP1-iris-AR
CPS
Binding Energy [eV]

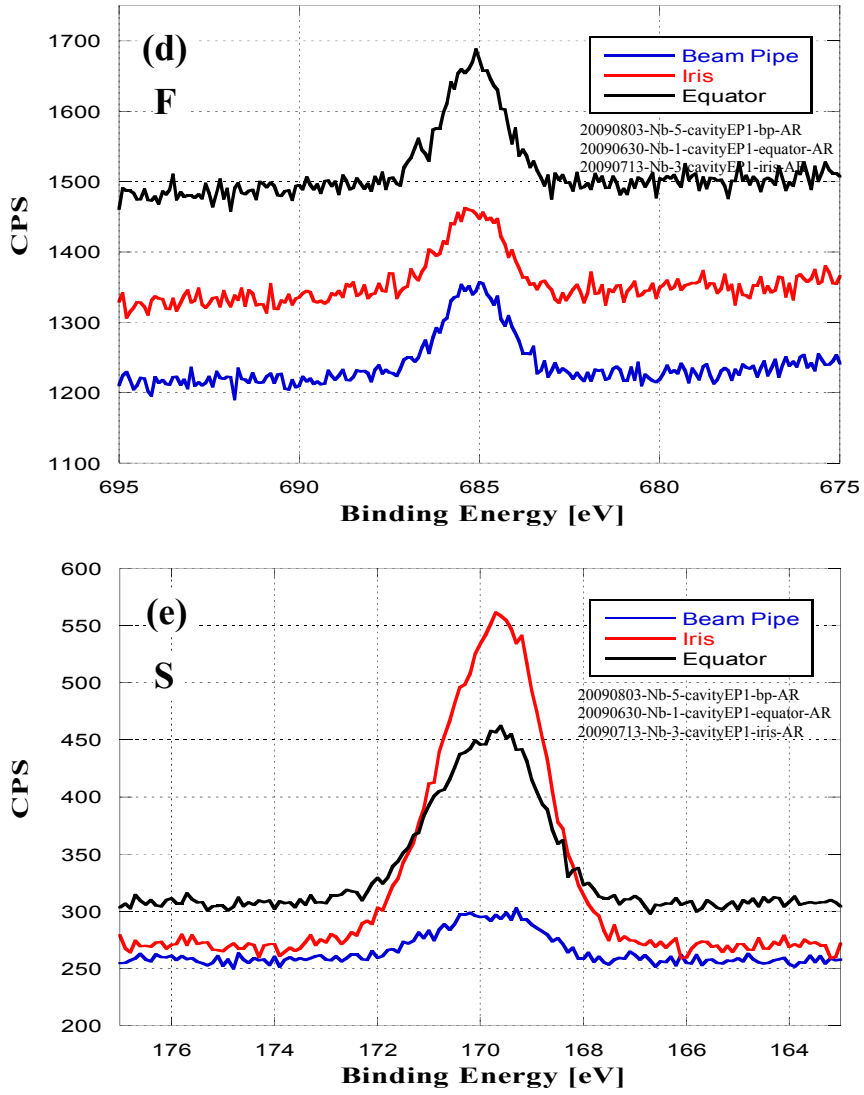

Fig. 4.5 : Comparison of XPS spectra among equator, iris, and beam pipe samples EPed in cavity EP 2 experiment, (a) Nb spectrum, (b) Carbon spectrum, (c) Oxygen spectrum, (d) Fluorine spectrum and (e) Sulfur spectrum.

The binding energy of a shifted oxygen peak was around 532.3 eV and it was around 169.5 eV in case of a sulfur peak. The original binding energy corresponding to the oxygen and sulfur peak is 531.7 eV and 164.4 eV respectively.

The peak shift in a sulfur spectrum reveals the existence of sulfur in the oxidation form at the samples surface. The chemical state of sulfur is found as a mixture of SO_4^{--} and SO_3^{-} [4.3].

The depth profiles of the samples treated in a cavity EP 2 experiment show that the sulfur was reduced drastically after 0.5 nm depth and the sulfur peak was shifted toward the original binding energy which

demonstrates that the sulfur oxide layer was present only at top surface. After 0.5 nm, a peak shift in the oxygen spectrum towards the oxygen original binding energy was also observed which shows some relevance with the presence of sulfur.

The depth profiles show that the fluorine and sulfur were present up to 1 nm in case of the equator as well as beam pipe samples while in case of an iris sample, it was present up to 2 nm. The oxide layer FWHM was 1.5 nm at an equator sample surface, 2.5 nm at an iris sample surface and 1.9 nm in case of a beam pipe sample surface.

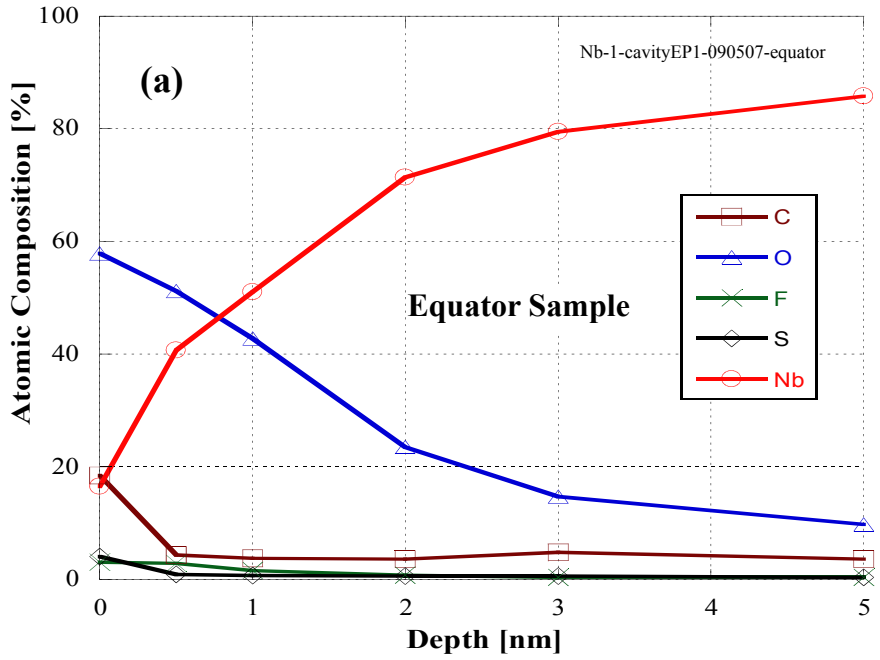

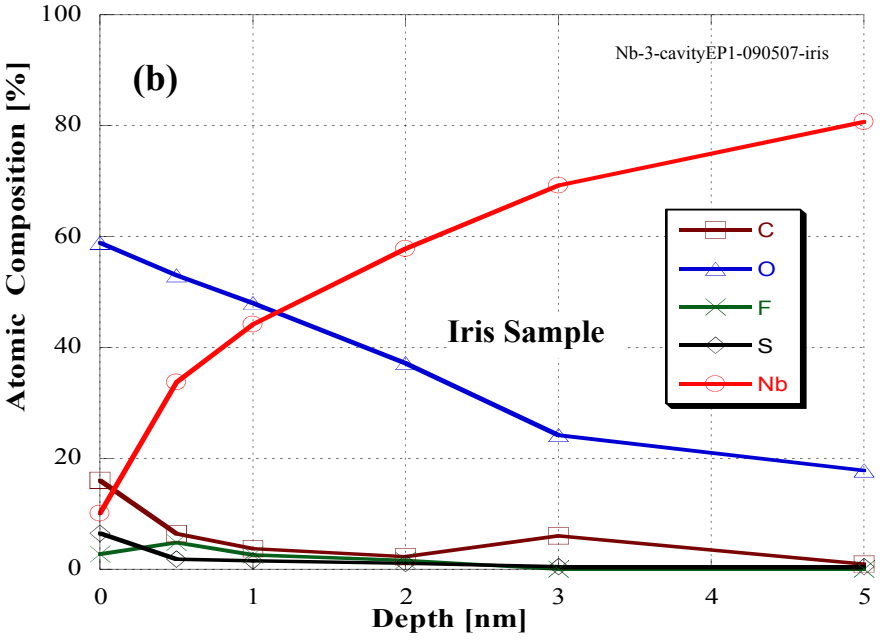

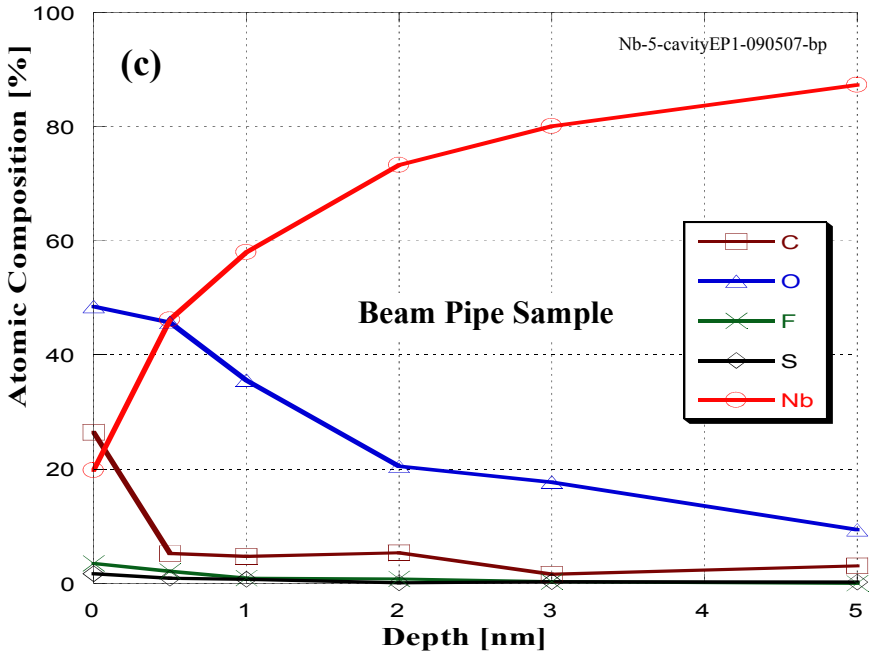

Fig. 4.6 : Depth profiles of the EPed samples in the cavity EP 2 experiment up to 5 nm, (a) Equator sample, (b) Iris Sample and (c) Beam pipe sample.

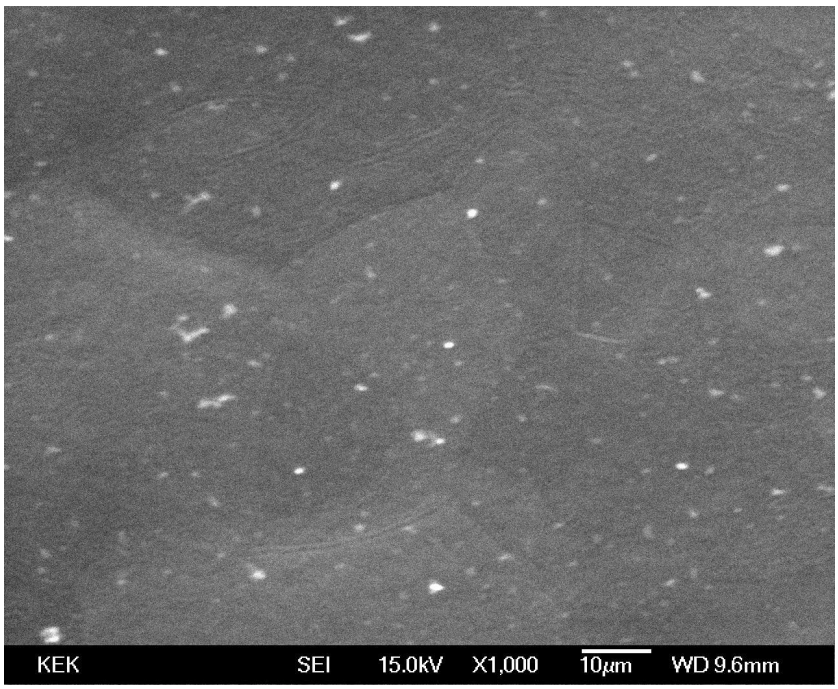

Fig 4.7 : A typical SEM image of the beam pipe sample surface treated in cavity EP 2 experiment.

The SEM images of the samples treated in the cavity EP 2 experiment show that the surfaces were covered with many particles of the size of several sub micrometers to few micrometers similar to the particles found in the cavity EP 1 experiment. The high density of such particles was found on the surfaces in case of the samples EPed in the cavity EP 2 experiment.

4.1.1.3. Cavity EP 3 : The current density plays an important role in performance of the EP. Therefore it is essential to characterize the effect of low current density in EP. In order to see the effect of low current density including aged EP acid, the third cavity EP experiment was conducted. The table 4.6 summarizes the experimental conditions :

Average Current Density (mA/cm^2)	**EP Acid Temperature (^0C)**	**Nb Conc. in EP acid (g/l)**	**Removal depth (µm)**
30	25	6	20

Table 4.6 : The experimental conditions of cavity EP 3 experiment.

The XPS results of the cavity EP 3 experiment reveal that the sulfur and fluorine were present at the surfaces. The quantity of sulfur and fluorine is found very less in comparison with the cavity EP 2 experiment.

Elements	**Equator sample surface (atomic %)**	**Iris sample surface (atomic %)**	**Beam pipe sample surface (atomic %)**
Nb	18	17	16
C	35	29	33
O	45	54	51
F	0.9	0.2	0.4
S	0.5	< 0.1	0.2

Table 4.7 : Atomic percentages of the elements present on the samples surface after cavity EP 3 experiment.

The chemical state of sulfur was found same as it was found in a cavity EP 2 experiment as the chemical shift in the peak was found around 169.5 eV. There was no peak shift found in any of other spectra because the quantity of sulfur was too low. The amount of sulfur was found least in case of an iris sample while it was found maximum in case of an equator sample in the cavity EP 3 experiment (table 4.7).

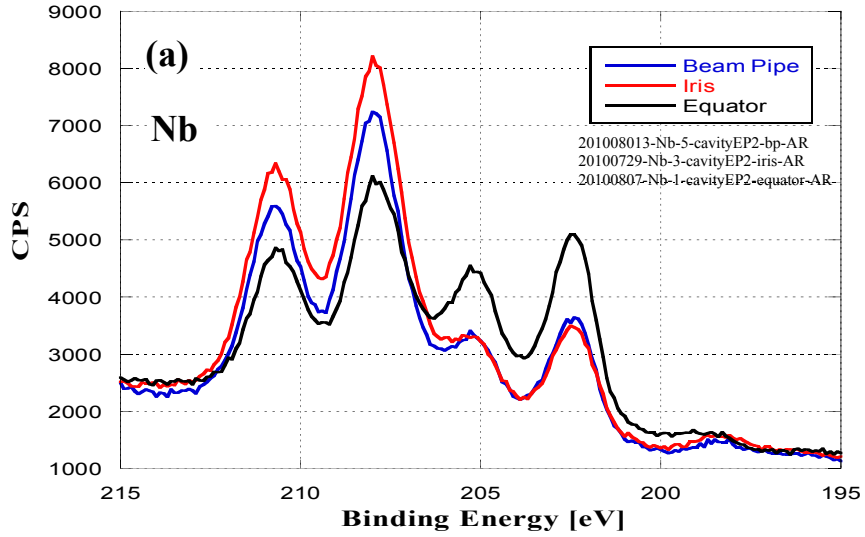
(a)
Nb
Beam Pipe
Iris
Equator
201008013-Nb-5-cavityEP2-bp-AR
20100729-Nb-3-cavityEP2-iris-AR
20100807-Nb-1-cavityEP2-equator-AR
CPS
Binding Energy [eV]

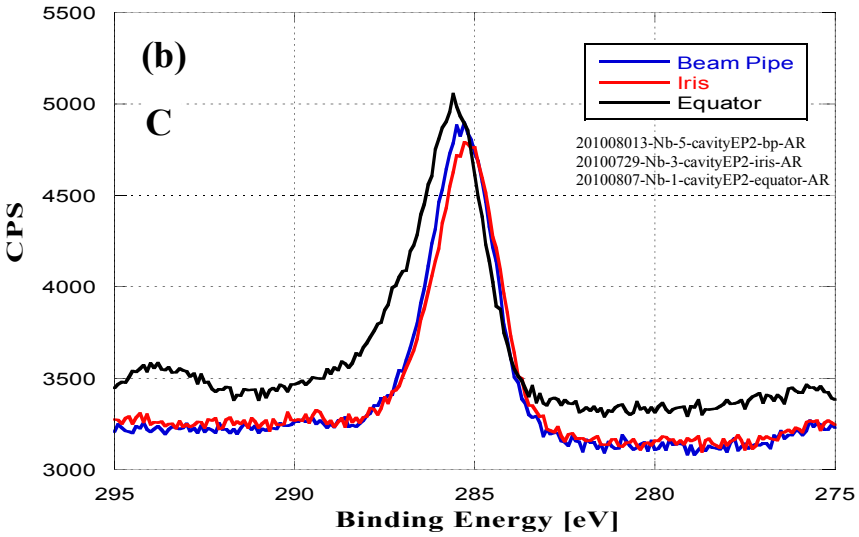
(b)
C
Beam Pipe
Iris
Equator
201008013-Nb-5-cavityEP2-bp-AR
20100729-Nb-3-cavityEP2-iris-AR
20100807-Nb-1-cavityEP2-equator-AR
CPS
Binding Energy [eV]

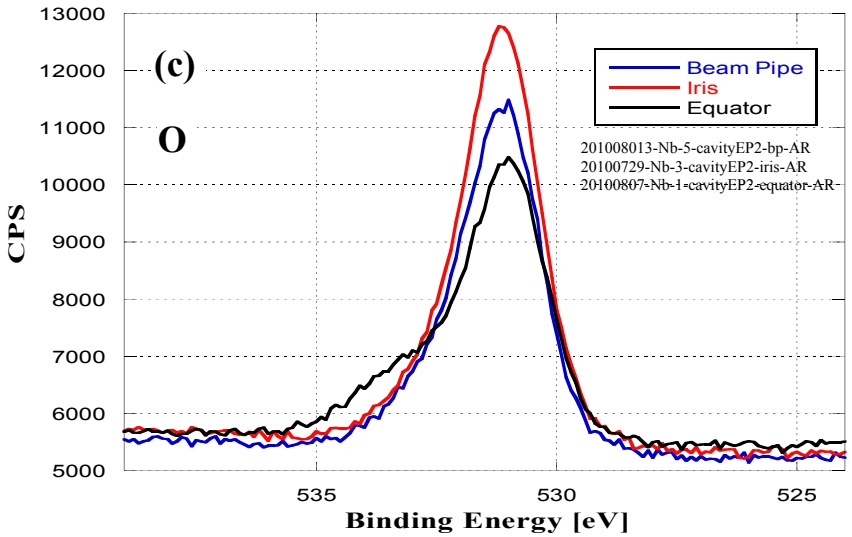
(c)
O
Beam Pipe
Iris
Equator
201008013-Nb-5-cavityEP2-bp-AR
20100729-Nb-3-cavityEP2-iris-AR
20100807-Nb-1-cavityEP2-equator-AR
CPS
Binding Energy [eV]

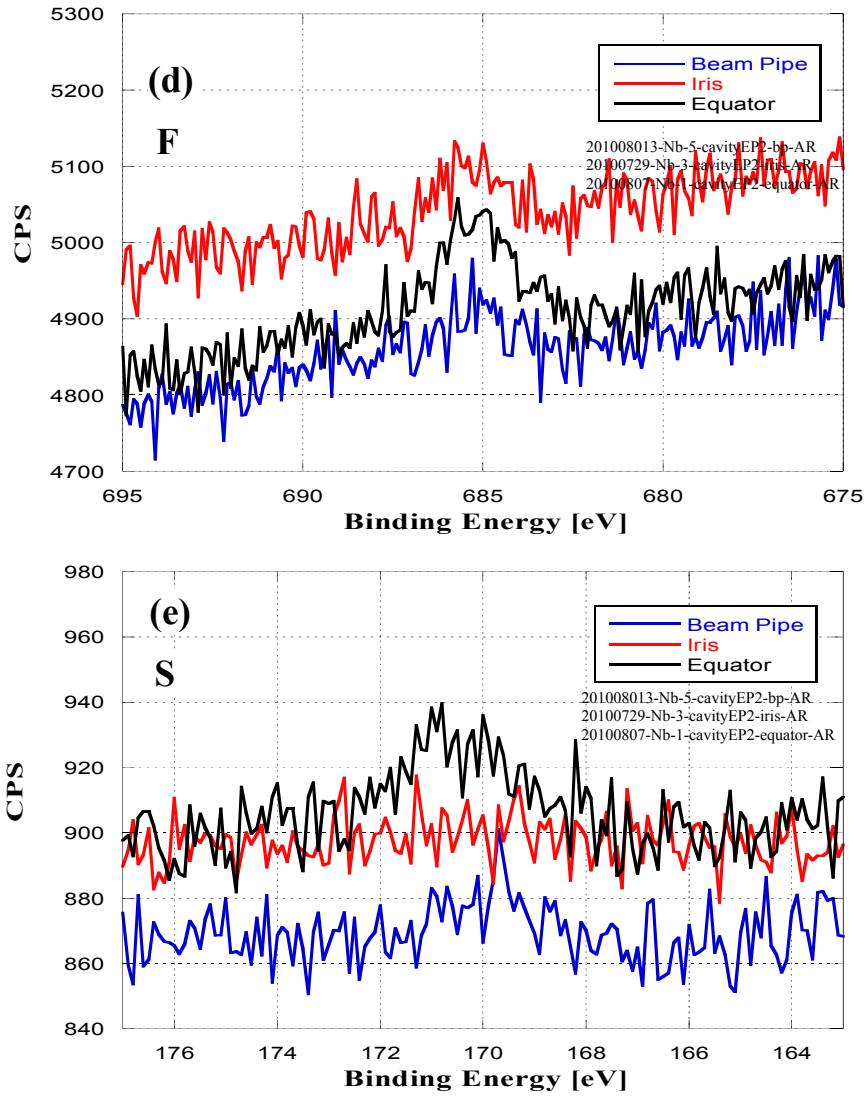

Fig. 4.8 : Comparison of XPS spectra among equator, iris, and beam pipe samples EPed in cavity EP 3 experiment, (a) Nb spectrum, (b) Carbon spectrum, (c) Oxygen spectrum, (d) Fluorine spectrum and (e) Sulfur spectrum.

The depth profiles of the samples treated in the cavity EP 3 experiment show that the sulfur and fluorine were present only at top surface. The FWHM of oxide layer was found 1.5 nm at an equator sample surface, 1.8 nm at an iris sample surface and 1.8 nm in case of a beam pipe sample surface. However, the thickness (FWHM) of the oxide layer was similar as cavity EP 1 and 2 experiments but it can also be seen from the depth profiles that the total thickness of the oxide layer was increased in the samples. The reason of quite thick oxide layer is still unclear.

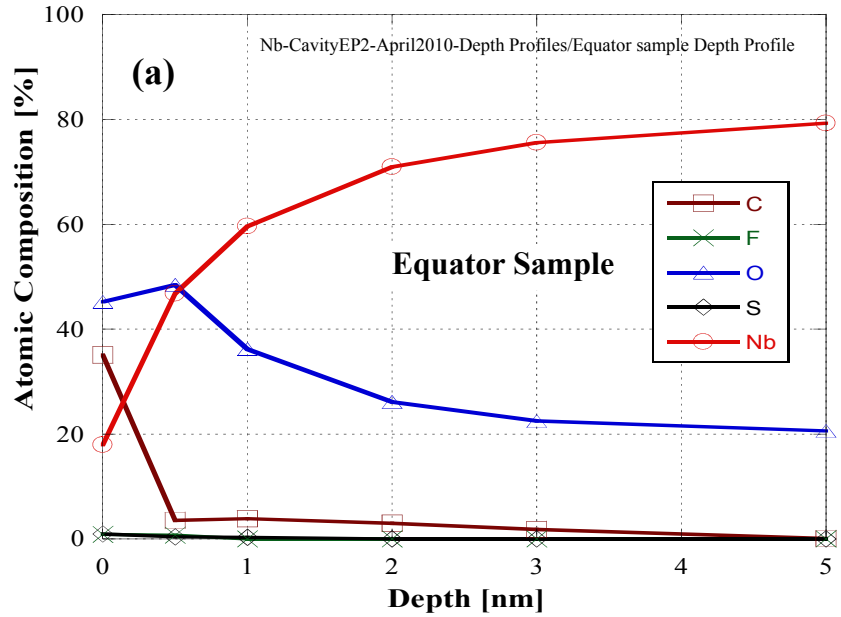
(a)
Nb-CavityEP2-April2010-Depth Profiles/Equator sample Depth Profile
Atomic Composition [%]
Depth [nm]
Equator Sample
C
F
O
S
Nb
0
20
40
60
80
100
0
1
2
3
4
5

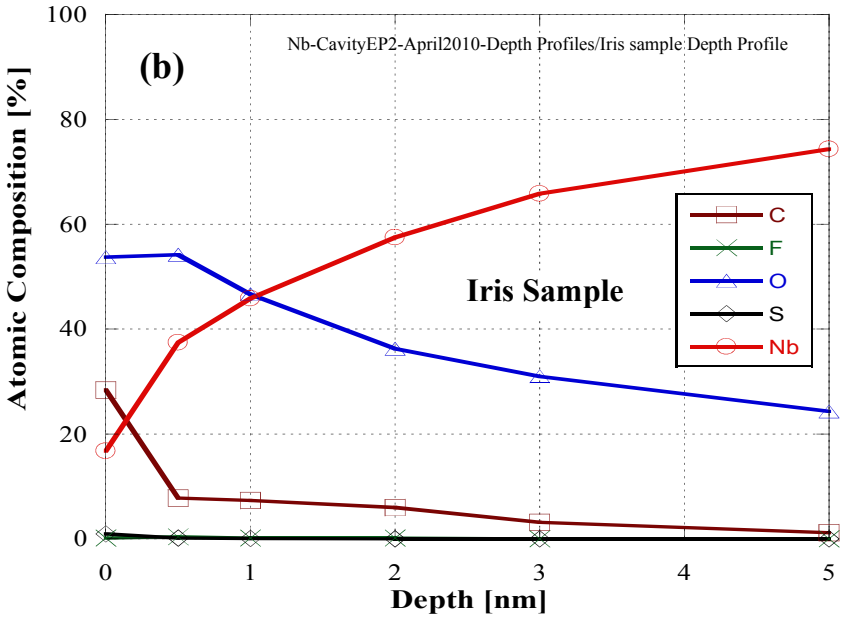
(b)
Nb-CavityEP2-April2010-Depth Profiles/Iris sample Depth Profile
Atomic Composition [%]
Depth [nm]
Iris Sample
C
F
O
S
Nb
0
20
40
60
80
100
0
1
2
3
4
5

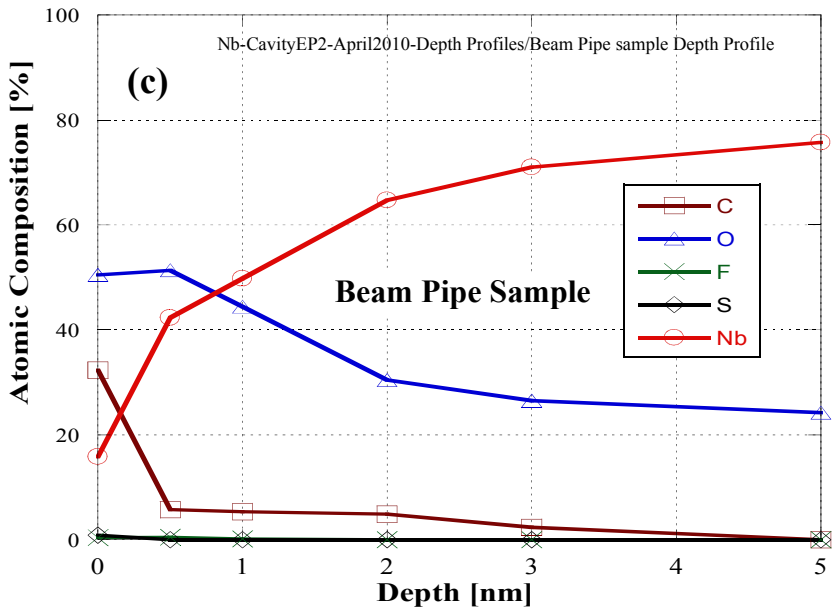

Fig. 4.9 : Depth profiles of the EPed samples in the cavity EP 3 experiment up to 5 nm, (a) Equator sample, (b) Iris Sample and (c) Beam pipe sample.

4.1.2. Laboratory EP : In order to confirm the effect of a current density on fluorine and sulfur generation, two laboratory EP experiments were conducted. Table 4.8 describes the experimental conditions.

Experiments	**Average Current Density (mA/cm^2)**	**EP Acid Temperature (^0C)**	**Nb Conc. in EP acid (g/l)**	**Removal Depth (µm)**	**Purpose**
Lab EP 1	33	27	7.3	20	To see the effect of low current density
Lab EP 2	50	30	7.6	20	To see the effect of high current density

Table 4.8 : Summary of the experimental conditions of Lab EP experiments.

The XPS results showed that the sulfur was not found on the surface EPed with a low current density while a large amount of sulfur was detected on the samples treated with a high current density. Table 4.9 gives the atomic composition present at the top surface.

Elements	Lab EP 1 Experiment with low current density (atomic %)	Lab EP 2 Experiment with high current density (atomic %)
Nb	16.5	5.1
C	29.7	25
O	53.7	60
F	<0.1	<0.1
S	0.3	10.3

Table 4.9 : Atomic percentages of the elements present on the samples surface after Laboratory EP experiments.

The XPS results of the laboratory EP were quite consistent with the Cavity EP 2 and Cavity EP 3 experiments. A peak shift in sulfur as well as oxygen spectra was also found in similar manner which confirms the sulfur chemical state is in oxidation form.

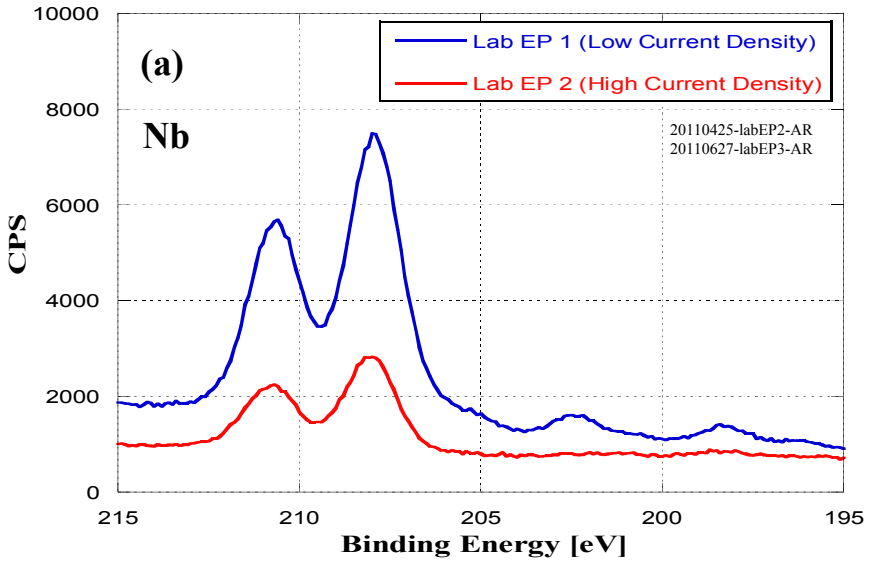

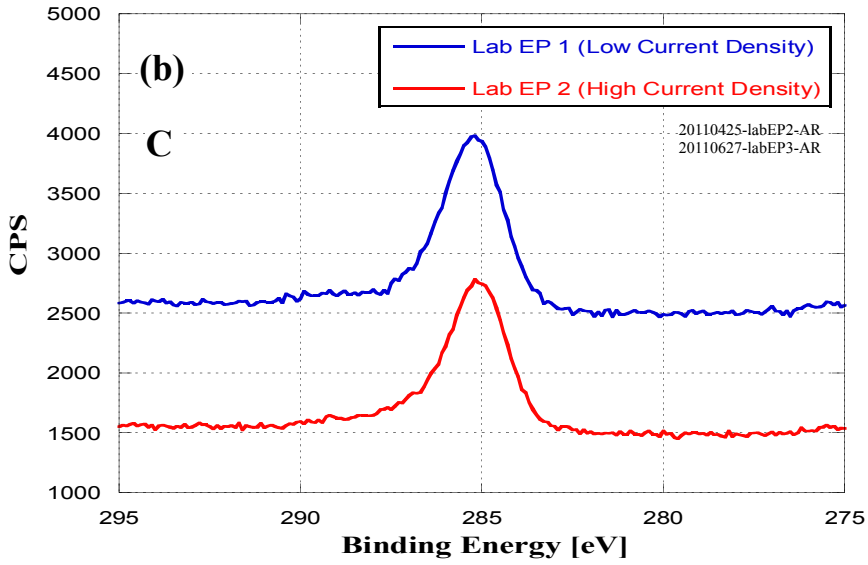
(b)
C
Lab EP 1 (Low Current Density)
Lab EP 2 (High Current Density)
20110425-labEP2-AR
20110627-labEP3-AR
CPS
5000
4500
4000
3500
3000
2500
2000
1500
1000
295
290
285
280
275
Binding Energy [eV]

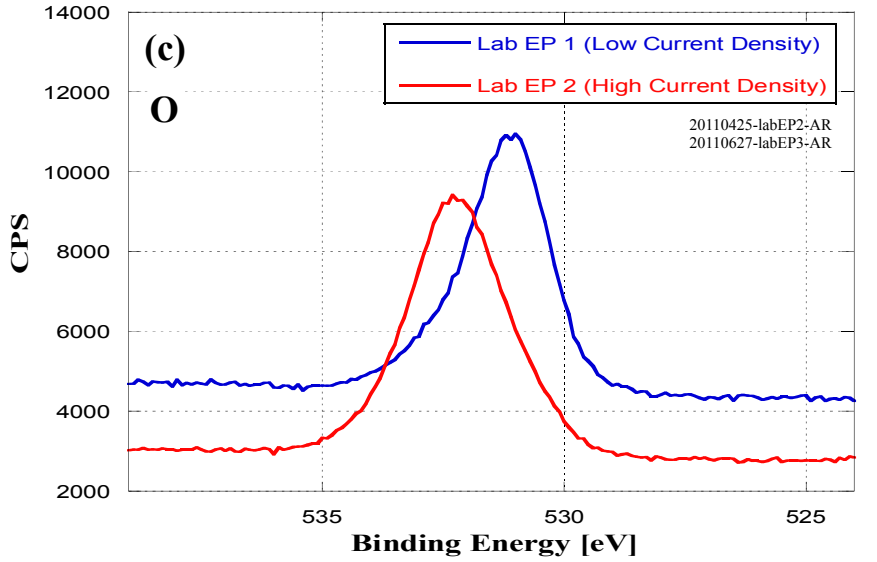
(c)
O
Lab EP 1 (Low Current Density)
Lab EP 2 (High Current Density)
20110425-labEP2-AR
20110627-labEP3-AR
CPS
14000
12000
10000
8000
6000
4000
2000
535
530
525
Binding Energy [eV]

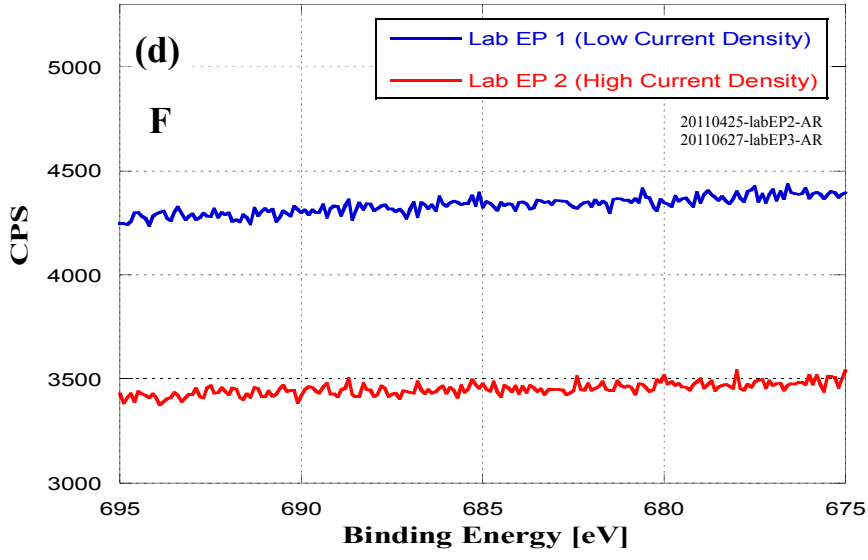
(d)
F
Lab EP 1 (Low Current Density)
Lab EP 2 (High Current Density)
20110425-labEP2-AR
20110627-labEP3-AR
CPS
5000
4500
4000
3500
3000
695
690
685
680
675
Binding Energy [eV]

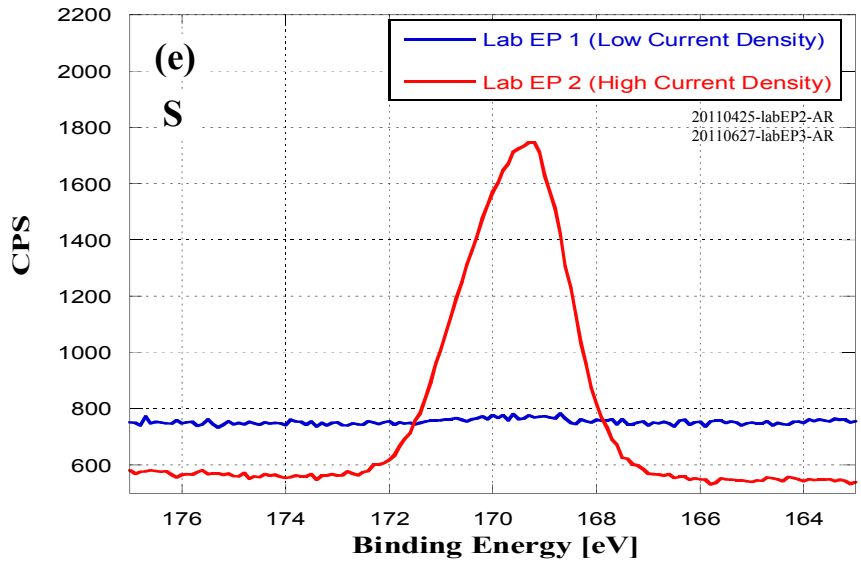

Fig. 4.10 : Comparison of XPS spectra among samples treated in lab EP 1 and 2 experiments, (a) Nb spectrum, (b) Carbon spectrum, (c) Oxygen spectrum, (d) Fluorine spectrum and (e) Sulfur spectrum.

As it can be confirmed from the XPS results of the Lab EP 1 and 2 as well as Cavity EP 2 and 3 that the sulfur generation is proportional to a high current density. The chemical state of sulfur at surfaces of samples treated in Lab EP 2 with a high current density was found as a sulfate/sulfide in the similar manner as it was found in case of the cavity EP 2 experiment.

4.2. High Pressure Rinsing Experimental Results

4.2.1. Cavity EP 4 and HPR : In order to evaluate the performance of KEK HPR facility in reality, we carried out a HPR experiment by using a real Nb cavity assembled with samples. The detailed experimental procedure is explained in the section 3.2.2 of chapter 3. The table 4.10 gives the EP conditions :

Average Current Density (mA/cm^2)	EP Acid Temperature (^0C)	Nb Conc. in EP acid (g/l)	Removal depth (µm)
50	20	2.1	20

Table 4.10 : The experimental conditions of cavity EP 4 experiment.

After the cavity EP 4 experiment, the cavity was subjected to HPR. The HPR pressure was 8 MPa which is a usual pressure for ILC cavities rinsing at KEK. The HPR was carried out for 2 hrs. and 25 min, which is an equivalent dose (0.79 l/cm^2) of normal HPR of ILC cavity at KEK.

Elements	Equator sample surface (atomic %)	Iris sample surface (atomic %)	Beam pipe sample surface (atomic %)
Nb	23	25	17
C	25	17	29
O	52	58	54
F	0.3	0.6	0.3
S	<0.1	<0.1	<0.1

Table 4.11 : Atomic percentages of the elements present on the samples surface after cavity EP 4 experiment followed by HPR.

The XPS results of the experiment show that the fluorine was found lowest at the equator and beam pipe sample while it was higher on an iris sample. The table 4.11 gives the atomic composition present on the samples surface.

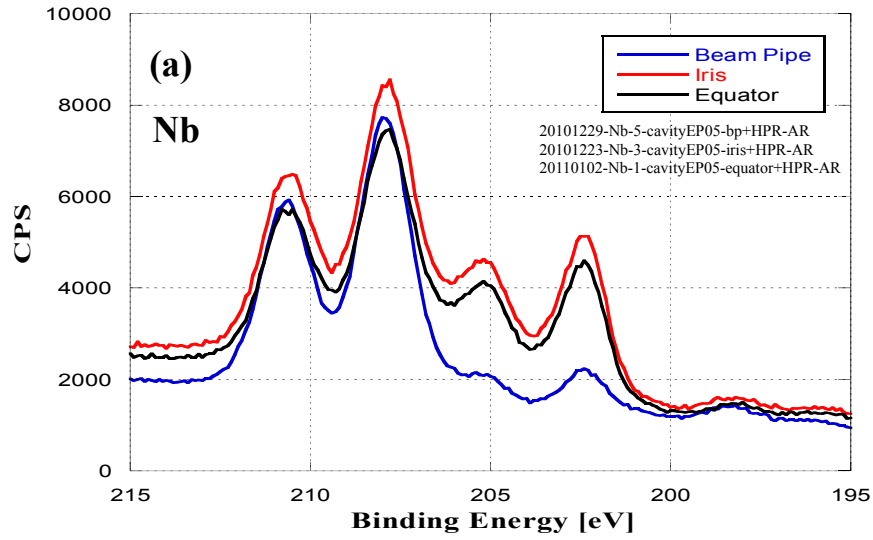
(a)
Nb
Beam Pipe
Iris
Equator
20101229-Nb-5-cavityEP05-bp+HPR-AR
20101223-Nb-3-cavityEP05-iris+HPR-AR
20110102-Nb-1-cavityEP05-equator+HPR-AR
CPS
Binding Energy [eV]

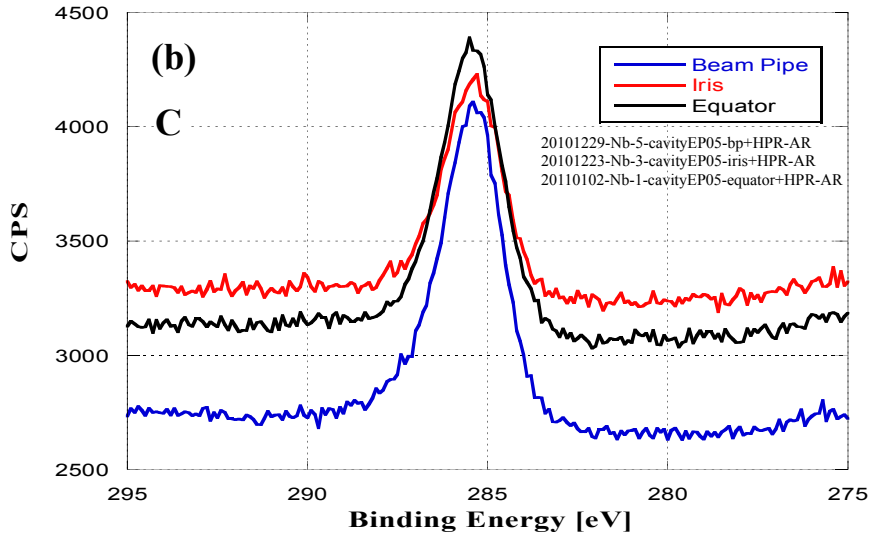
(b)
C
Beam Pipe
Iris
Equator
20101229-Nb-5-cavityEP05-bp+HPR-AR
20101223-Nb-3-cavityEP05-iris+HPR-AR
20110102-Nb-1-cavityEP05-equator+HPR-AR
CPS
Binding Energy [eV]

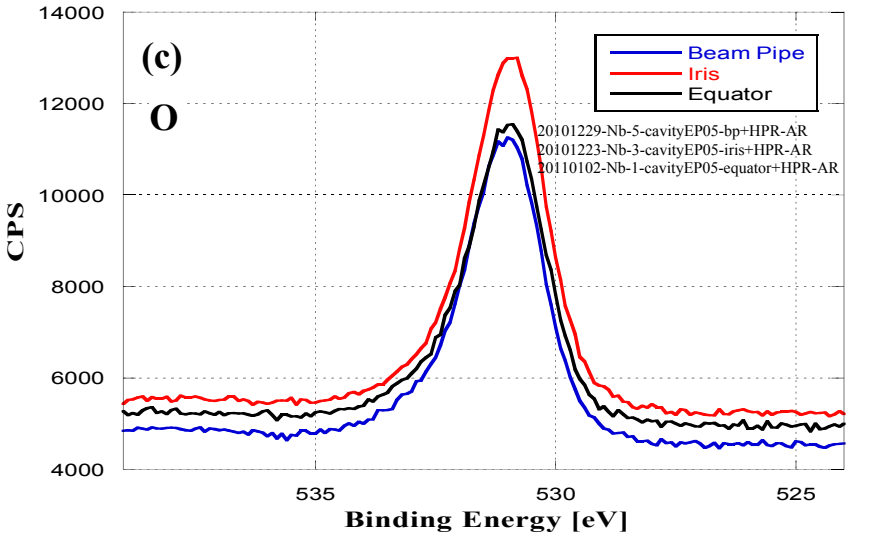
(c)
O
Beam Pipe
Iris
Equator
20101229-Nb-5-cavityEP05-bp+HPR-AR
20101223-Nb-3-cavityEP05-iris+HPR-AR
20110102-Nb-1-cavityEP05-equator+HPR-AR
CPS
Binding Energy [eV]

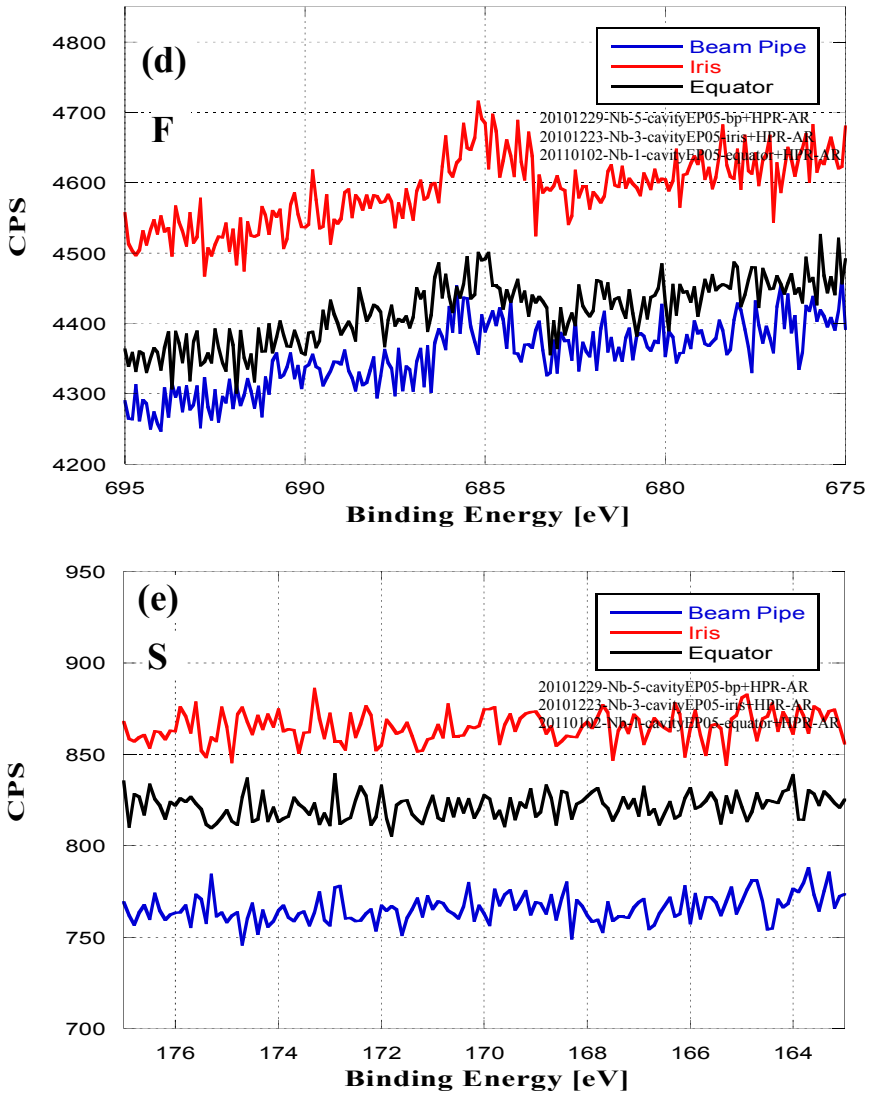

Fig. 4.11 : Comparison of XPS spectra among equator, iris, and beam pipe samples EPed in cavity EP 4 followed by HPR experiment, (a) Nb spectrum, (b) Carbon spectrum, (c) Oxygen spectrum, (d) Fluorine spectrum and (e) Sulfur spectrum.

The XPS spectra showed that the sulfur was not found at any of the samples surface within the detection limit. According to XPS results, either the HPR was quite effective to remove the sulfur and/or sulfur compounds from the surface or sulfur was not present on the samples surface since beginning as EP acid used was not very aged. The fluorine was still found at all the surfaces which shows that the either a high pressure or dose was not sufficient for removing fluorine from the surfaces. The Nb spectra of all the samples show the strong peak of Nb_2O_5 over the Nb metallic peak which indicates the presence of thicker oxide layers at samples surface.

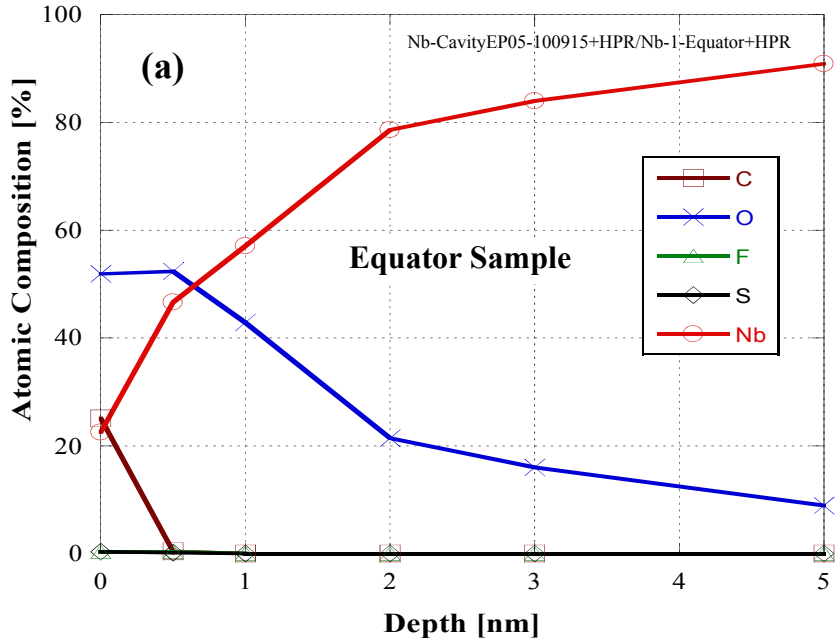
(a)
Nb-CavityEP05-100915+HPR/Nb-1-Equator+HPR
Equator Sample
C
O
F
S
Nb
Atomic Composition [%]
Depth [nm]
0
20
40
60
80
100
0
1
2
3
4
5

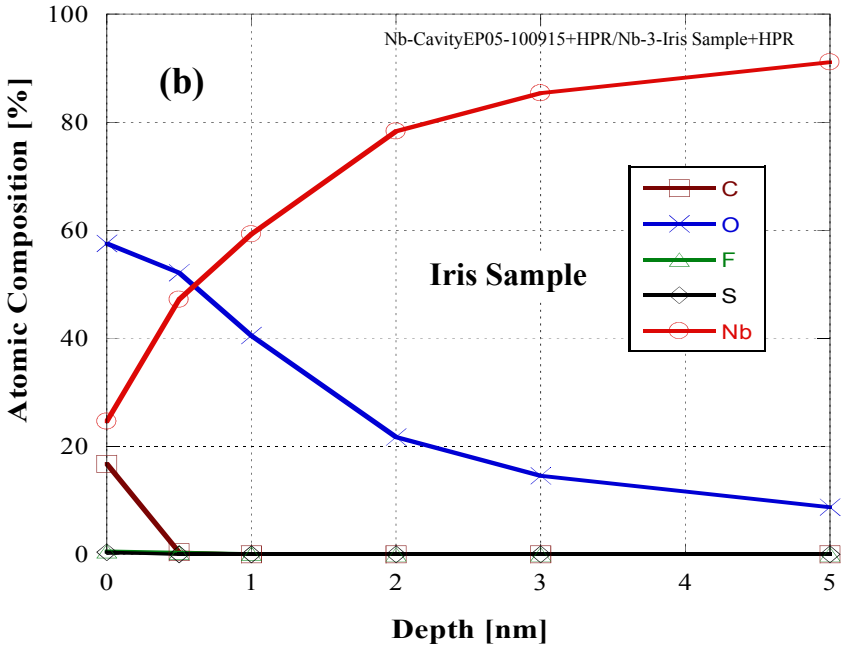
(b)
Nb-CavityEP05-100915+HPR/Nb-3-Iris Sample+HPR
Iris Sample
C
O
F
S
Nb
Atomic Composition [%]
Depth [nm]
0
20
40
60
80
100
0
1
2
3
4
5

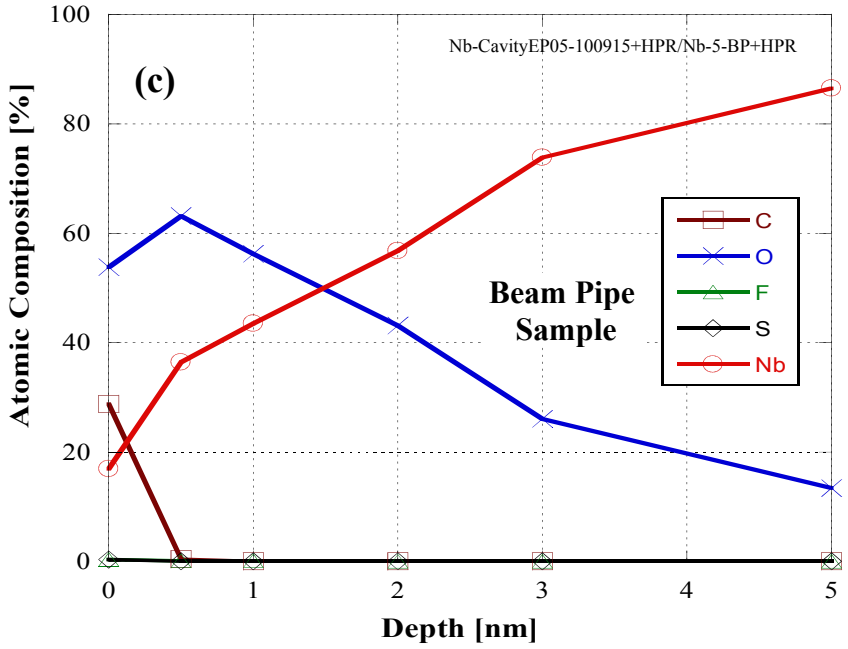

Fig. 4.12 : Depth profiles of the EPed samples in cavity EP 4 followed by HPR experiment up to 5 nm, (a) Equator sample, (b) Iris Sample and (c) Beam pipe sample.

The FWHM of oxide layer was 1.8 nm at an equator sample surface, 1.5 nm at an iris sample surface and 2.5 nm in case of a beam pipe sample surface. The reason of increase in the thickness (FWHM) of oxide layer of beam pipe sample can be explained in terms of the higher pressure at beam pipe position as nozzle distance is the shortest among all three positions.

4.2.2 Laboratory HPR : In order to characterize the effect of different high pressures on mitigation of the contaminants from the Nb surface after the BCP, a laboratory HPR experiment was conducted with the different pressures and doses [4.4]. The details of the experimental procedure and the definition of dose are explained in the section 3.2.1 of chapter 3. For the HPR experiment, All the samples were initially BCPed and a depth of 20 µm was removed. Then these BCPed samples were subjected to the HPR with two different doses for each pressure. Each sample was scanned for 1 second for a dose of 0.78 l/cm^2 and for 10 second for a dose of 7.9 l/cm^2.

Each sample was subjected to HPR at different places and one separator was used, which separates the sample in two parts in order to avoid the effect of rinsing of another position by side-streams of the water beam. The table 4.12 describes the atomic composition present at top surface of the samples.

Elements	Atomic Composition Present at Samples Surface (atomic %)						
	Dose = 0.78 l/cm² (1 S)			Dose = 7.8 l/cm² (10 S)			UPW rinsing
	8 MPa	10 MPa	15 MPa	8 MPa	10 MPa	15 MPa	
Nb	19	20	16	18	22	19	24
C	17	17	28	17	21	19	23
O	62	54	55	63	57	62	45
F	1.5	1.2	1	1.2	0.3	0.3	7

Table 4.12 : The atomic composition present at top surface of the samples after HPR with different pressures as a function of dose.

XPS results of the BCPed sample followed by UPW rinsing only, show that a huge amount of fluorine was found at top surface. The depth profile of the UPW rinsed sample shows the thickness (FWHM) of oxide layer was around 1.5 nm.

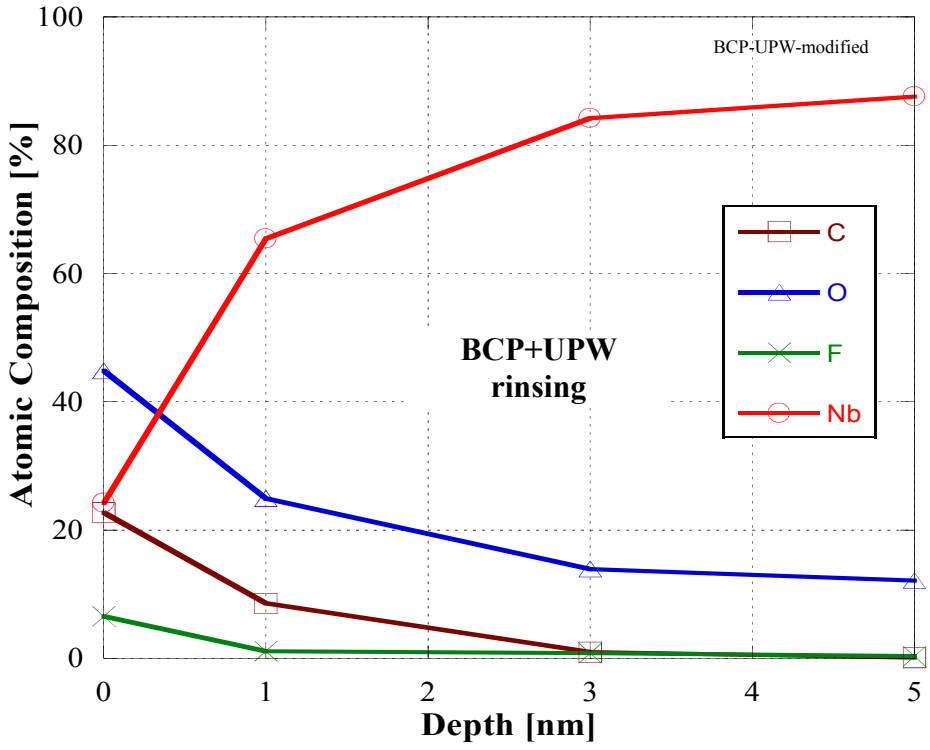

Fig. 4.13 : Depth profile of the BCPed samples followed by UPW rinsing up to 5 nm.

As it can also be encountered from the table 4.12 that the HPR was quite effective to mitigate the fluorine from the sample surfaces. The lowest fluorine was found on the surfaces treated with the higher dose.

It is evident from XPS results that not only the higher pressure is effective in order to mitigate the chemical contaminants from the surface but higher dose is more advantageous over the high pressure. As expected, all the depth profiles of the BCPed samples subjected to HPR show a great increment in the thickness of oxide layer after the HPR. The FWHM of oxide layer was 2.5 nm in case of the sample subjected to 8 MPa HPR with a low dose and 2.7 nm in case of a high dose. The difference in thickness (FWHM) of oxide layer between low and high dose was found 0.2 nm.

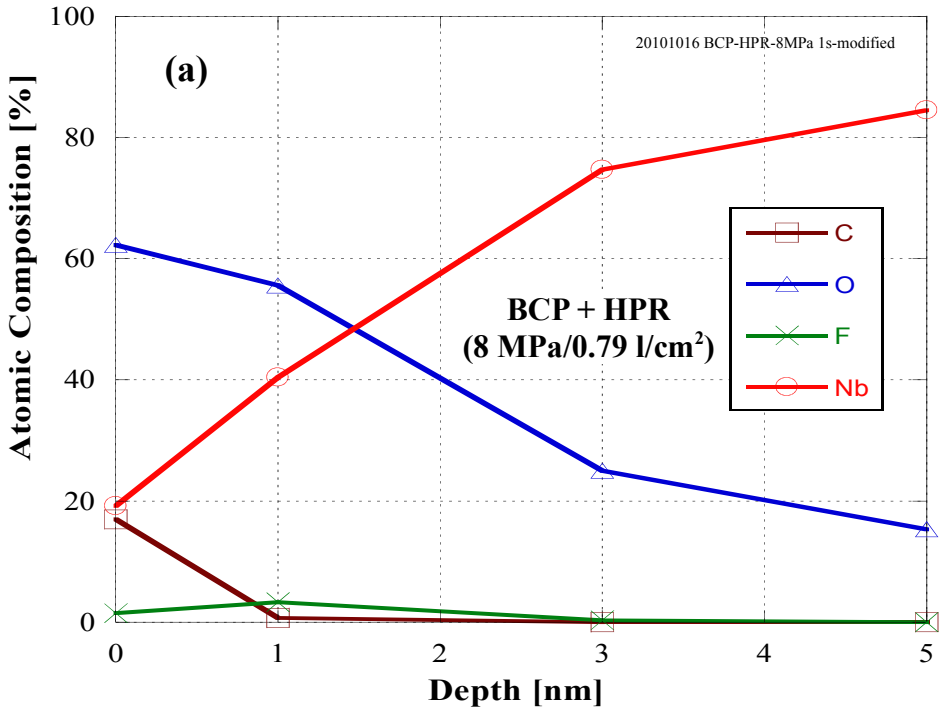

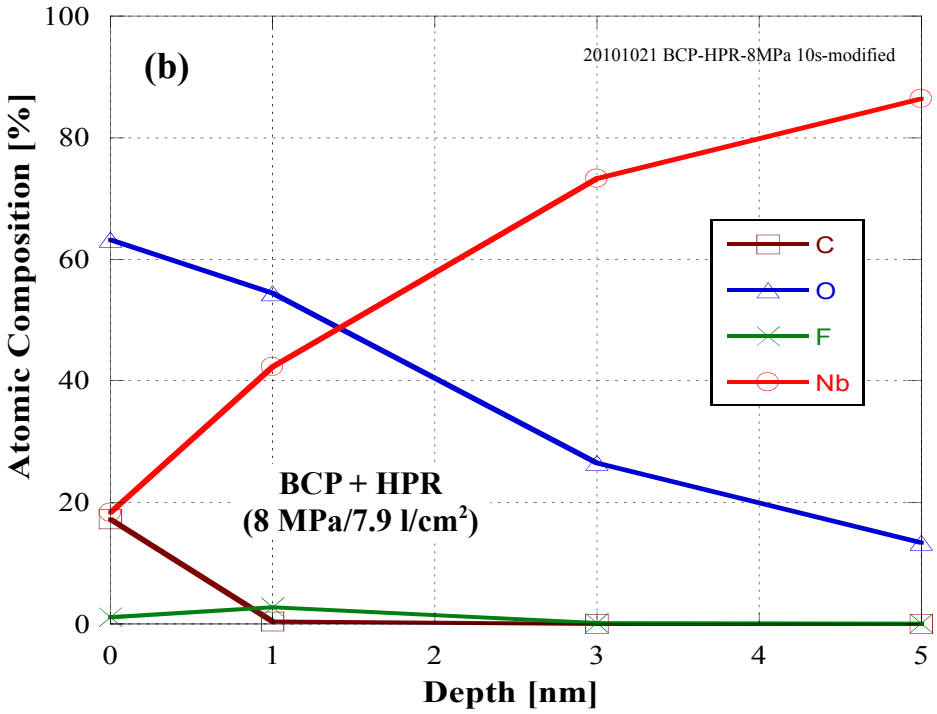

Fig. 4.14 : Depth profiles of the BCPed samples followed by HPR experiment with 8 MPa up to 5 nm, (a) With a dose of 0.79 l/cm^2 and (b) With a dose of 7.9 l/cm^2.

From the depth profiles of the samples subjected to 10 MPa HPR, it can be seen that the thickness of oxide layer was 2.4 nm in case of a low dose and 3.8 in case of a high dose. The dose dependent difference in an oxide layer thickness was 1.4 nm in case of samples subjected to HPR with 10 MPa.

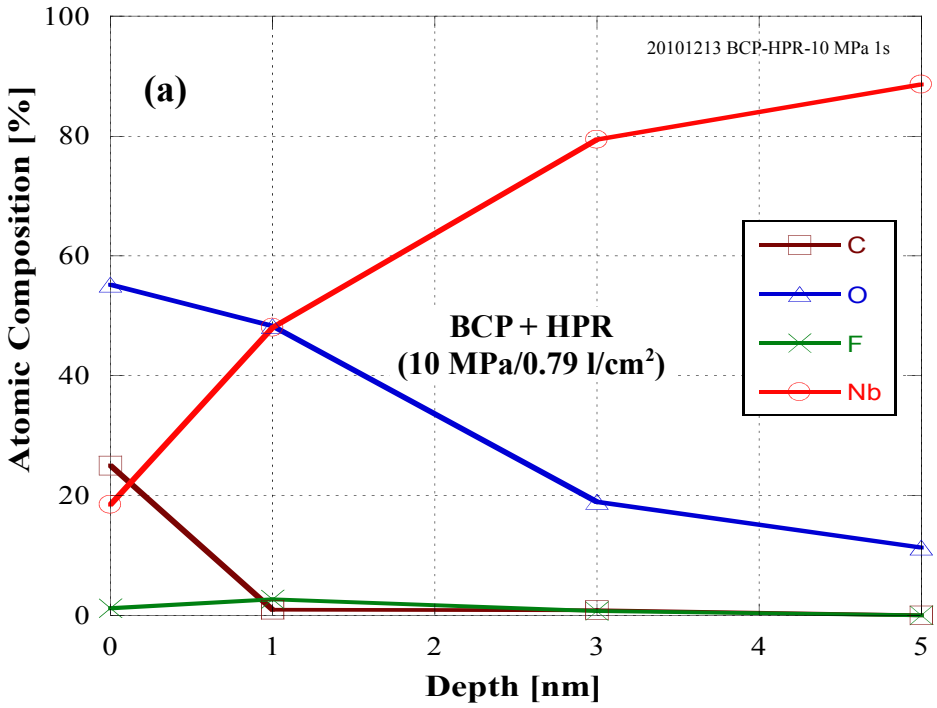

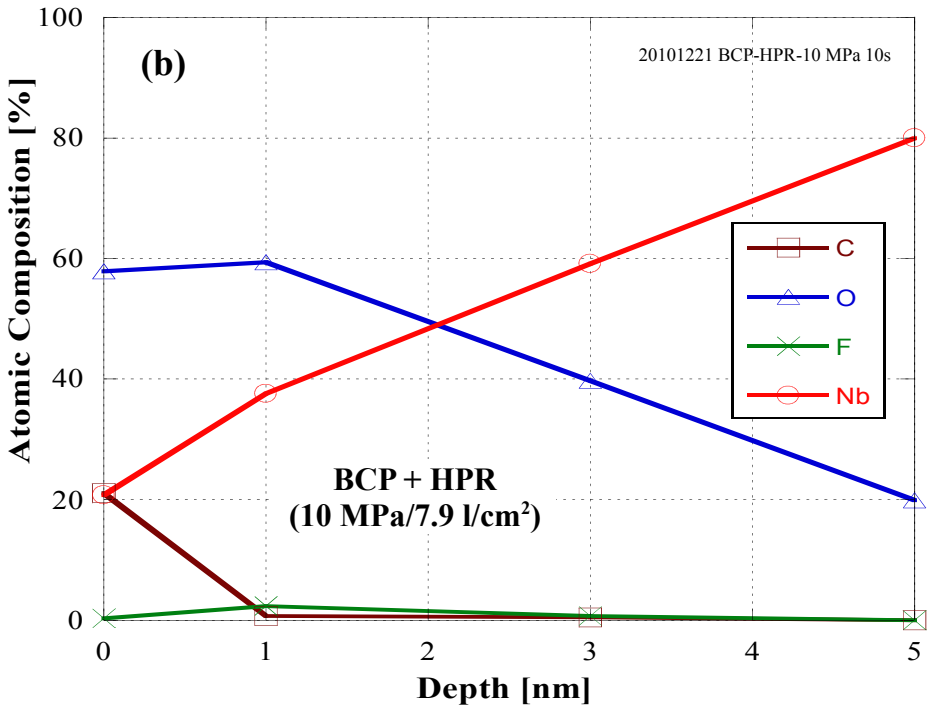

Fig. 4.15 : Depth profiles of the BCPed samples followed by HPR experiment with 10 MPa up to 5 nm, (a) With a dose of 0.79 l/cm^2 and (b) With a dose of 7.9 l/cm^2.

As it is evident from the depth profiles of the samples subjected to 15 MPa HPR that the FWHM of oxide layer was 3.2 nm in case of a low dose and it was 4.5 nm in a high dose case.

As it can be seen from the table 4.12 that the amount of fluorine present at sample surface after the HPR was same in the case of 10 MPa and 15 MPa with a high dose while the FWHM oxide layer was found 0.7 nm thicker in case of 15 MPa than 10 MPa with a high dose. It is also noticed that the amount of fluorine was increased at 1 nm depth and was similar in all the cases which shows that the HPR is effective to mitigate the contaminants from top layer of surface (<0.5 nm) only.

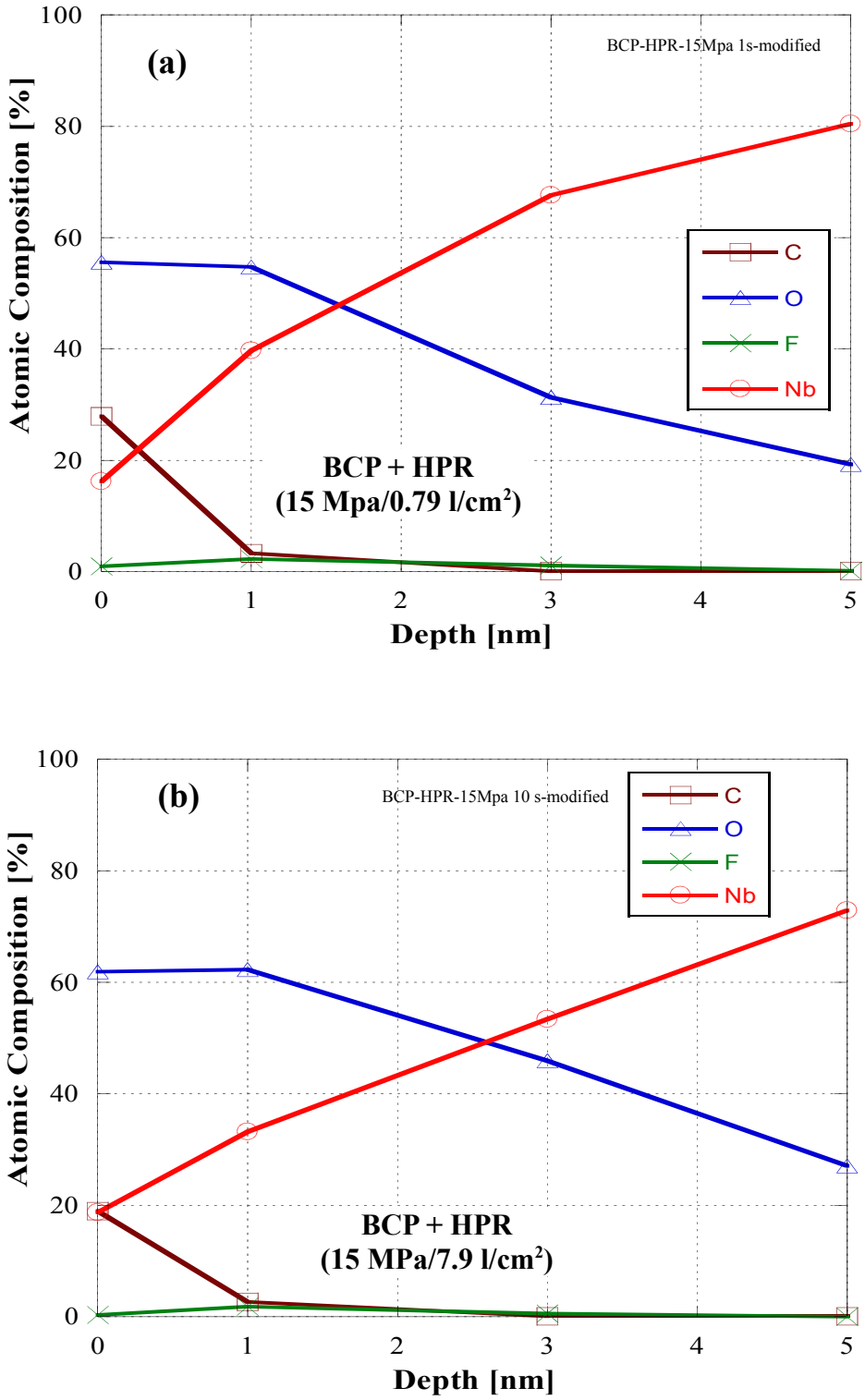

Fig. 4.16 : Depth profiles of the BCPed samples followed by HPR experiment with 15 MPa up to 5 nm, (a) With a dose of 0.79 l/cm^2 and (b) With a dose of 7.9 l/cm^2.

The reduction of same amount of fluorine with a different oxide layer thickness make the HPR pressure and doses more important from the point of view of SRF application.

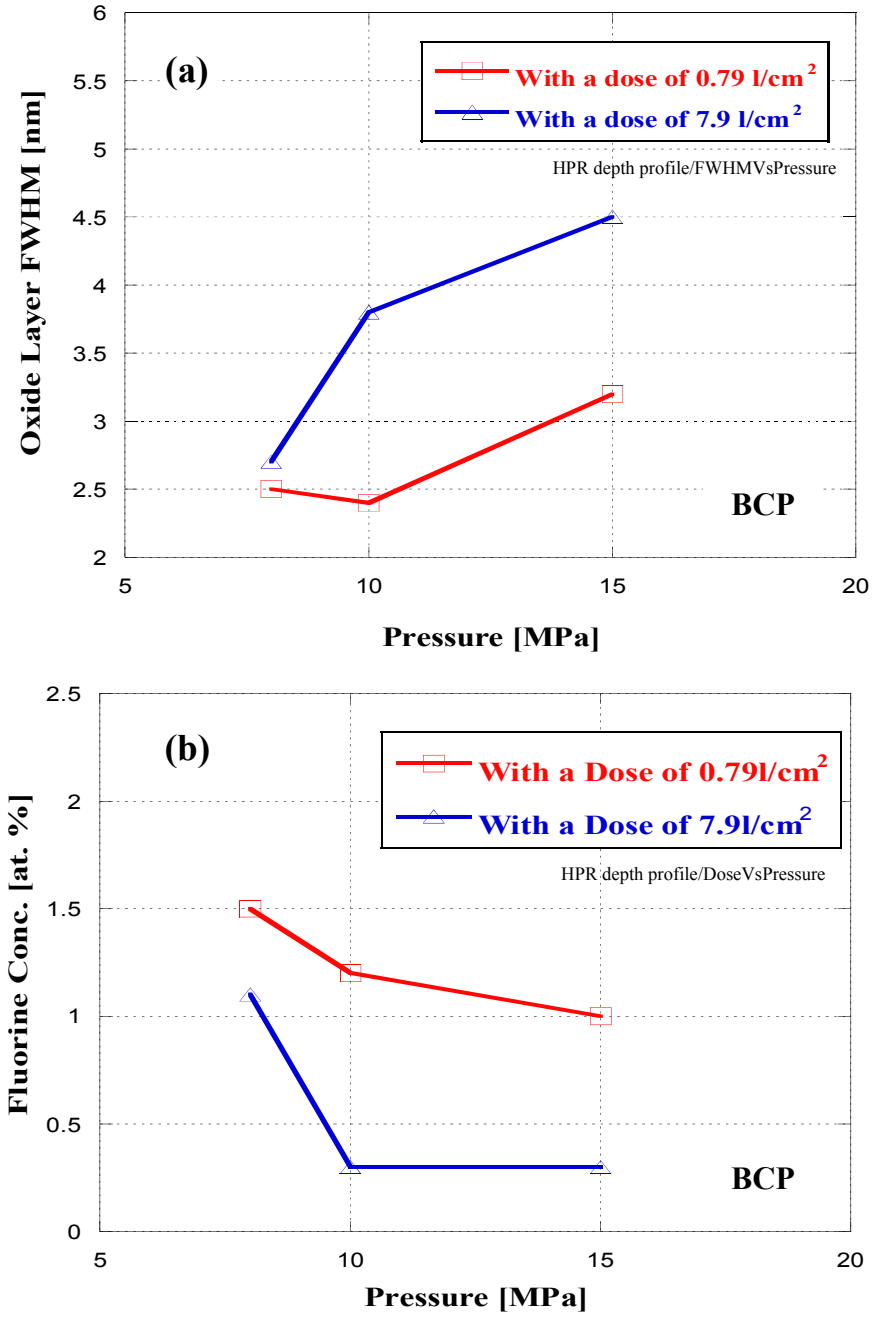

Fig. 4.17 : (a) Variation of oxide layer FWHM as a function of pressure and dose. (b) Reduction in fluorine concentration based on pressure and dose.

From the laboratory HPR experiment, it can be seen that the same high dose of 10 MPa and 15 MPa HPR mitigate the fluorine in the same amount but HPR with 15 MPa and a high dose produces a thicker oxide layer.

4.3. Dry Ice Cleaning Experimental Results

The dry ice cleaning (DIC) experiment was performed on the Nb samples EPed in the lab EP1 experiment. The rectangular type Nb sample was used for the DIC experiments and half of the sample was covered with another Nb sample in order to avoid the DIC effect on another side. The two DIC experiments were conducted; one in a normal environment (Air) and other in a nitrogen environment. The ice formation was observed at the surface during the experiment in air because of the high humidity which disturbed the experiment. Therefore the second experiment was performed under the presence of nitrogen in order to avoid the ice formation. The following table 4.13 summarizes the experimental conditions :

Experiments	Nozzle Distance (mm)	Cleaning Time (min.)	Cleaning Environment	Remarks	Experimental Method
Dry Ice 1	10	3	Air	The ice was formed at top surface during the experiment because of a high humidity	With a 5 min interval after 1 min cleaning in order to melt ice
Dry Ice 2		1	Nitrogen	No ice was formed during the experiment	Continuously for 1 min.

Table 4.13 : The experimental conditions of DIC experiments.

The XPS analysis of the samples surface after the DIC experiments didn't show a significant difference between DIC and non-DIC areas in both the DIC experiments. The similar atomic composition of sulfur and fluorine was found at both the areas (DIC and non-DIC). The table 4.14 gives the atomic composition present at top surface in both the experiments.

Elements	DIC in Air		DIC in Nitrogen	
	Non-DIC Area (atomic %)	DIC Area (atomic %)	Non-DIC Area (atomic %)	DIC Area (atomic %)
Nb	15.6	16.6	13.8	16
C	31.1	26.5	35.2	26.6
O	52.9	56.2	50.6	56.7
F	0.3	0.4	0.1	0.3
S	0.3	0.4	0.3	0.4

Table 4.14 : Atomic composition present at top surface after the DIC experiments in both the conditions.

Although there is a little difference found in atomic compositions between DIC and non-DIC area which is mainly because, some of the hydrocarbons in adsorbate should have been removed.

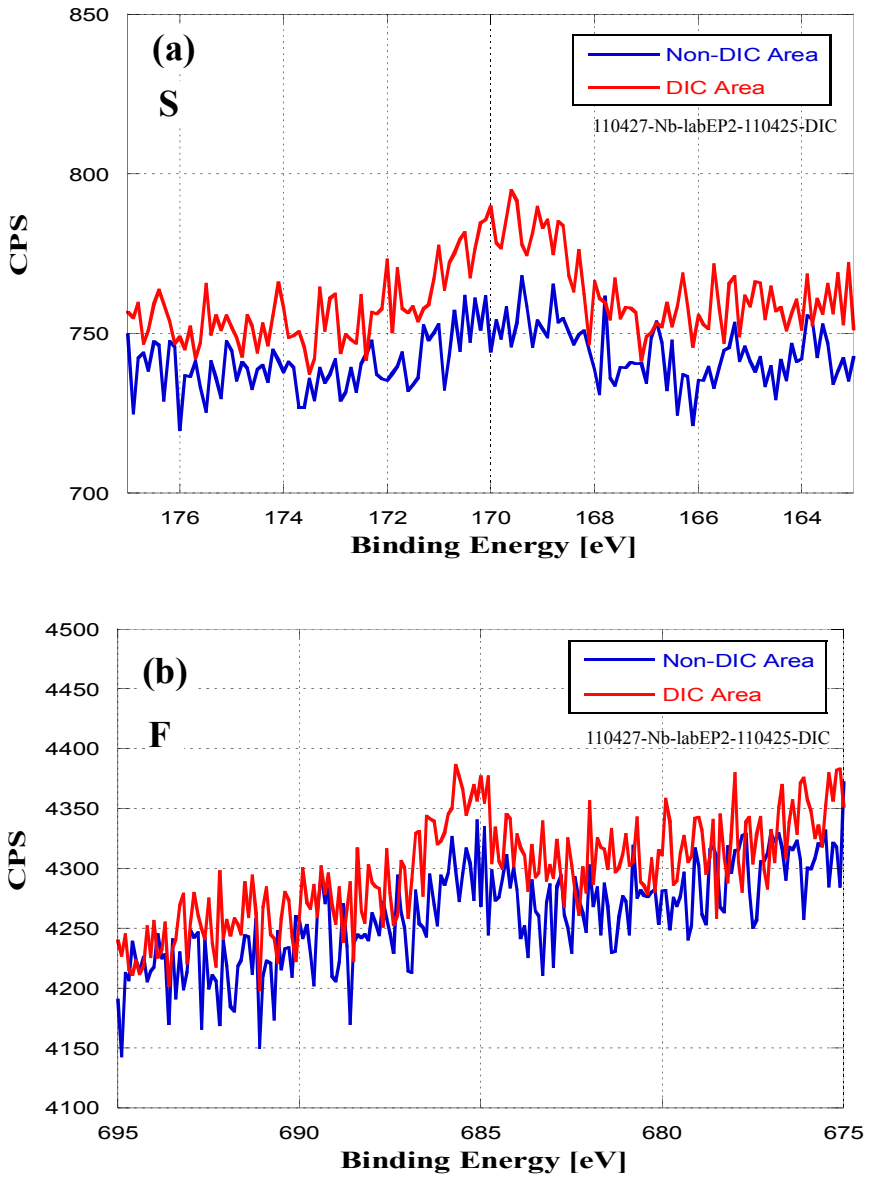

Fig. 4.18 : The XPS spectra of sample surface after the DIC experiment in normal environment. (a) Sulfur and (b) Fluorine.

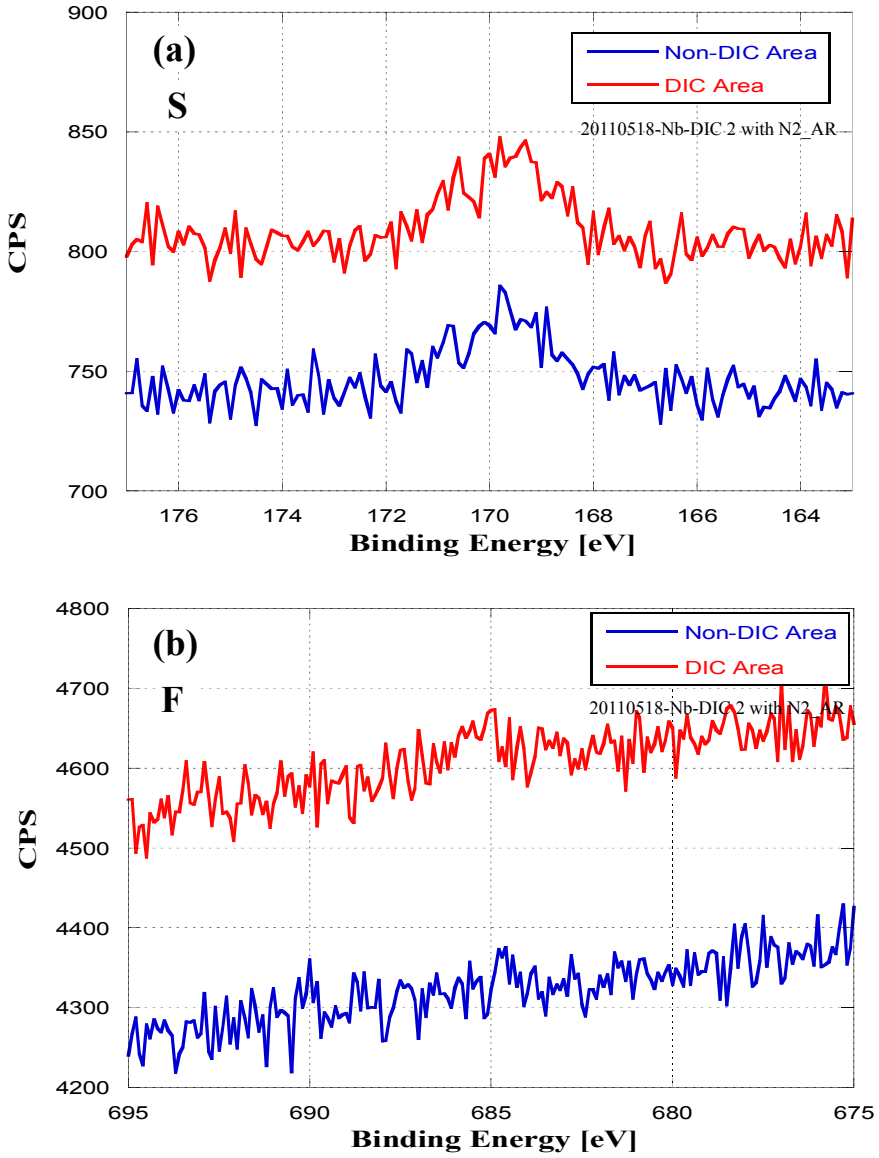

Fig. 4.19 : The XPS spectra of sample surface after the DIC experiment in nitrogen environment. (a) Sulfur and (b) Fluorine.

As it is clear from the XPS spectra of the Nb samples after DIC experiments that the DIC was not so effective to mitigate the chemical contaminants from the surface. Although some of the dust particles can be removed by using DIC, still it can not be utilized for the cleaning of real Nb cavities in these conditions. There may be some chances that DIC can work effectively if the density of dry ice particles and pressure is increased. Therefore much research and efforts are required to explore the possibility of DIC to use it on the Nb cavities.

4.4. References

[4.1] M. Nishiwaki et. al, “Surface study using niobium sample coupons for superconducting rf cavity”, Proc. PAC 2009, Vancouver, Canada.

[4.2] P. V. Tyagi, et. al, “Surface analyses of electro-polished niobium samples for SRF cavity”, JVST A, 28, (2010), 634.

[4.3] Daichi Imamura, “Effect of potential on sulfur-poisoning of Pt/C catalyst”, ECS Transactions, 16, (2008), 807.

[4.4] P. V. Tyagi et. al, "Various rinsing effects to mitigate contaminates brought by BCP on Niobium SRF cavity surface", Proc. of IPAC10, 2010, Kyoto, Japan.

Chapter 5 Conclusions

A systematic study concerning about the surface preparation of the ILC SRF cavities with many new findings for the first time in the world is presented in this thesis. The inner surface of the SRF cavities plays the most important role in the achievement of the high E field, therefore the understanding of the surface treatments behavior inside a real cavity and effect of the post treatments processes are essential. In order to understand the real conditions inside a cavity after the EP, we used a real Nb cavity assembled with Nb samples for the experiments and EPed in the same procedure as ILC cavities are employed. As a post EP processes, we also conducted a HPR experiment on the Nb cavity assembled with Nb samples just after the EP to see the effect of HPR on mitigation of contaminants. To characterize the performance of HPR dependent on different high pressures and doses, we carried out a laboratory HPR experiment on BCPed samples. The dry ice cleaning experiments were also carried out on Nb surfaces after the lab EP in order to clean the surface. The surfaces of all the samples were investigated by using the surface analytical tools at our surface analysis laboratory. Many systems like the vacuum suitcases to carry the samples while keeping in vacuum, the load lock 2 and 3 for the surface analysis system to transfer the sample from suitcase, an experimental set up to perform HPR etc. were improved/constructed for the experiments.

5.1. Conclusions of Electropolishing Experiments

5.1.1. Conclusions of Cavity EP Experiments : In order to see the performance of EP inside a real Nb cavity, a series of cavity EP experiments were conducted by using a real Nb test cavity. The table 5.1 summarizes the experimental results of all cavity EP experiments.

5.1.1.1. Conclusion of Cavity EP 1 Experiment : The cavity EP 1 experiment was conducted to see the presence of contaminants mainly sulfur and fluorine at Nb surface after the EP with fresh EP acid. The experimental results show that the sulfur and fluorine were not found at any of the samples surface treated in the cavity EP 1 experiment under the detection limit (<0.5 at. % for sulfur and <0.4 at. % for fluorine) of our XPS. The depth profiles of the samples show the FWHM of oxide layer at equator sample, the iris sample and the beam pipe sample were 1.5 nm, 1.8 nm and 2 nm respectively. The SEM images of the samples showed that the surfaces were covered with many particles of the size of sub micrometer to few micrometers which were confirmed as the sulfate/sulfide particles in TOF-SIMS analysis.

5.1.1.2. Conclusion of Cavity EP 2 Experiment : In order to see the effect of the aging of EP acid in terms of contaminants presence at the cavity surface, we conducted the cavity EP 2 experiment with the aged EP acid in the similar style of the cavity EP 1 experiment. The Nb concentration in aged EP acid

solution was 7.9 g/l. In comparison with the cavity EP 1 experimental results, the XPS results showed a huge quantity of sulfur and fluorine was present at samples surface in case of the cavity EP 2 experiment. A chemical shift was also observed in the sulfur and oxygen spectra which confirms the presence of sulfur as a sulfate and/or sulfide form. Atomic percentage of sulfur was found maximum (7 at. %) at iris sample surface while the minimum was found at beam pipe sample. Additionally, a notable quantity of nitrogen was found on the surfaces of iris and equator samples. The depth profiles of the samples showed that the sulfur was present only at top surface and the FWHM thickness of oxide layer at equator sample, the iris sample and the beam pipe sample were 1.5 nm, 2.5 nm and 1.9 nm respectively. The SEM observations showed the high density of particles on the surfaces in comparison with the cavity EP 1 experiment.

Experiments	**Aim**	**Average Current Density (mA/cm^2)**	**Nb Conc. in EP acid (g/l)**	**Removal Depth (µm)**	**Sample Position**	**Results**		
						Atomic Percentages Present on the Surface (at. %)		**Oxide Layer Thickness (FWHM nm)**
						F	**S**	
Cavity EP 1	To see the performance of EP with fresh EP acid inside a real cavity	48	0	20	Equator	<0.4	<0.5	1.5
					Iris	<0.4	<0.5	1.8
					Beam Pipe	<0.4	<0.5	2
Cavity EP 2	To see the aging effect of the EP acid on EP performance	48	7.9	50	Equator	3	4	1.5
					Iris	3	7	2.5
					Beam Pipe	4	2	1.9
Cavity EP 3	To see the effect of the low current density with aged EP acid on EP performance	30	6	20	Equator	0.9	0.5	1.5
					Iris	0.2	<0.1	1.8
					Beam Pipe	0.4	0.2	1.8

Table 5.1 : The summary of experimental results of the cavity EP experiments.

5.1.1.3. Conclusion of Cavity EP 3 Experiment : The cavity EP 3 experiment was conducted to characterize the effect of current density on presence of contaminants at Nb surface after the EP with aged acid. The experimental results demonstrated a reduction in amount of sulfur and fluorine at the

samples surface after the EP with low current density. The XPS results showed the low current density is helpful in order to reduce the sulfur and fluorine presence/generation at Nb surface EPed with aged EP acid. The depth profiles of the samples show that the sulfur was present only at top surface and the FWHM of oxide layer at equator sample, iris sample and beam pipe sample were 1.5 nm, 1.8 nm and 1.8 nm respectively. The FWHM of oxide layer was similar to the cavity EP 1 and 2 experiments but in case of cavity EP 3 experiment, it was present in the bulk also. The reason of quite deeper oxide layer is still unclear.

5.1.2. Conclusion of Laboratory EP Experiments : Two lab EP experiments with low and high current density and aged EP acid were conducted in order to confirm the results of the cavity EP 2 and 3 experiments. Following table 5.2 gives the summary of experimental conditions and results.

Experiments	Aim	Average Current Density (mA/cm^2)	Nb Conc. in EP acid (g/l)	Removal Depth (µm)	Atomic Percentages Present on the Surface (at. %)	
					F	S
Lab EP 1	To see the effect of low current density at laboratory scale.	33	7.3	20	<0.1	0.3
Lab EP 2	To see the effect of high current density at laboratory scale.	50	7.6	20	<0.1	10.3

Table 5.2 : The summary of experimental results of the laboratory EP experiments.

5.1.2.1. Conclusion of Lab EP 1 Experiment : The lab EP 1 experiment was conducted with the low current density and aged EP acid at laboratory scale on the rectangular type Nb samples fixed at a Nb base plate. The Nb concentration in aged EP acid solution was 7.3 g/l and a current density during the experiment was maintained at 33 mA/cm^2. The XPS results showed that a very small quantity of sulfur (up to 0.3 at. %) and fluorine (<0.1 at. %) were found at top surface. The lab EP 1 experiment with a low current density and aged EP acid in conjunction with cavity EP 3 experiment confirmed that the low current density is very helpful to reduce the generation of contaminations at Nb surface.

5.1.2.2. Conclusion of Lab EP 2 Experiment : In order to confirm the effect of a high current density with aged EP acid solution in conjunction with cavity EP 2 experiment, the lab EP 2 experiment was carried out at a laboratory level. The Nb concentration in the aged EP acid solution and current density during the experiment were 7.6 g/l and 50 mA/cm^2 respectively. The XPS results of the lab EP 2 experiment were quite consistent with the cavity EP 2 experimental results and showed a huge quantity

of sulfur (up to 10.3 at. %) was present at the surface. A peak shift in sulfur as well as oxygen spectra was found in the same manner as it was found in the cavity EP 2 experiment and confirms the sulfur presence in oxidation state. On the basis of surface analysis results of cavity EP 2 and lab EP 2 experiments it can be concluded that the sulfur generation is proportional to the high current density.

5.2. Conclusions of High Pressure Rinsing Experiments

5.2.1. Conclusion of Cavity EP 4 and HPR : In order to see the effect of HPR after the EP, we conducted a cavity EP 4 experiment followed by HPR. The pressure and duration of HPR were 8 MPa and 2 hr. 25 min respectively. The HPR duration was calculated in order to keep the same dose of 0.79 l/cm^2 as similar dose of ILC cavity HPR.

Experiments	**Average Current Density (mA/cm^2)**	**EP Acid Temperature (^{0}C)**	**Nb Conc. in EP acid (g/l)**	**Sample Position**	**Results**		
					Atomic Percentage Present on the Surface (at. %)		**Oxide Layer Thickness (FWHM nm)**
					F	**S**	
Cavity EP 4 (20 µm removal) + HPR with 8 MPa (2 hrs. 25 min.)	50	20	2.1	Equator	0.3	<0.1	1.8
				Iris	0.6	<0.1	1.5
				Beam Pipe	0.3	<0.1	2.5

Table 5.3 : The experimental results of the cavity EP 4 followed by the HPR experiment.

The XPS results of the samples surface showed that the sulfur was not present at the surface while fluorine was found at the surface (table 5.3). The maximum fluorine (0.6 at. %) was found on the iris sample. According to surface analyses results, either the HPR was quite effective to remove sulfur and/or sulfur compounds from the surface or the sulfur was not present on the samples surface since beginning as EP acid used was not very aged. From our results, it can be seen that the HPR pressure/dose was not sufficient to remove the fluorine. The FWHM of oxide layer at equator sample, the iris sample and the beam pipe sample were 1.8 nm, 1.5 nm and 2.5 nm respectively. The FWHM oxide layer, in case of equator and iris was small or similar to other cavity EP experiments while it was increased in case of beam pipe sample. The reasons would be the following : as the distance between nozzle and the equator is quite large in comparison of iris and beam pipe positions, the actual HPR pressure would be weak at the sample surface fixed at equator position while in case of the sample fixed at iris, the sample was not subject to water beam properly as the geometry of cavity at iris position is very complicated and the beam pipe sample was exposed to high pressure water beam very effectively as the distance to nozzle is the shortest among all the samples.

5.2.2. Conclusion of lab HPR experiment : The laboratory HPR experiment with different pressures and doses was conducted in order to see the effect of mitigation of contaminants by HPR at a laboratory level. For the experiment, three Nb rectangular type samples were BCPed and subjected to two different doses (0.79 l/cm^2 and 7.9 l/cm^2) of HPR with 8 MPa, 10 MPa and 15 MPa. The table 5.4 describes the experimental conditions and results.

The XPS results show that the huge amount of fluorine (7 at. %) was found on the BCPed samples and HPR with high pressures and dose was quite effective in order to reduce the fluorine concentration from the surface. The fluorine was found least (0.3 at. %) on the samples surface treated with a high dose of 10 MPa and 15 MPa. The first finding of the increase in the oxide layer as a function of pressure and dose was also reported.

Experimental Conditions			**Results**	
Removal Depth By BCP (µm)	**Rinsing Procedure**	**Dose (l/cm^2)**	**F (at. %)**	**Oxide Layer Thickness (FWHM nm)**
20 µm	8 MPa	0.79	1.5	2.5
		7.9	1.1	2.7
	10 MPa	0.79	1.2	2.4
		7.9	0.3	3.8
	15 MPa	0.79	1	3.2
		7.9	0.3	4.5

Table 5.4 : The experimental results of the BCP experiment followed by the HPR with different pressures and doses.

After the HPR with a high dose of 10 MPa and 15 MPa, the fluorine was reduced to the same amount in both cases while a thicker oxide layer was found in case of sample subjected to 15 MPa with high dose. The oxide layer in case of HPR with 15 MPa and high dose was found 0.7 nm thicker than 10 MPa and high dose with the reduction of fluorine in the same amount. Therefore it can be concluded from our results that the HPR with 10 MPa with high dose is a better process to remove the fluorine from the Nb surface. To obtain the best HPR effect, multiple nozzles in single wand would be a good way to increase dose in the same time.

5.3. Conclusions of Dry Ice Cleaning Experiment

The dry ice cleaning experiment was conducted on EPed rectangular Nb samples in normal and nitrogen environment. The table 5.5 includes the experimental conditions and results.

Experiments	**Experimental Conditions**			**Results**	
				F (at. %)	**S (at. %)**
ECB	In Air	For 3 min. with an interval of 5 min. after every 1 min in order to melt the ice	At DIC Area	0.4	0.4
			Non-DIC Area	0.3	0.3
	In Nitrogen	Continuously for 1 min.	DIC Area	0.3	0.4
			Non-DIC Area	0.1	0.3

Table 5.5 : The experimental results of the DIC experiment in air and nitrogen.

During the experiment in air, an ice was formed at Nb surface due to the high humidity therefore an additional DIC experiment was conducted in the nitrogen environment. The surface analysis results didn't show much difference between DIC area and non-DIC area in both the experiments (air and nitrogen). Therefore, it can be concluded from our DIC experimental results that the DIC is not an affective cleaning method in terms of chemical contaminants removal with these conditions and can't be used for Nb surface cleaning.

Appendix :

Table of the surface analysis system specifications :

Equipments	**Model/Type**	**Manufacturer**
X-ray source	XR-50	Specs
Electron gun	EQ22/35	Specs
Ion gun	IQE 12/38	Specs
Electron energy analyzer	Phoibos 100 MCD5	Specs
Electron energy analyzer Software control	Speclab2 and Spleclab 1	Specs

Tables of specifications of X-ray source :

Anode :

Anode	Positive high voltage
Anode material	Al, Mg
Anode base material	Ag-tipped
Anode voltage	+15 kV max
Power dissipation	1 kW max
Continuous load	400 W for Al, 300 W for Mg
Anode cooling	Water, 15 - 22^0C
Anode to sample distance	15 mm

Cathode :

Cathode	ThO_2 coated Tungsten (spiral)
Power consumption	Max 30 W

Table of Ion gun operating parameters :

Ion source	Ar^+
Operating energy	5 keV
Emission current	10 mA
Rastering area on a sample	5×5 mm^2
Ar^+ ion Faraday current	160-180 nA (at 1 E-2 Pa Ar pressure in I-gun)
Beam diameter [FWHM]	~800 μm

Table of operating modes of electron energy analyzer :

Mode	**Acceptance Area**	**Acceptance Angle**	**Typical Application**
Large area	Ø 12 mm independent on slit size	$\pm 0.5^0$ to $\pm 5^0$ dependent on slit size	Large area XPS and UPS ADXPS and XPD
Medium area (angular resolved)	Ø 8 mm independent on slit size	$\pm 0.5^0$ to $\pm 5^0$ dependent on slit size	XPS and UPS high resolution applications and ADXPS/ADUPS
Medium magnification* (spatially resolved)	2×7 mm^2 to Ø 0.3 mm dependent on slit size	up to $\pm 0.4^0$ decreasing with smaller sizes	XPS and UPS
High magnification (spatially resoled)	0.75×2.5 mm^2 to Ø 125 μm dependent on slit size	up to $\pm 0.9^0$ decreasing with smaller slit sizes	Small area XPS/UPS, AES, ISS and synchrotron studies

*The medium magnification mode has been used for the current study.